

2

NAVAL POSTGRADUATE SCHOOL MONTEREY, CALIFORNIA

AD-A273 373



ALL INFORMATION CONTAINED
HEREIN IS UNCLASSIFIED
EXCEPT WHERE SHOWN
OTHERWISE IN BLACK AND
WHITE

DTIC
ELECTE
DEC 06 1993
S B D

THESIS

A NUMERICAL STUDY OF AIRPLANES FLYING IN
PROXIMITY

by

David B. Porter

September 1993

Thesis Advisor:

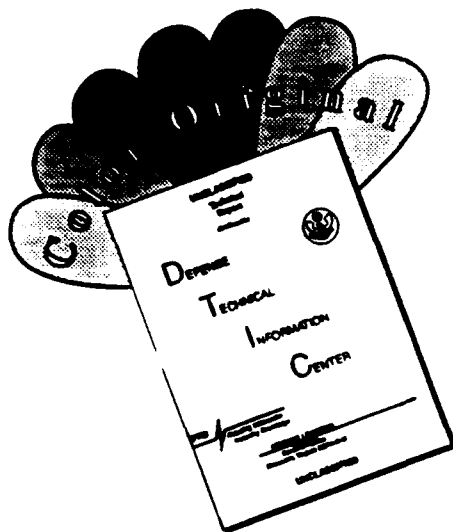
Richard M. Howard

Approved for public release; distribution is unlimited.

93 12 3 013

140pt
93-29529

DISCLAIMER NOTICE



THIS DOCUMENT IS BEST QUALITY AVAILABLE. THE COPY FURNISHED TO DTIC CONTAINED A SIGNIFICANT NUMBER OF COLOR PAGES WHICH DO NOT REPRODUCE LEGIBLY ON BLACK AND WHITE MICROFICHE.

REPORT DOCUMENTATION PAGE

1a. REPORT SECURITY CLASSIFICATION Unclassified		16. RESTRICTIVE MARKINGS	
2a. SECURITY CLASSIFICATION AUTHORITY		3. DISTRIBUTION/AVAILABILITY OF REPORT Approved for public release; distribution is unlimited.	
2b. DECLASSIFICATION/DOWNGRADING SCHEDULE			
4. PERFORMING ORGANIZATION REPORT NUMBER(S)		5. MONITORING ORGANIZATION REPORT NUMBER(S)	
6a. NAME OF PERFORMING ORGANIZATION Naval Postgraduate School	6b. OFFICE SYMBOL (If Applicable) AA	7a. NAME OF MONITORING ORGANIZATION Naval Postgraduate School	
6c. ADDRESS (city, state, and ZIP code) Monterey, CA 93943-5000		7b. ADDRESS (city, state, and ZIP code) Monterey, CA 93943-5000	
8a. NAME OF FUNDING/SPONSORING ORGANIZATION	8b. OFFICE SYMBOL (If Applicable)	9. PROCUREMENT INSTRUMENT IDENTIFICATION NUMBER	
8c. ADDRESS (city, state, and ZIP code)		10. SOURCE OF FUNDING NUMBERS	
		PROGRAM ELEMENT NO.	PROJECT NO.
		TASK NO.	WORK UNIT ACCESSION NO.
11. TITLE (Include Security Classification) A NUMERICAL STUDY OF AIRPLANES FLYING IN PROXIMITY			
12. PERSONAL AUTHOR(S) Porter, David B.			
13a. TYPE OF REPORT Master's Thesis	13b. TIME COVERED FROM TO	14. DATE OF REPORT (year, month, day) September 1993	15. PAGE COUNT 140
16. SUPPLEMENTARY NOTATION The views expressed in this thesis are those of the author and do not reflect the official policy or position of the Department of Defense or the U.S. Government.			
17. COSATI CODES		18. SUBJECT TERMS (continue on reverse if necessary and identify by block number)	
FIELD	GROUP	Formation Flying, Panel Method, Stability and Control	
19. ABSTRACT (Continue on reverse if necessary and identify by block number)			
<p>During an emergency such as an unsafe landing gear indication, a second aircraft is often used to perform an airborne visual inspection of the landing gear. The chase airplane may be quite dissimilar in size and wing loading and consequently experience unexpected aerodynamic forces and moments caused by the other airplane. A numerical study of the inherent danger involved with the aerodynamic interaction of aircraft flying in proximity was made using the low-order panel code PMARC (Panel Method Ames Research Center). PMARC validation was made by comparing wind tunnel and analytically-derived stability data for T-34 and F-14 models with PMARC results. A T-34 was then placed at various distances underneath an F-14 to determine changes in lift and pitching moments on the T-34. Color illustrations of pressure coefficients were used to highlight the changes in aerodynamic forces and moments as vertical separation between the two aircraft was decreased. PMARC showed that 4.5 deg. of elevator trim change were required as a T-34 approached to within its semispan of an F-14.</p>			
20. DISTRIBUTION/AVAILABILITY OF ABSTRACT <input checked="" type="checkbox"/> UNCLASSIFIED/UNLIMITED <input type="checkbox"/> SAME AS RPT. <input type="checkbox"/> DTIC USERS		21. ABSTRACT SECURITY CLASSIFICATION Unclassified	
22a. NAME OF RESPONSIBLE INDIVIDUAL Richard M. Howard		22b. TELEPHONE (Include Area Code) (408) 656-2870	22c. OFFICE SYMBOL AA/HO

ORIGINAL COPIES
SHOULD BE IN BLACK AND
...
...

Approved for public release; distribution is unlimited.

A Numerical Study of Airplanes Flying in Proximity

by

David B. Porter
Lieutenant Commander, United States Navy
B.S.A.E., United States Naval Academy, 1980

Submitted in partial fulfillment of the requirements for
the degree of

MASTER OF SCIENCE IN AERONAUTICAL ENGINEERING

from the

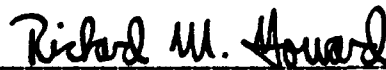
NAVAL POSTGRADUATE SCHOOL
September, 1993

Author:



David B. Porter

Approved by:



Richard M. Howard, Thesis Advisor



Oscar Biblarz, Second Reader



Daniel J. Collins, Chairman,
Department of Aeronautics and Astronautics

ABSTRACT

During an emergency such as an unsafe landing gear indication, a second aircraft is often used to perform an airborne visual inspection of the landing gear. The chase airplane may be quite dissimilar in size and wing loading and consequently experience unexpected aerodynamic forces and moments caused by the other airplane. A numerical study of the inherent danger involved with the aerodynamic interaction of aircraft flying in proximity was made using the low-order panel code PMARC (Panel Method Ames Research Center). PMARC validation was made by comparing wind tunnel and analytically-derived stability data for T-34 and F-14 models with PMARC results. A T-34 was then placed at various distances underneath an F-14 to determine changes in lift and pitching moments on the T-34. Color illustrations of pressure coefficients were used to highlight the changes in aerodynamic forces and moments as vertical separation between the two aircraft was decreased. PMARC showed that 4.5 degrees of elevator trim change were required as a T-34 approached to within its semispan of an F-14.

DTIC QUALITY INSPECTED 3

Accession For	
NTIS GRA&I	<input checked="" type="checkbox"/>
DTIC TAB	<input type="checkbox"/>
Unannounced	<input type="checkbox"/>
Justification	
By _____	
Distribution/	
Availability Codes	
Diat	Avail and/or Special
A-1	

TABLE OF CONTENTS

I.	INTRODUCTION	1
II.	BACKGROUND.....	3
A.	NAVY FORMATION FLYING	3
B.	PREVIOUS FORMATION FLYING STUDIES.....	6
C.	COMPUTER CODES.....	7
1.	PMARC Background.....	8
a.	PMARC Description.....	8
b.	Operating Systems.....	9
c.	Coordinate Systems	9
d.	Geometry Modeling.....	10
e.	Wake Modeling.....	11
2.	GVS Background.....	12
a.	GVS Description	12
b.	Operating Systems.....	12
III.	GROUNDWORK AND PMARC VALIDATION.....	14
A.	ANALYTIC DERIVATION OF T-34 STABILITY DERIVATIVES.....	14
1.	T-34 Lift-Curve Slope, $C_{L\alpha}$	14
2.	T-34 Change in Pitching Moment with Angle of Attack, $C_{m\alpha}$	14
3.	T-34 Change in Lift Coefficient with Elevator Deflection, $C_{L\delta}$	16
4.	T-34 Change in Pitching Moment with Elevator Deflection, $C_{m\delta}$	16
B.	T-34 DERIVATIVE COMPARISON WITH SIMILAR AIRPLANES.....	17
C.	PMARC AND MODELING VALIDATION.....	17
1.	NACA 4415 Airfoil Evaluation.....	18
a.	PMARC Data Versus 2-D Airfoil Data	18
b.	Computer-Generated Versus Operator-Defined Wakes.....	19
2.	T-34 Geometry Evaluation	21
3.	F-14 Geometry Validation	24

IV. ANALYSIS OF AIRPLANES FLYING IN PROXIMITY	30
A. LARGE WING AND T-34 WING AND TAIL IN PROXIMITY	30
B. F-14 AND T-34 IN PROXIMITY	35
1. Vertical Separation	35
2. Horizontal Separation.....	40
3. F-14 Jet Intake Effects.....	45
V. CONCLUSIONS AND RECOMMENDATIONS.....	47
A. CONCLUSIONS.....	47
B. RECOMMENDATIONS	48
APPENDIX A PMARC/GVS FIGURES.....	50
APPENDIX B PMARC F-14/T-34 INPUT	71
LIST OF REFERENCES	128
INITIAL DISTRIBUTION LIST.....	130

NOMENCLATURE

ac	aerodynamic center
a_t	tail lift curve slope
a_w	wing lift curve slope
AR	aspect ratio
\bar{c}	length of mean aerodynamic chord
cg	center of gravity
C_{l_α}	local section lift curve slope
$C_{l_\alpha \text{ tail}}$	local section lift curve slope for the tail
$C_{l_{\delta_e}}$	change in section lift coefficient due to elevator deflection
C_L	lift coefficient
C_{L_α}	change in lift coefficient with angle of attack (lift curve slope)
$C_{L_\alpha \text{ tail}}$	tail lift curve slope
$C_{L_{\alpha \text{ wing}}}$	wing lift curve slope
$C_{L_{\delta_e}}$	change in lift coefficient due to elevator deflection
C_m	pitching moment coefficient
C_{m_α}	change in pitching moment coefficient with angle of attack
$C_{m_{\delta_e}}$	change in pitching moment coefficient due to elevator deflection
$d\varepsilon/d\alpha$	change in downwash angle due to change in angle of attack
$\Delta\delta_e$	change in elevator deflection
$\varepsilon_{l \text{ wing}}$	induced-angle span efficiency factor of wing
$\varepsilon_{l \text{ tail}}$	induced-angle span efficiency factor of tail
h	cg position, in fraction of mac
h_{acwb}	position of aerodynamic center for wing-body, in fraction of mac

l_{tail}	length from cg to horizontal tail aerodynamic center
mac	mean aerodynamic chord
η_t	efficiency factor for tail, q_{tail} / q
ρ	air density
q	dynamic pressure ($1/2\rho V^2$)
q_{tail}	tail dynamic pressure ($1/2\rho V_t^2$)
V	free-stream velocity
S_w	wing area
S_t	horizontal tail area
V_H	horizontal tail volume coefficient
V_t	free-stream velocity at tail

ACKNOWLEDGMENTS

This study could not have been completed without the help and generosity of many people. Dan Lyon's initial instruction and guidance on PMARC fundamentals were instrumental in getting this project started. Stephen Bachner and Mark Byers of NAWC AD spent considerable time gathering and discussing F-14 and T-34 data. Steve Keith of Sterling Software was always available for help with GVS. He developed a truly great product in GVS and to him I give credit for the outstanding images in Appendix A. Matthew Koebbe's expertise in UNIX and the NPGS Visualization Lab was instrumental in the production of the video associated with this thesis.

I would especially like to thank Dr. Richard Howard, my thesis advisor, for all of his help and guidance. Finally, a very special recognition goes to Mr. Dale Ashby of NASA Ames. His unselfish dedication and technical expertise with PMARC kept the project on track.

I. INTRODUCTION

On 14 January 1992, an F-14A experienced an unsafe landing gear indication prior to recovery at a Naval air station. The F-14 air crew requested a chase aircraft to conduct a visual inspection of their landing gear in accordance with Naval Air Training and Operating Procedures Standardization Program (NATOPS) procedures. A T-34C with instructor and student pilot joined on the F-14 to inspect the landing gear. Shortly after notifying the F-14 crew that their gear looked good, the T-34 collided with the substantially larger aircraft. Significant damage to T-34 control surfaces resulted in uncontrolled flight and subsequent loss of the aircraft and its air crew. The F-14 received minor damage and returned to the Naval air station without further incident.

A study of Navy and Air Force mid-air collisions involving formation flying over the past ten years has shown that pilot error is the predominant common denominator. Task saturation; preoccupation with cockpit duties; and failures to judge closure rates and take sufficient, timely and appropriate action to avoid collision, are major factors in mishap findings [Refs. 1 and 2]. Mutual interference of the flow patterns around aircraft in proximity is rarely discussed in mishap findings or even flight training, yet may be a significant causal factor. Interference of airflow over lifting surfaces such as wings and tails can alter the aerodynamic characteristics of the aircraft. Unexpected changes in lift and pitching moments may occur that affect closure rate and task saturation of the unaware or uninformed pilot.

Very little information is available to military aviators concerning changes in aerodynamic forces and moments that result when airplanes fly close to each

other. NAVAIR has subsequently tasked the Naval Postgraduate School to investigate mutual interference of aircraft flying in formation. The desires for better insight into the aerodynamic interactions between formation aircraft and a means to educate military aviators about them form the impetus for this study.

This study is a numerical investigation in aerodynamic trim changes of dissimilar aircraft flying in formation. The low-order panel code PMARC was used to determine aerodynamic pressures, forces and moments on various wings, wing-bodies and aircraft in proximity. Discussions include PMARC validation, numerical results, and limitations associated with the computer code for this type of study. Color illustrations and histograms are used to present the changes in pressure coefficients on a T-34 wing and tail as its vertical separation from an F-14 decreases. Subsequent changes in elevator trim position and lift are addressed to provide the aviator with a better understanding of the aerodynamic effects one airplane has on the other.

This study is offered as a supplement to existing formation flying literature and training aids. A video that graphically depicts the numerical results with narration oriented toward the student aviator has been produced as a training tool for aviation safety and formation flying education. Its purpose is to expose student pilots to changes in airplane trim and handling characteristics brought about by disturbances associated with formation flying. This research ultimately provides AIR-530 with an engineering approach to investigate the aerodynamics of formation flying.

II. BACKGROUND

A. NAVY FORMATION FLYING

Military pilots are instructed in the fundamentals of formation flying throughout their training syllabus. Ultimately, formation flying becomes standard operating procedure for most tactical aviators. Unfortunately the fundamentals are often limited to basic procedures and visual cues for flying in formation with similar type aircraft.

Student Naval aviators begin primary flight training in the T-34C. After solo and basic instrument instruction, the student is taught basic procedures for flying in formation with other T-34C airplanes. Classroom emphasis is placed on operating area familiarization, join-up, formation and breakup procedures with appropriate visual cues. Visual cues are used to judge closure rates, and to maintain proper separation and placement in level flight, turn and cross-under maneuvers. Classroom instruction does not include a thorough discussion of interference between airplanes in flight. Interference from lead aircraft prop wash and its effects on lateral-directional stability of airplanes in trail is addressed, however.¹ Aircraft in trail or performing cross-under maneuvers experience a weather-vane effect when flying in the lead aircraft's prop wash. This phenomenon is discussed with students and often demonstrated in flight.

Primary flight instructors come from diverse backgrounds. Most come from P-3, C-130, E-2 and helicopter communities where formation flying is not a

¹ Phone Conversation, 28 July 1993 between author and Lt. Freeman, VT-6, Milton NAS, FL

primary means of operation. This is not to say that these pilots do not make good formation pilots; but rather they have relatively little formation flying experience outside the basic principles they were taught during flight training and their more recent T-34 instructor under training (IUT) syllabus. Without vast experience in formation flying they rely heavily on "textbook" procedures and visual cues. The instructors may not be able to provide detailed information about potential changes in airplane aerodynamic characteristics caused by flying in proximity.

The latest revision of the T-34C Flight Training Instruction has a new subsection addressing formation flight with dissimilar aircraft, specifically during landing gear inspections. This inclusion is attributed to the F-14 and T-34 mid-air collision and is evidence of the need for increased awareness of formation flying hazards. Adverse aerodynamic conditions that cause upward pitching moments and trim changes to maintain control of the aircraft are discussed. The instruction now stipulates [Ref. 3]:

...If the wing man does not anticipate this trim change, it could cause a significant controllability problem which could result in airborne collision. The magnitude of this flow interference is related to the configuration, speed, weight and distance between the two aircraft.

The actual aerodynamic flow between a T-34C and a dissimilar aircraft will not normally be known. Because of the inherent danger involved when inspecting landing gear of dissimilar aircraft, the inspection pilot should be aware of the possible adverse flight conditions and avoid them.

Advanced flight training for tactical aviators is taught in the Navy's T-2, A-4 and T-45 aircraft. Formation training again places instructional emphasis on area and formation procedures and visual cues, with little formal instruction on mutual interference of flow patterns. Primary positions such as parade and line are discussed with video highlights. Hand signals, radio communications and maneuvers are also presented with video support. The new T-45 training program provides flight simulators to aid in formation flying instruction.

Simulators expose the student pilot to section take-off, TACAN rendezvous, breakup and rendezvous, turns, cross-under and acrobatic formation maneuvers. Formation flight instruction in the T-45 primarily emphasizes procedures and visual cues, but pilots are also exposed to changes in aircraft stability as T-45's get closer together. A T-45 flight instructor from VT-21 in Kingsville, Texas, indicated that formation pilots, lead and wing man, can feel the presence of each other's airplane through changes in trim conditions as they get closer.² Instructor pilots warn the students of the danger in flying too close and demonstrate how to maneuver back to the ideal position, but the aerodynamic cause and effect do not seem to be addressed at this level. Formation flying is limited to groups of similar aircraft as the students prepare for carrier qualifications and fleet aircraft selection.

Formation flying becomes routine in most fleet tactical squadrons as airplanes sortie together for low-level navigation, strikes, combat air patrol, in-flight refueling and escort operations. Procedures and visual cues remain primary instructional tools, but complexities and variations arise due to the diversity of carrier aircraft. Without a basic understanding of potential aerodynamic interferences between airplanes flying in formation, the inexperienced fleet aviator may have few resources to call upon when joining on a different type aircraft, especially for the first time.

The truth is that most formation flying instruction appears to be passed down from aviator to aviator. Procedural standards and techniques are presented to the students and fleet aviators for their type aircraft, but there is very little textbook information to supplement the mechanics of formation flying. Even the Blue

² Phone Conversation, 28 July 1993 between author and Lt. Renner USN, VT-21, Kingsville NAS, TX

Angels aerial demonstration team relies on basic techniques that are passed from one formation pilot to the next. A diamond formation pilot for the Blue Angels could not pinpoint any known literature used by the team to teach potential interference effects between airplanes in the formation.³

Aerodynamics For Naval Aviators, by H. H. Hurt, is the only Navy textbook found by the author that addresses disturbances in flow patterns caused by formation flying. Besides describing the phenomenon, Hurt points out [Ref. 4:p. 385]:

A common collision problem is the case of an airplane with a malfunctioning landing gear. If another airplane is called to inspect the malfunctioning landing gear, great care must be taken to maintain adequate separation and preserve orientation. Many instances such as this have resulted in a collision when the pilot of the trailing airplane became disoriented and did not maintain adequate separation.

In-flight refueling and supersonic flight issues pertaining to formation flying are also addressed, though recommended procedures are lacking.

To maintain proficiency, combat readiness and safety, Naval aviators receive continuous training in the cockpit, simulator and classroom. To this end, a more thorough understanding of formation flying aerodynamics provided by this study can enhance pilot awareness and safety.

B. PREVIOUS FORMATION FLYING STUDIES

Many studies have been conducted involving formation flying. Topics include formation flight trainer evaluations, formation station keeping concepts, wakes at large distances (up to 250 chords) from wings, airplane formation flying qualities, and potential benefits of flying aircraft in formation on extended range

³ Phone Conversation, 21 July 1993 between author and LCdr. Packer USN, Blue Angels Flight Demonstration Team, Pensacola NAS, FL

missions. Human factor and physiology issues have also been addressed. There seems to be very little information available, however, concerning the issue of aerodynamic interference between airplanes flying in formation. [Refs. 5-8]

Vortex lattice calculations have been used to study the benefits of formation flying. Maskew [Ref. 8] applied a quadrilateral vortex-lattice method to a formation of three wings. Force and moment data were used in estimating potential benefits to flying aircraft in formation on extended range missions. Only echelon and double row formations were presented, but Maskew did point out that trimming in roll was required for the echelon formation.

C. COMPUTER CODES

Computational fluid dynamics have become an integral part of aircraft design and analysis. Most recently, powerful computer systems and codes provide solutions to Navier-Stokes and Euler equations for simple three-dimensional wing-body configurations. Potential flow panel codes have been developed for the past 25 years to aid in the design and analysis of arbitrary three-dimensional wing-bodies. Today's engineer has the option to choose from an abundance of computational programs based on project scope, available computer resources and problem complexity.

The potential-flow panel code PMARC (Panel Method Ames Research Center) was used for this study. PMARC was designed to numerically predict flow fields around complex three-dimensional bodies. Adjustable size arrays permit tailoring of the code for the size problem being solved and the available computer hardware. The decision to use PMARC was also based on past success using the code at the Naval Postgraduate School to conduct aerodynamic studies

of the Pioneer unmanned air vehicle and the Service Aircraft Instrumentation Package (SAIP) [Refs. 9 and 10].

PMARC data are displayed by GVS 3.1 (General Visualization System) software. Designed specifically for PMARC, the program is ideal for visual representations of aerodynamic data on complex geometries.

1. PMARC Background

a. PMARC Description

PMARC is a low-order, potential flow panel code that is patterned after Analytical Methods Inc. VSAERO (Vortex Separation Aerodynamics Program). Surface geometries are broken up into panels with constant strength source and doublet distributions over each panel. These singularities distributed with constant strength over each panel qualify PMARC as a low-order panel method. Higher-order methods allow the singularity strengths to vary linearly or quadratically over each panel. Better accuracy is obtained by the higher-order methods at the expense of code complexity and computation time [Ref. 11: p. 2]. Experience and research have shown, however, that low-order panel methods can provide nearly identical results as higher-order methods over a wide range of cases. PMARC's potential flow model theory can be found in Ref. 11.

PMARC version 11 is written in FORTRAN 77. Adjustable size arrays within the code permit simple to very complex geometries, wakes, off-body velocity scans and streamlines. Basic input data include body geometry and coordinate systems, free-stream conditions, angular position and rates, symmetry parameters and requests for off-body velocity scans and streamlines. Outputs consist of geometries, wakes, aerodynamic parameters, off-body velocities and off-body streamline data. Aerodynamic data provide doublet strength, velocity

components, pressure coefficient, and local Mach number for each panel. Forces and moments for panel sections, components and entire geometries are summed and put in coefficient form. Force and moment coefficients are then expressed for wind, stability and body axes.

b. Operating Systems

PMARC is designed to run on computers ranging from personal computers (Macintosh II based) to the powerful Cray Y-MP. Disk space and memory requirements for operating the code are dependent on the size of the operator-selected arrays. This research used approximately 2,350 geometry panels. According to Ref. 11, the scratch disk space required to run PMARC is approximately 67 Mb for this application. Memory requirements for storing the executing instructions and output data are difficult to predict and are significantly effected by dimensioning the code.

The Naval Postgraduate School's Cray Y-MP EL 8/2048 was used to operate PMARC for this study. There was ample storage on the Cray with 2 Gigabytes of main memory and several 50-Gigabyte local disks. Eight vector processors provided a peak operation of 133-MFLOP (Million Floating point Operations) per processor [Ref. 12].

c. Coordinate Systems

Aircraft geometries are described in a body-fixed coordinate system. PMARC assumes that the body-fixed coordinate system is coincident with the origin of an inertial reference frame. Assembly and component coordinate systems are also provided for complex geometries and configurations. Separate component and assembly coordinate systems were used in this analysis to differentiate between the F-14 and T-34, for example.

Constant velocity vectors and constant angular rotation rates about the three coordinate axes are used to describe geometry motion. Normalized velocities with zero angular rotation rates were used throughout this analysis. The geometry incrementally moved through the prescribed motion in a series of time steps. Solutions were computed at each incremental time step that included updated surface source strengths. Instantaneous free-stream velocity vectors in the body-fixed reference frame were subsequently computed from the surface source strengths.

d. Geometry Modeling

PMARC geometries are modeled by a set of panels. Complex geometries such as aircraft, are subdivided into several pieces and modeled with sets of panels called patches. Patches are formed from two or more sections. A section is a set of points defining a cross-sectional area of the modeled object. Patches are usually four sided but fewer sides can exist for complex or intricate shapes. Wings, for example, are made by folding a patch over onto itself to form a common edge. [Ref. 11:p. 14]

Low-order panel methods do not demand exact matching between panels as higher-order methods do. This difference becomes important when trying to model from three-view drawings with little detail. Small gaps and panel mismatches that may arise due to modeling inaccuracies or ambiguities can be tolerated in PMARC without severe penalties in data accuracy.

The T-34 geometry sections were defined using the three-view drawing in Appendix A, Figure A1. Airfoil data were obtained from Ref. 13. The tailless F-14 model, Appendix A, Figure A2, was used by Naval Air Warfare Center, Weapon Division (NAWC WD), China Lake, to conduct stores separation

analysis. Horizontal and vertical tails were added with small gaps between them and the fuselage to simplify the model and minimize deformities. F-14 tail airfoil data were obtained from Ref. 14. Half-plane models were used with the assumption that the airflow and geometry are symmetric around the XZ plane. PMARC automatically adds the influence of the mirror image when calculating the total force and moment coefficients.

e. Wake Modeling

Wakes are shed from user-specified separation lines on the surface geometry. PMARC has provisions for three wake options. A time-stepping wake model is developed that moves downstream with the local velocity field. This option requires significant processing, particularly with complex and high-density panel geometries. Alternatively, the user can specify an initial wake that allows analysis of the steady-state problem without going through several time steps to reach a steady-state condition. A no-wakes option is also available, but its use for this study's application was limited to geometry-only plotting.

Initial wakes were specified for the majority of data runs in this analysis. The decision to use initial-wake specifications vice time-stepping wakes was based on discussions with PMARC's principal programmer, Dale Ashby. Numerical results between the two wake options are generally within five to seven percent of each other as long as the wake is reasonably approximated. Part of the wake should separate at or near the wing trailing edge, for example. Verification data are presented in Chapter III.

Wake separation lines and initial specifications must be handled with great care because they affect numerical results. User-defined wake sections must all go in the same direction as the separation line [Ref. 11:p. 16]. Defining

the wake separation line becomes an art as the user stitches it along wing and fuselage panel edges. If the separation line changes direction or is incomplete, due to input coding errors, inaccurate and often unrealistic data will result. Specified wakes must also carry downstream approximately 20 chord lengths in order to provide reliable data.⁴

2. GVS BACKGROUND

a. GVS Description

GVS is designed to display PMARC data in a variety of formats. One of two PMARC output files is used by GVS to display geometries, wakes, and on-body and off-body streamlines that are collectively called objects. PMARC phenomena such as component velocities, pressure coefficients, doublet strengths and Mach numbers are qualitatively displayed in color on the various objects. A quantitative association for the data is provided by a histogram that identifies a numerical value for each color displayed, depending upon the observed phenomenon. Displayed objects can be rotated, translated and scaled for ease in data analysis.

b. Operating Systems

GVS is designed to run on Silicon Graphics Incorporated (SGI) Iris™ computer graphics workstations. It is a computationally intensive program that requires a great deal of memory and disk resources. A minimum of 72 Megabytes of disk space is required [Ref. 15]. Main memory requirements are difficult to estimate. GVS was designed on a system with 24 Megabytes of RAM and a 20 MHz processor but has run on Naval Postgraduate School SGI Iris

⁴ Conversations between author and Dale Ashby, NASA Ames Research Center, April - June 1993.

machines running at 16 MHz with 16 Megabytes of RAM. The graphics monitor must provide 24-bit color; otherwise the color display of phenomenon data will be distorted. The program is designed to compile and run using IRIX 3.0.x and IRIX 4.0.x system software.

A SGI 4D/380, model VGX, Iris™ workstation was used for GVS data analysis, display and reproduction. The Naval Postgraduate School's Visualization Lab SGI system operates at 36 MHz and provides 128 Megabytes of RAM and 4 Gigabytes of disk space [Ref. 12:p. 4]. Color graphics were provided by a Shinko color Postscript printer.

III. GROUNDWORK AND PMARC VALIDATION

A. ANALYTIC DERIVATION OF T-34 STABILITY DERIVATIVES

The Navy did not buy stability derivative data when the T-34C was procured.⁵ Several derivatives were required for this analysis, however, in order to determine elevator trim changes and to compare with PMARC output data. Stability and control data were consequently estimated from Smetana [Ref. 16], and from Perkins and Hage [Ref. 17]. Stability derivatives were then compared with typical values for other airplanes. Table I contains aerodynamic parameters and assumptions used in calculating T-34 stability derivatives for the cruise configuration, defined as gear and flaps retracted.

1. T-34 Lift-Curve Slope, $C_{L\alpha}$

Equation (1) [Ref. 16:p. 57] was used to approximate the lift curve slope of the T-34C. The contribution of the fuselage was assumed to be negligible.

$$C_{L\alpha} = C_{L\alpha \text{ wing}} + C_{L\alpha \text{ fuselage}} + C_{L\alpha \text{ tail}} \left(1 - \frac{d\epsilon}{d\alpha} \right) \frac{S_{\text{tail}}}{S_{\text{wing}}} \eta_{\text{tail}} \quad (1)$$

Substitution of data from Table I into equation (1) yielded: $C_{L\alpha} = 0.0894/\text{deg}$.

2. T-34 Change in Pitching Moment with Angle of Attack, $C_{m\alpha}$

The change in pitching moment coefficient with angle of attack has significant impact on an airplane's longitudinal stability. It determines the response of the airframe to elevator motions, gusts and other aerodynamic disturbances. $C_{m\alpha}$ is estimated by equation (2) [Ref. 16:pp. 67-69].

⁵ Phone conversation between author and Mr. Buck Buchannon, NAVAIRSYSCOM Detachment PMA(F)-227, T-34C Class Desk, 5 August 1993.

TABLE I T-34 STABILITY AND CONTROL DERIVATIVE DATA

Wing Airfoil Type (1)	NACA 23012
C_{l_α} (2)	0.107/deg.
S_W (1)	179.56 ft ²
Wing Aspect Ratio (1)	6.22
$C_{L_\alpha \text{ wing}}$ (6)	0.0812/deg.
$\epsilon_{1 \text{ wing}}$ (3)	0.99
$d\epsilon/d\alpha$ (4)	0.45
Tail Airfoil Type (1)	NACA 0008.2
$C_{l_\alpha \text{ tail}}$ (5)	0.10965/deg.
S_t (1)	37.15 ft ²
Tail Aspect Ratio (1)	3.99
V_H (1)	0.5628
l_{tail} (1)	14.74 ft
$\epsilon_{1 \text{ tail}}$ (3)	0.97
$C_{L_\alpha \text{ tail}}$ (6)	0.0723/deg.
η_t (7)	1.0

1. Ref. 13

2. Ref. 18

3. Ref. 16

4. Ref. 17

5. $2\pi / 57.3$

6.
$$C_{L_\alpha} = \frac{C_{l_\alpha}}{1 + C_{l_\alpha} \frac{57.3}{\pi \epsilon_1 AR}} \quad [\text{Ref. 16:p. 58}]$$

7. Assumed

$$C_{m\alpha} = a_w \left[(h - h_{ac_{wb}}) - V_H \frac{a_t}{a_w} \left(1 - \frac{d\epsilon}{d\alpha} \right) \right] \quad (2)$$

The aircraft cg was assumed to be at the aerodynamic center. $C_{m\alpha}$ equals -0.0339/deg.

3. T-34 Change in Lift Coefficient with Elevator Deflection, $C_{L\delta}$

The change in lift coefficient due to elevator deflection is approximated by equation (3) [Ref. 16:p. 94].

$$C_{L\delta_e} = 1.05 C_{l\delta_e} \frac{C_{L\alpha_t}}{C_{l\alpha_t}} \frac{S_t}{S_w} \eta_t \quad (3)$$

A positive elevator deflection is defined as trailing-edge down. The derivative represents the change in overall lift from a change in tail camber caused by an elevator deflection. Everything else remains constant; therefore angle of attack and associated lift changes are not considered in this derivative. The derivative is normally positive and small for conventional aircraft. Substitution of data from Table I into (3) yields: $C_{L\delta_e} = 0.00745/\text{deg}$.

4. T-34 Change in Pitching Moment with Elevator Deflection, $C_{m\delta}$

The change in pitching moment coefficient with change in elevator deflection is commonly referred to as "elevator power" or "elevator effectiveness." The sign is usually negative due to the way elevator deflection is defined. Therefore, a positive deflection provides a negative pitching moment, making elevator power negative. A numerical value for elevator power is obtained from equation (4) [Ref. 16:p.101].

$$C_{m\delta_e} = -\frac{l_{tail}}{\bar{c}} C_{L\delta_e} \quad (4)$$

Substituting (3) into (4) yields a $C_{m\delta_e}$ value of -0.02026/deg.

B. T-34 DERIVATIVE COMPARISON WITH SIMILAR AIRPLANES

Stability and control derivatives for three similar aircraft are presented in Table II for comparison to estimated T-34C derivatives. The approximations appear reasonable and fall within Smetana's typical values. Further validation will be made by comparing the derivatives to PMARC results in subsequent sections.

TABLE II STABILITY DERIVATIVES OF VARIOUS AIRPLANES (1)

Derivative	C-172 (2)	Navion (3)	Jet Trainer (4)	T-34C
$C_{L\alpha}$	0.0803	0.0775	0.0960	0.0894
$C_{m\alpha}$	-0.0155	-0.0119	-0.0042	-0.0339
$C_{L\delta_e}$	0.0075	0.0062	0.0066	0.0075
$C_{m\delta_e}$	-0.0223	-0.0161	-0.0154	-0.0203

1. All derivatives are per degree and for a cruise configuration.
2. Ref. 19:p. 592
3. Ref. 20:p. 252
4. Ref. 19:p. 609

C. PMARC AND MODELING VALIDATION

PMARC was evaluated first using a simple wing test case. PMARC data from the test case were compared with data derived from 2-D airfoil theory for validity. Data from computer-generated wake models were then compared with data associated with operator-defined wake models. Geometry models for the T-34 and the F-14 were also validated by comparing PMARC results with analytically-derived stability data or wind tunnel report data. Observations and conclusions from these evaluations constituted the groundwork for the more complex analysis of two airplanes in proximity presented in Chapter IV.

1. NACA 4415 Airfoil Evaluation

a. PMARC Data Versus 2-D Airfoil Data

A NACA 4415 wing with an aspect ratio of 15 was analyzed at various angles of attack. Appendix A, Figure A3 shows the 4415 wing and its initial wake. The wake was defined by the author and extended 20 chord lengths aft of the trailing edge. Figure 1 shows the lift curve slope generated from PMARC data and corresponding information derived from a 2-D NACA 4415 airfoil from Abbott and Doenhoff [Ref. 18:p. 490]. Data from Ref. 18 were corrected for aspect ratio using the equation in Table I, note 6. Figure 2 shows analogous data for pitching moment coefficient versus angle of attack.

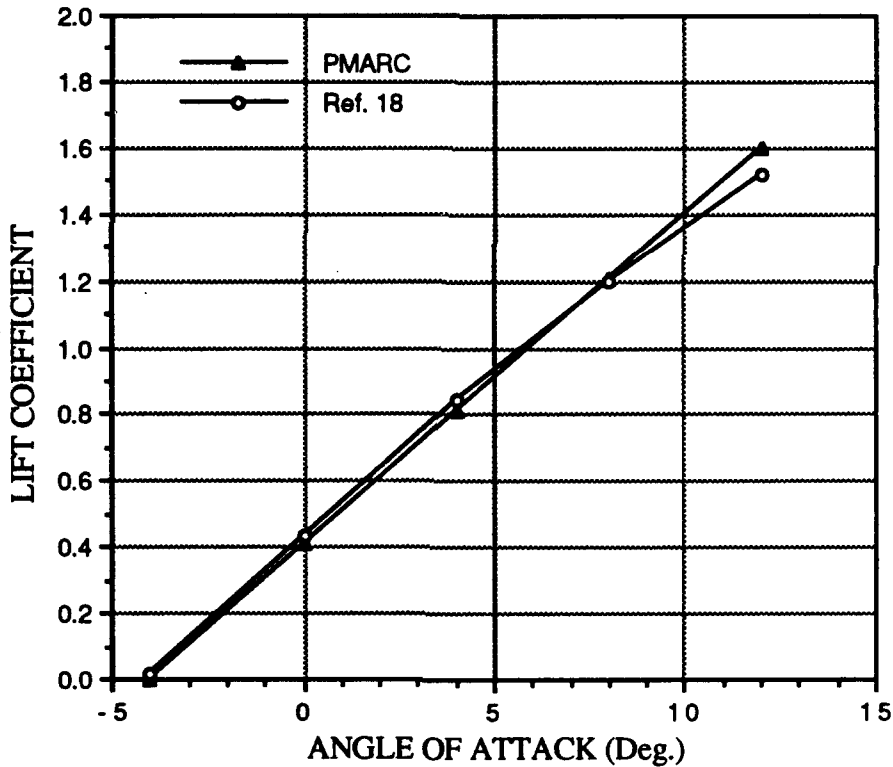


Figure 1. NACA 4415 Wing Lift Curve Slope

Upon inspection, PMARC results for a high-aspect-ratio wing correspond well with corrected 2-D data, especially at lower angles of attack.

Larger differences at higher angles of attack could be associated with the fact that the flow starts to separate, moving the effective aerodynamic center forward. A less negative pitching moment subsequently results. Indications of flow separation and subsequent stall are not predictable by panel codes. Within the scope of this analysis, however, PMARC results sufficiently agree with theoretical data.

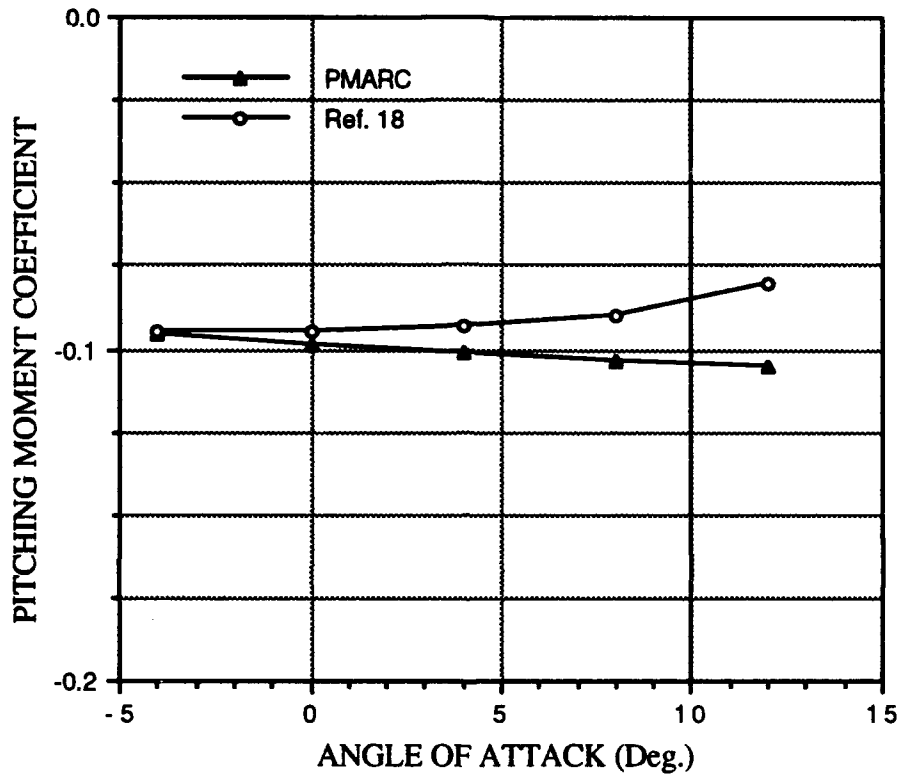


Figure 2. NACA 4415 Wing C_m (cg @ 0.25 mac) versus Angle of Attack

b. Computer-Generated Versus Operator-Defined Wakes

An experiment was made to determine the differences between PMARC results for geometries with user-defined wakes and those with computer-generated wakes. The motivation for this test was a reduction of high CPU times associated with computer-generated wakes without sacrificing data accuracy. Results indicate that data from a well-defined wake model are within two percent of the computer-generated wake model data as shown in Figures 3

and 4. An NACA 4415 wing and its computer-generated wake are found in Appendix A, Figure A4. Table III indicates the CPU times for each run. A three-fold saving in CPU time was made with very little sacrifice in data accuracy.

TABLE III CPU TIMES FOR PMARC WAKE MODELS

Wake Model	CPU Time (sec.)
User-defined	48
Computer-generated	170

It is important to emphasize that the CPU times in Table III are for a very simple geometry with 315 panels. The CPU times for test cases of the F-14 and T-34 together with operator-defined wakes were approximately 25 minutes. In contrast, a PMARC execution of a T-34 geometry with computer-generated wake experienced a CPU time-out after 2.5 hours.

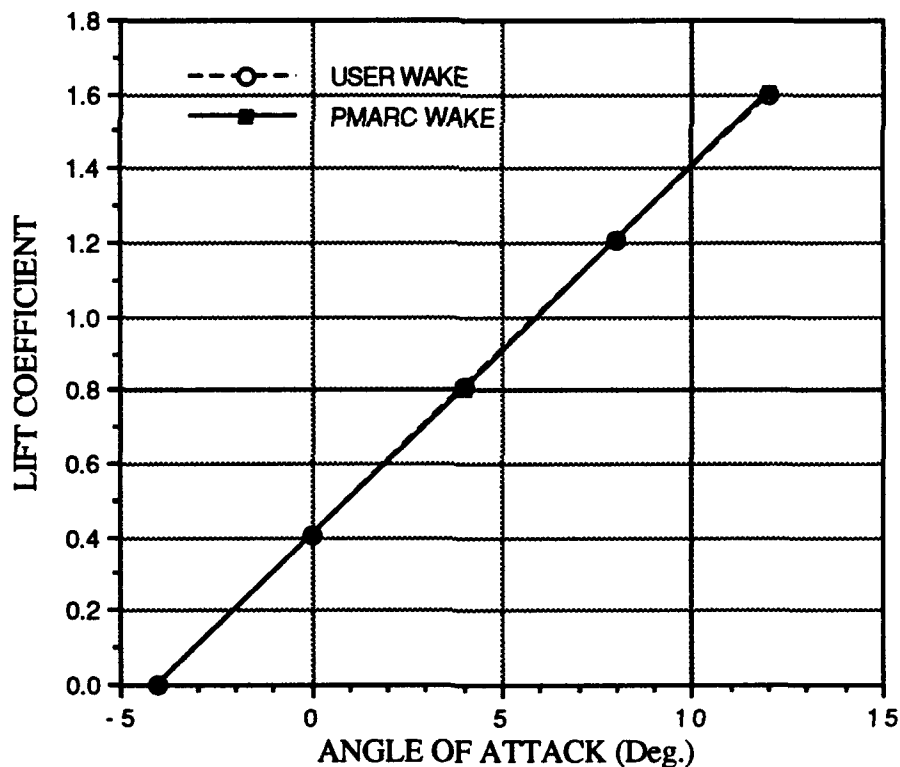


Figure 3. NACA 4415 Wing Lift Curve Slope

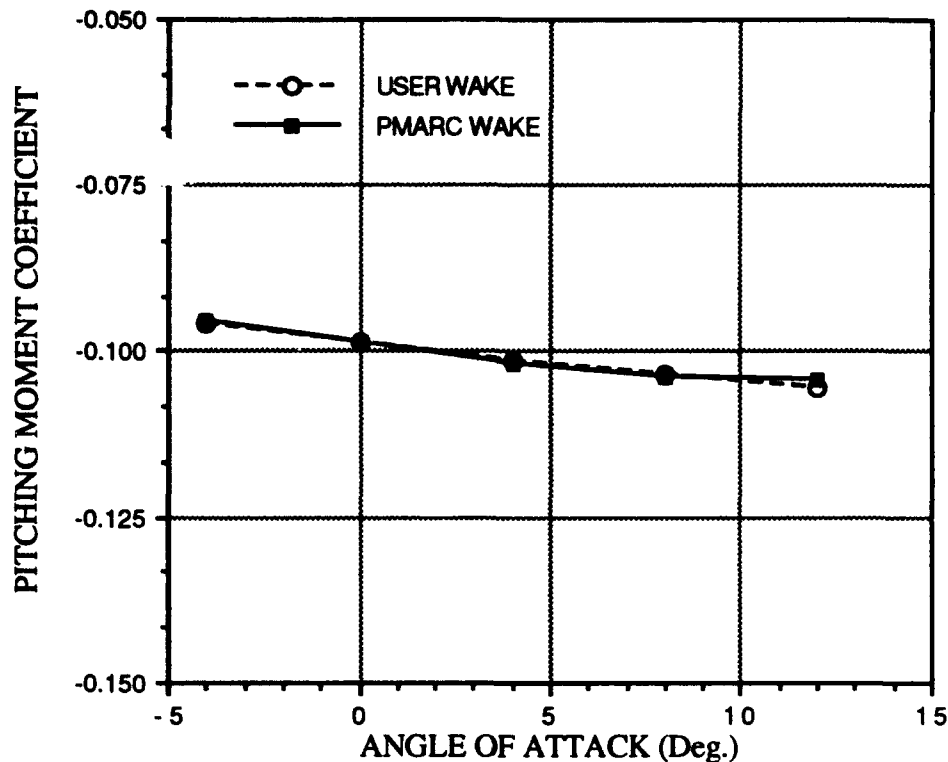


Figure 4. NACA 4415 Wing C_m (cg @ 0.25 mac) versus Angle of Attack

User-defined wakes were implemented for the remainder of the analysis based on the small differences in data sets between the computer-generated and user-defined wake geometries. The savings in CPU time permitted greater diversity of tests and test conditions within research time constraints.

2. T-34 Geometry Evaluation

A T-34 wing and tail were initially modeled to compare PMARC data with analytically-derived stability and control data described earlier. Appendix A, Figure A5 contains a T-34 wing and tail at five degrees angle of attack. Streamlines generated by PMARC are also included. Wakes on all remaining geometries are not shown to avoid clutter. A complete T-34 was then modeled with similar comparisons made. A T-34 model at one degree angle of attack is

shown in Appendix A, Figure A6. Streamlines are moved outboard to observe the flow over the wing and tail vice the fuselage.

PMARC-generated lift and pitching moment coefficients are plotted against angle of attack in Figures 5 and 6 respectively. A cg location at 0.25 of the mean aerodynamic chord (mac) was assumed and used for all PMARC executions.

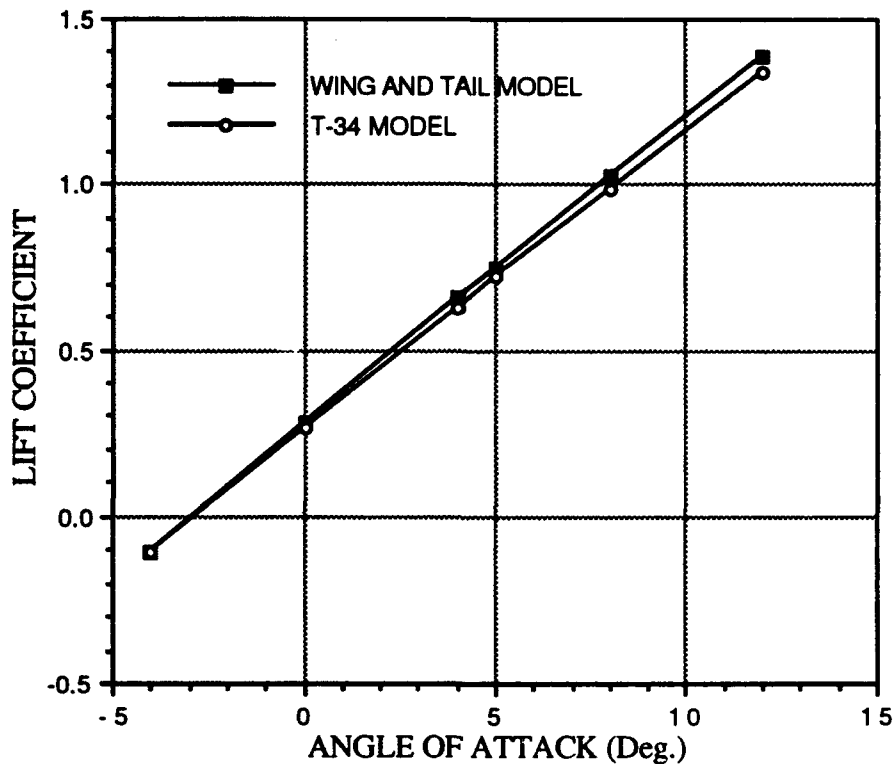


Figure 5. T-34 Geometry Lift Curve Slope

Lift curve slopes for each model were determined from Figure 5 by simple curve fits. The corresponding changes in pitching moment with angle of attack were obtained from curve fits of Figure 6. Stability derivatives are presented in Table IV for comparison with analytical results.

The lift curve slopes of each model are within five percent of analytical data. Pitching moment changes are within 34 percent of estimated data. The

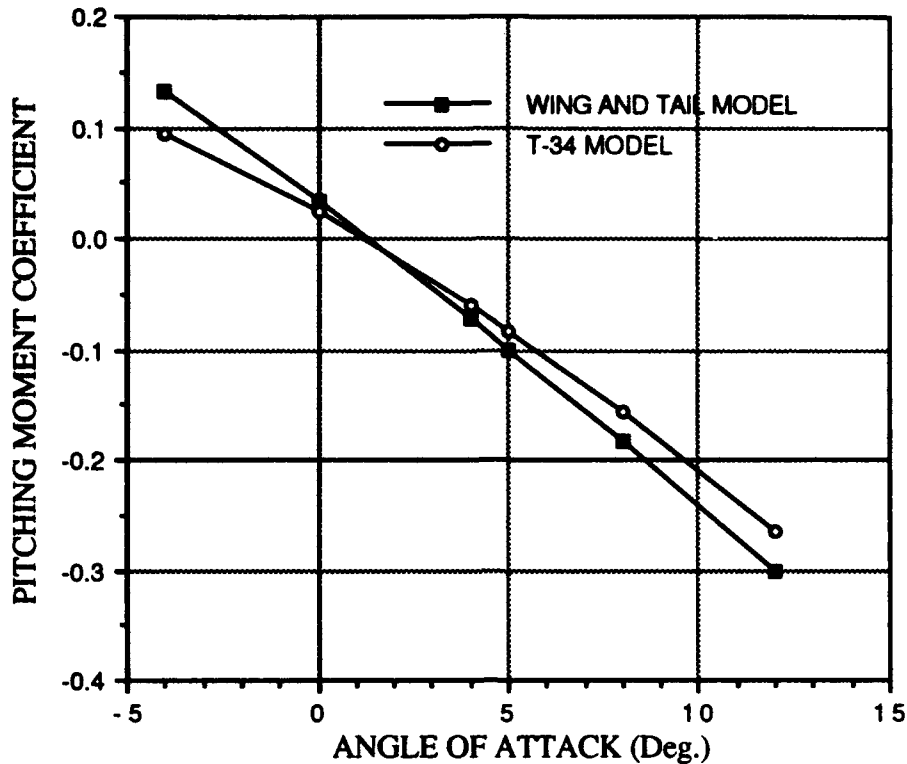


Figure 6. T-34 Geometry C_m (cg @ 0.25 mac) versus Angle of Attack

larger disparity in pitching moment data may be attributed to approximations for the geometric coordinates of the 0.25 mean aerodynamic chord location. PMARC uses these coordinates to compute forces and moments. Discrepancies

TABLE IV T-34 STABILITY DERIVATIVES

Derivative	T-34 Wing and Tail	T-34	Analytic Estimation
$C_{L\alpha}$	0.0933	0.0908	0.0894
$C_{m\alpha}$	-0.0271	-0.0224	-0.0339

between surface areas used in the analytical approximations and those generated from PMARC input geometries may also affect accuracy. Rounded T-34 wing and tail tips were truncated and modeled with little detail in order to keep the geometries as simple as possible.

It is important to emphasize that the analytic derivations used as reference standards for comparison were just estimates. A comparison of data in Tables II and IV shows that PMARC and analytic estimations are fairly close to expected values for the T-34's category of aircraft. The only exception is the estimate for the change in pitching moment with angle of attack. PMARC results appeared more consistent; therefore, the data were considered sufficiently accurate to conduct an investigation in the changes in trim conditions caused by airplanes flying in proximity.

3. F-14 Geometry Validation

A tailless F-14 model was obtained from NAWC WD, China Lake, CA. China Lake engineers used the model, written in VSAERO, to study stores separation characteristics. The code was converted to PMARC and used for this analysis. Thirty degrees of flaps were added to the model before conducting PMARC studies. Figures 7 and 8 show PMARC generated lift and moment coefficients versus angle of attack respectively. Geometry data from Ref. 14 were used to approximate a cg location at 0.25 of the wing's mean aerodynamic chord. The position was estimated by adding 0.25 of the mean geometric chord length to the longitudinal station coordinates of the mean geometric chord's leading edge. This center of gravity location was taken as noted with no verification by further analysis.

The tailless F-14's lift curve slope as a function of angle of attack was then determined by simple curve fit and is presented in Figure 9. Wind tunnel report data from Ref. 14 are included for comparison. The differences between PMARC and wind tunnel report data are attributed to variations in configuration

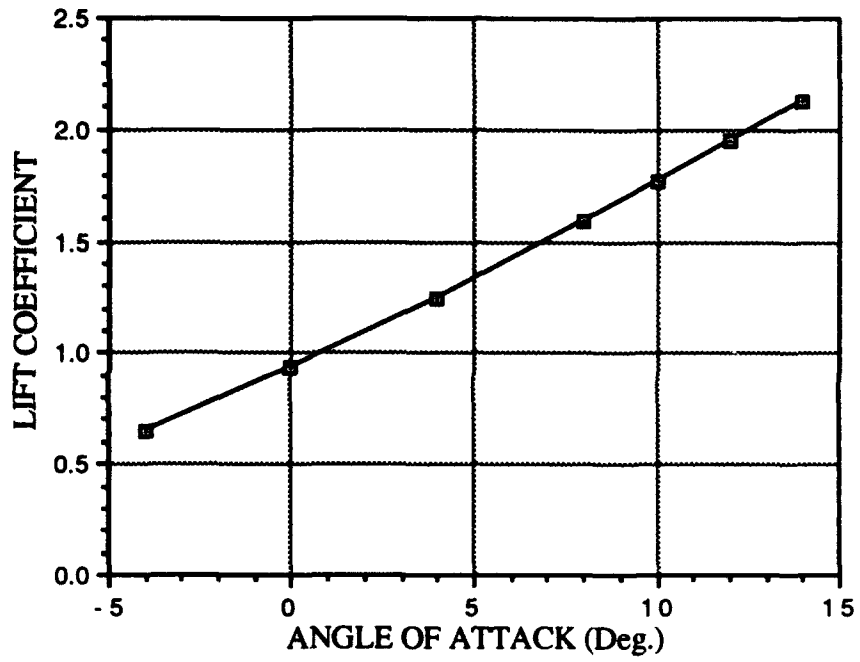


Figure 7. Tailless F-14 Lift Curve Slope

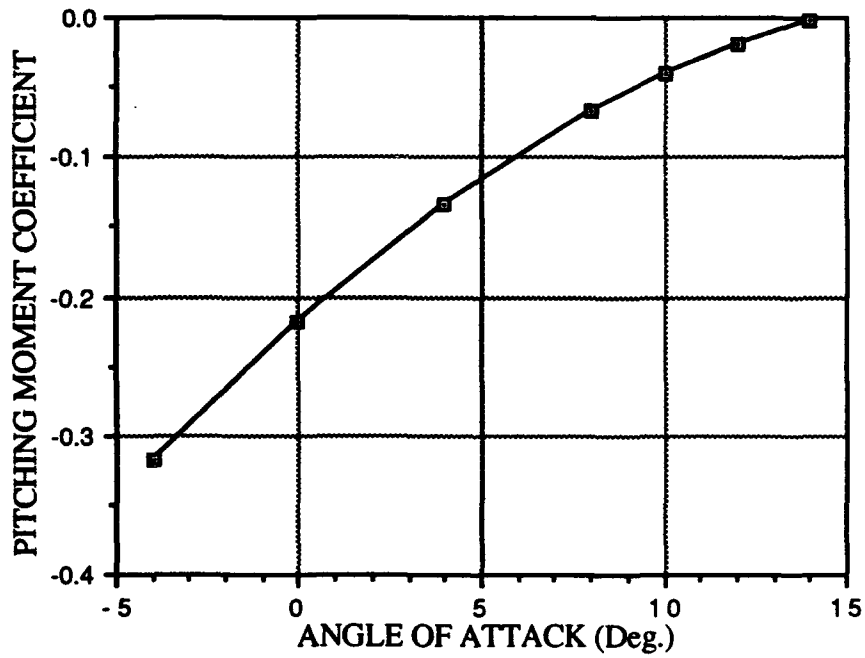


Figure 8. Tailless F-14 C_m (cg @ 0.25 mac) versus Angle of Attack

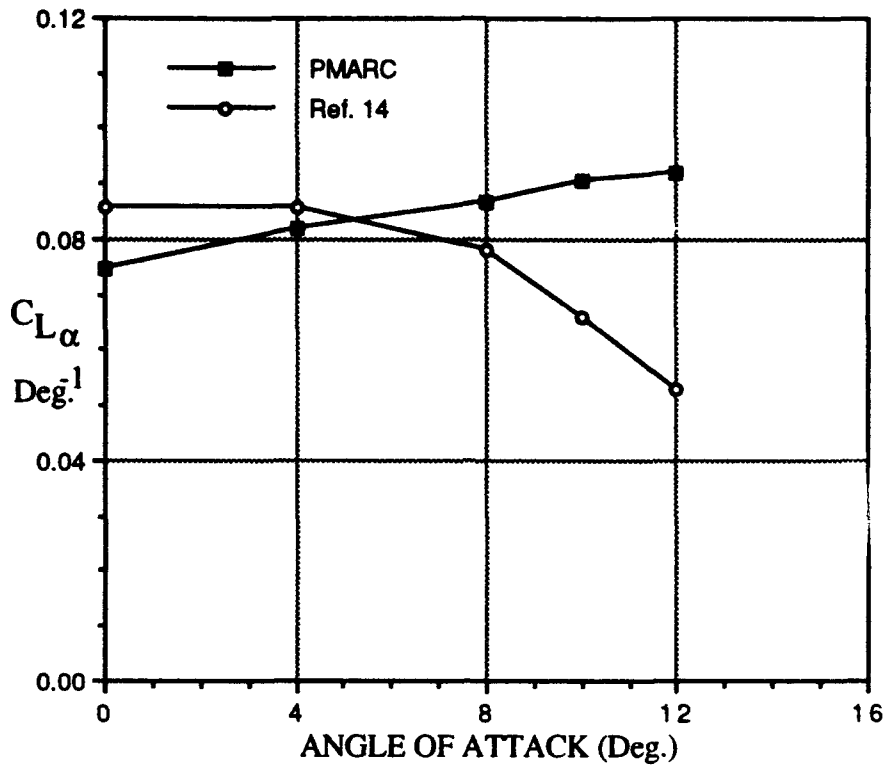


Figure 9. Tailless F-14 $C_{L\alpha}$ versus Angle of Attack

for each test. Table V shows the configurations used for each data set. Flow separation effects at high angles of attack, mentioned earlier for the 4415 wing evaluation, could also account for contrasts in data.

TABLE V F-14 TEST CASE CONFIGURATIONS

Test Case	Landing Gear	Flaps	Slats	Speed Brake	Direct Lift Control
PMARC	Up	30°	Retracted	Retracted	Stowed
Ref. 14	Down	35°	Extended	Extended	Stowed

Tails were then modeled based on airfoil information obtained from Ref. 14. The tail patches did not join the original model but were placed as close as possible. Small gaps between patch surfaces remained but did not appear to corrupt output data. This approach simplified the model and provided an

additional benefit of having moveable tail surfaces that were later used to trim the F-14. This modeling technique was not considered unrealistic, because the horizontal tail of the F-14 is an all moveable control surface attached to the airframe by a single pin.

The complete F-14 geometry used for this study is shown in Appendix A, Figure A7. PMARC-generated lift and pitching moment coefficients are plotted against angle of attack in Figures 10 and 11 respectively. A cg location at 0.25 mac was used for all PMARC applications. Computer simulation data from Ref. 21, are included for comparison. The simulation data were corrected to a cg location at 0.25 mac using equation (5) [Ref. 14:p. 1-3].

$$C_m = C_{m_{cg@0.162}} + C_L(h - 0.162) \quad (5)$$

The configurations were the same as those used for the tailless investigation presented in Table V. The horizontal tail used in the PMARC model was aligned with the body axis (zero relative angle of attack). The zero reference line for the F-14 tail angle of attack was not known, so data sets from several tail positions are presented in Figure 11. Differences between the PMARC body axes and the actual F-14 zero reference line could account for the PMARC data in Figure 11 lying between the +5 and 0 symmetric tail position data sets. Configuration differences mentioned in Table V and approximations for 0.25 mean aerodynamic chord location could also affect data.

The F-14 lift curve slope as a function of angle of attack was then determined by simple curve fit and is presented in Figure 12. Wind tunnel report data from Ref. 14 are included for comparison.

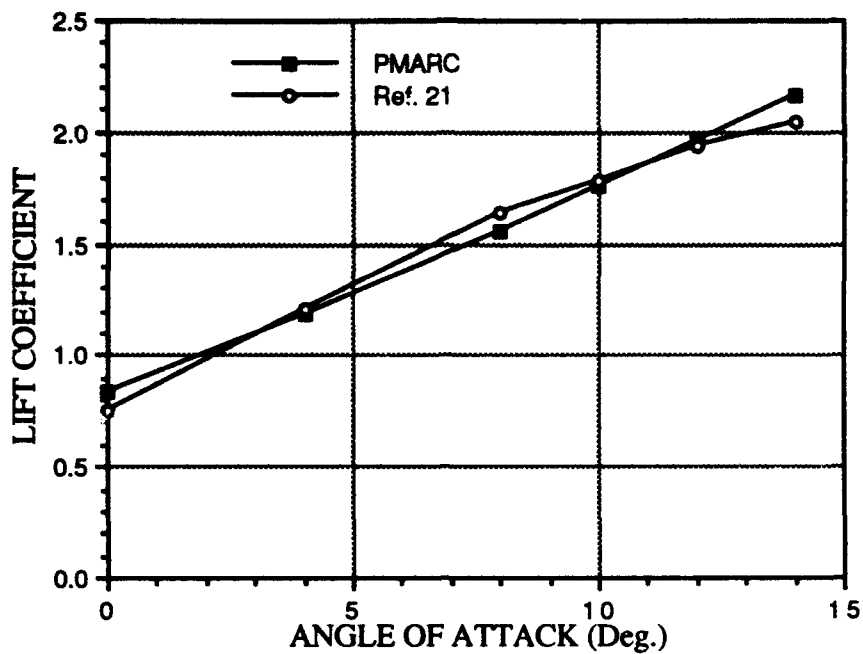


Figure 10. F-14 Lift Curve Slope

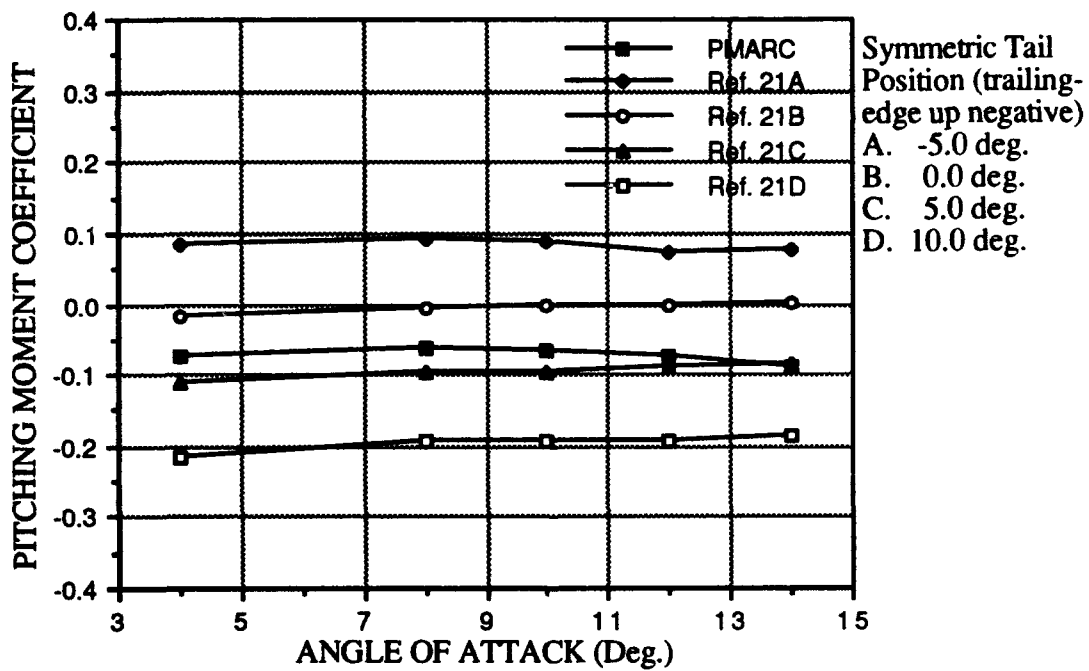


Figure 11. C_m (cg @ 0.25 mac) Versus Angle of Attack

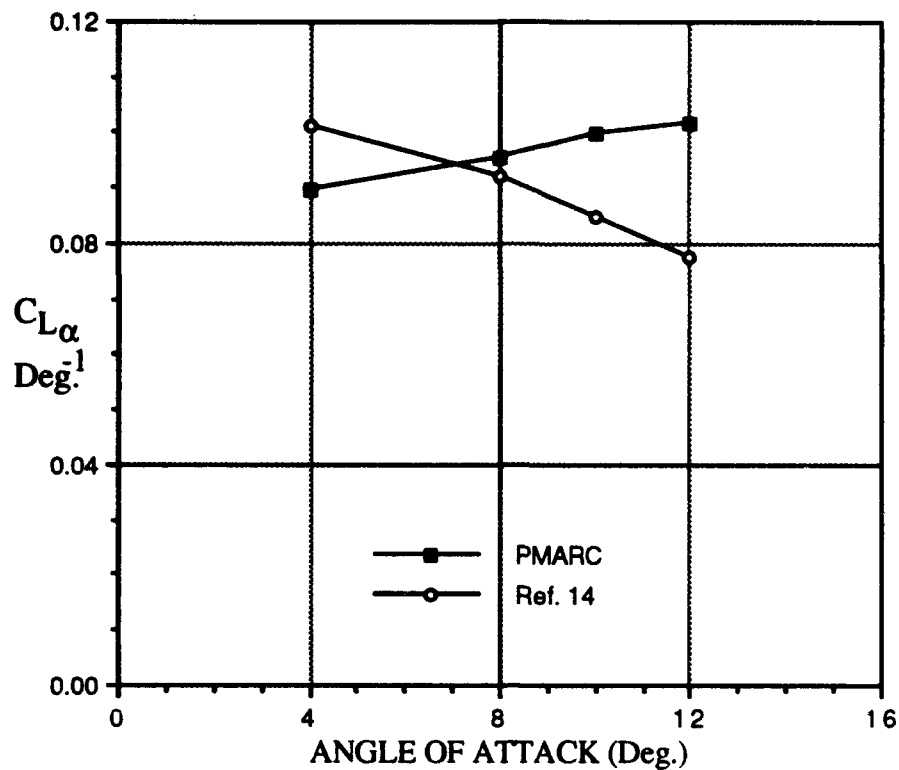


Figure 12. F-14 $C_{L\alpha}$ Versus Angle of Attack

PMARC validation based on the results found in Figures 7 through 12 was not possible due to the configuration variations among the data sets. Data similarities in magnitudes and trends were deemed adequate for this study, however. The F-14 model was considered a good representation for further investigation of dissimilar airplanes flying in proximity.

The F-14 was then "trimmed" at 11 degrees angle of attack for the remainder of this study. This flight condition was based on a gross weight of 57,000 lbs. and an airspeed of 135 kts. Detailed test conditions are presented in Chapter IV. A horizontal elevator position of 4.9 degrees trailing-edge up was used to zero the pitching moment of the F-14 model. This trim setting was facilitated by the fact that the horizontal tail was modeled separately and was free to rotate independently.

IV. ANALYSIS OF AIRPLANES FLYING IN PROXIMITY

Several combinations of PMARC geometries were used to study the aerodynamic disturbances between airplanes in proximity. A T-34 wing and tail geometry was observed first as the configuration approached a much larger wing. Then, the T-34 model was looked at as it flew closer to an F-14. An additional study kept the vertical separation between two airplanes constant and varied their relative longitudinal positions fore and aft. Disturbances created by jet intakes were also briefly examined. Streamlines, lift coefficients, pitching moments and pressure coefficients were observed at incremental distances between PMARC geometries. Data were provided by PMARC output tables and displayed by GVS. Data reduction included changes in elevator deflection required to maintain longitudinal trim of the smaller geometry as it approached the larger configuration.

Geometry separations for all of the PMARC studies were constrained to the XZ plane of symmetry. This limitation was due to the half-plane models used, so PMARC could automatically add the influence of the mirror image when calculating the total force and moment coefficients. Investigations in other planes would require full geometry models, adding complexity and computational burden to the analysis, and were beyond the scope of the current study.

A. LARGE WING AND T-34 WING AND TAIL IN PROXIMITY

A large untapered wing and a T-34 wing and tail were modeled as shown in Appendix A, Figure A8. The two bodies were aligned in the XZ plane such that the T-34 wing's ac was directly under the larger wing's ac. Distances between the two geometries varied between 170.83 and 8.33 feet. In terms of T-34 wing

spans, the distances varied between approximately 5.0 and 0.25. Test conditions and relative geometry sizes are presented in Table VI. Angles of attack for each geometry remained constant, as indicated in Table VI, throughout the PMARC executions. Variations in lift, moments and elevator trim requirements caused by aerodynamic interference could then be studied as a function of vertical separation only.

TABLE VI PMARC TEST CONDITIONS

Geometry	Airfoil	Span (ft)	Area (ft ²)	MAC (ft)	CG	AOA
Large Wing	4415	54.125	695.0	10.83	0.25 MAC	11 deg
T-34 Wing	23012	33.34	180.0	8.33	0.25 MAC	5 deg
T-34 Tail	0008	12.5	38.45	3.1	----	----

Figure 13 indicates a change in lift of the wing and tail as the vertical separation between modeled geometries decreases. The decrease in lift may be due to a reduction in local angle of attack caused by flow curvature under the larger wing or to increased ambient pressure due to the pressure side of the large wing. Figure 13 shows a 50 percent reduction in lift of the T-34 wing and tail when the model approaches the larger wing to within its own semi-span.

The pitching moment was also affected by changes in vertical separation as shown in Figure 14. At five degrees angle of attack, the T-34 configuration developed a nose-down pitching moment as expected. As the T-34 wing and tail approached the larger wing to within 12.5 feet, PMARC indicated that a nose-up pitching moment had developed. The nose-up pitching moment was approximately equal in magnitude to the nose-down moment obtained beyond the aerodynamic interference of the larger wing as shown in Figure 14.

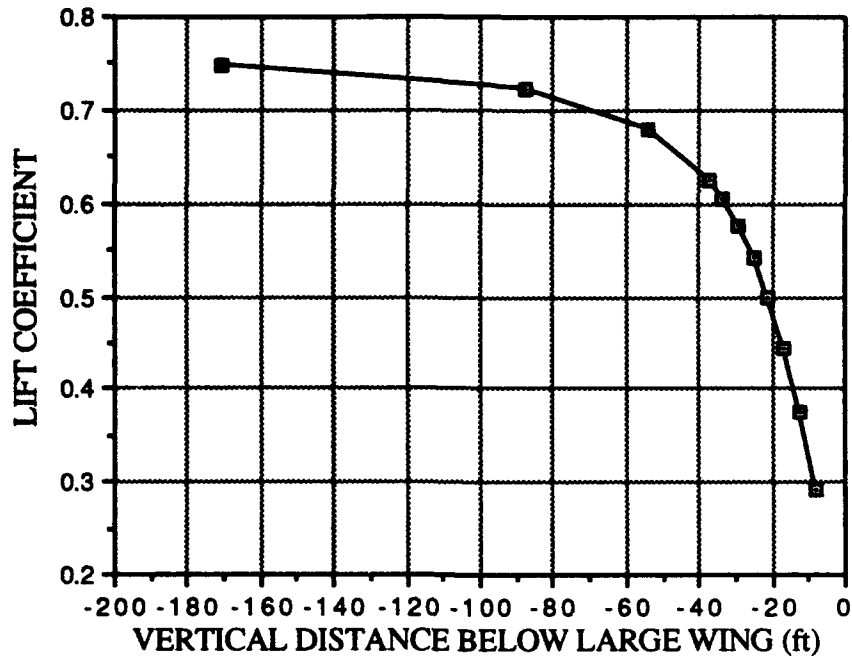


Figure 13. T-34 Wing and Tail Lift Coefficient Versus Vertical Separation

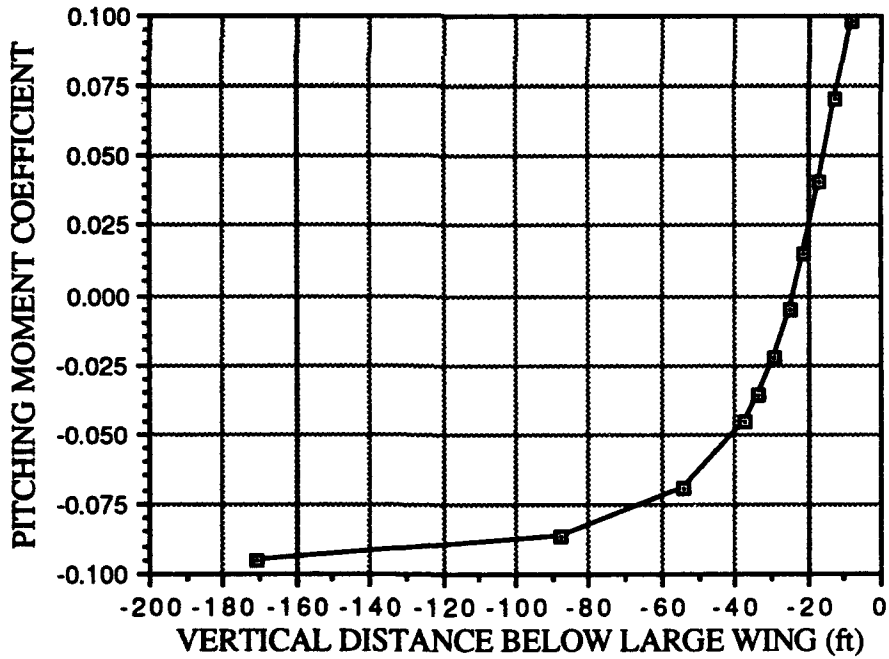


Figure 14. T-34 Wing and Tail C_m (cg @ 0.25 mac) Versus Vertical Separation

A baseline pitching moment coefficient of -0.10 was established for the T-34 wing and tail model at five degrees angle of attack, from Chapter III, Figure 6. The differences between the pitching moment coefficients for each vertical distance and the baseline were used to determine the changes in elevator deflection to maintain trim at five degrees angle of attack. The change in elevator deflection as a function of vertical separation was determined by equation (6).

$$C_{m_{\text{baseline}}} - C_{m_{\text{interference}}} = C_{m_{\delta_e}} \Delta\delta_e \quad (6)$$

Changes in elevator deflection data are presented in Figure 15. A positive change represents more trailing-edge down. PMARC data showed that a change

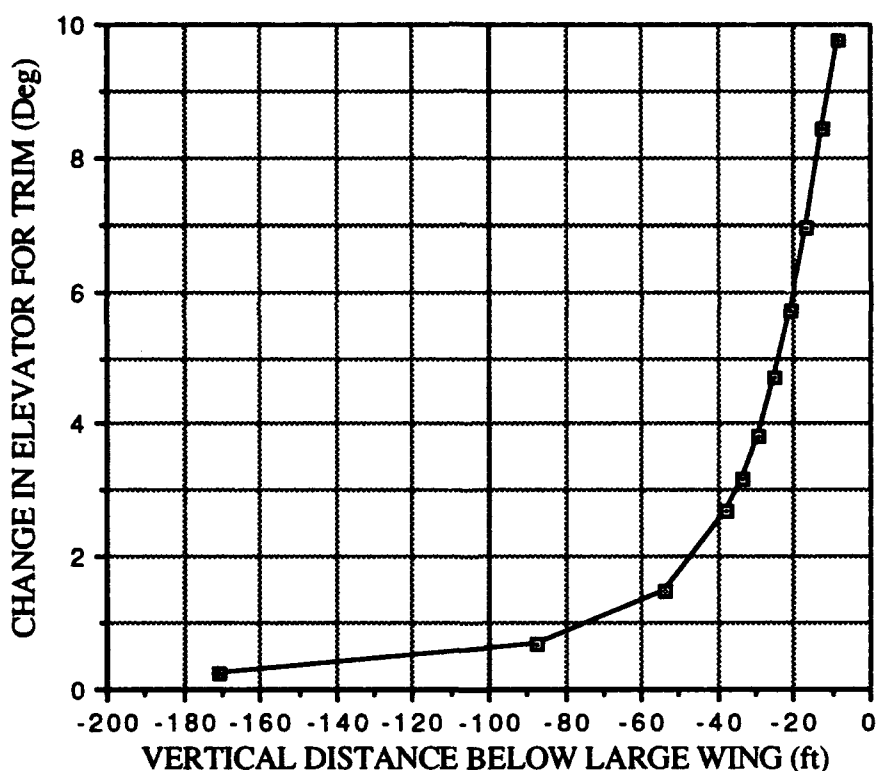


Figure 15. Change in Elevator Deflection Versus Vertical Separation

of 9.5 degrees in elevator deflection, more trailing-edge down, was required for trim as the T-34 wing and tail approached to within 8.33 feet of the large wing.

Streamlines plotted by GVS provided a qualitative analysis of the aerodynamic disturbances between the two configurations. Appendix A, Figure A9 shows just the T-34 wing and tail and associated streamlines. Appendix A, Figure A10 shows the streamlines when the T-34 wing and tail were 12.5 feet below the large wing. As the distance between the two models decreased, the streamlines were deflected slightly downward behind the large wing. This apparent downwash probably contributed to the positive pitching moment of the T-34 wing and tail. The downwash decreased the tail's relative angle of attack, decreasing positive lift and eventually producing lift in the downward direction.

The color display of pressure coefficients on the wing and tail also provided insights into the changes in pitching moment. Appendix A, Figure A11 shows the bottom of the T-34 tail when the wing and tail configuration was beyond any interference effects of other airplanes. The underside of the tail is predominantly yellow at the leading edge and blends to green toward the trailing edge. Free-stream conditions are represented by green. The histogram to the right of the figure indicates these pressures represent a small suction peak at the lower leading edge that tapers off to almost zero pressure coefficient, or free-stream pressure, at the trailing edge. Appendix A, Figure A12 shows the bottom of the tail when it is 8.33 feet from the large wing. A noticeable red band along the lower-surface leading edge has developed. A much stronger suction peak exists; therefore a greater downward force is acting on the tail. This downward force provided the positive pitching moment determined by PMARC and depicted in Figure 14.

B. F-14 AND T-34 IN PROXIMITY

1. Vertical Separation

An F-14 and T-34 were modeled as shown in Appendix A, Figure A13. The PMARC input code for this evaluation is presented in Appendix B. The two bodies were aligned in the XZ plane such that the T-34's cg was directly under the F-14's cg. Distances between the two geometries varied between 170.83 and 12.5 feet. In terms of T-34 wing spans, the distances varied between approximately 5.0 and 0.4. PMARC test conditions were determined from the data in Table VII. Angles of attack for each geometry remained constant, as indicated in Table VII, throughout the PMARC executions.

TABLE VII PMARC TEST CONDITIONS (F-14 AND T-34)

Configuration\A/C	T-34	F-14
Weight (lbs)	3760	57000
Velocity (kts)	135	135
Wing Area (ft ²)	180	565
C _L (1)	0.35	1.70
Angle of Attack	1°	11°
CG	0.25 MAC	0.25 MAC (2)

1. Standard day @ 1000 ft
2. Wing Mean Geometric Chord

Figure 16 shows a decrease in lift of the T-34 as it approaches the F-14. The T-34 loses approximately 55 percent of its lift when it is one wing span away from the larger aircraft and 91 percent of its lift when a semi-span away. Once again, the decrease in lift may be due to a decrease in the local angle of attack of the T-34 wing and the increased pressure felt by the upper wing surface due to its proximity to the pressure side of the F-14 wing. To the pilot, this loss of lift can correspond to a sensation of being pushed away by the F-14.

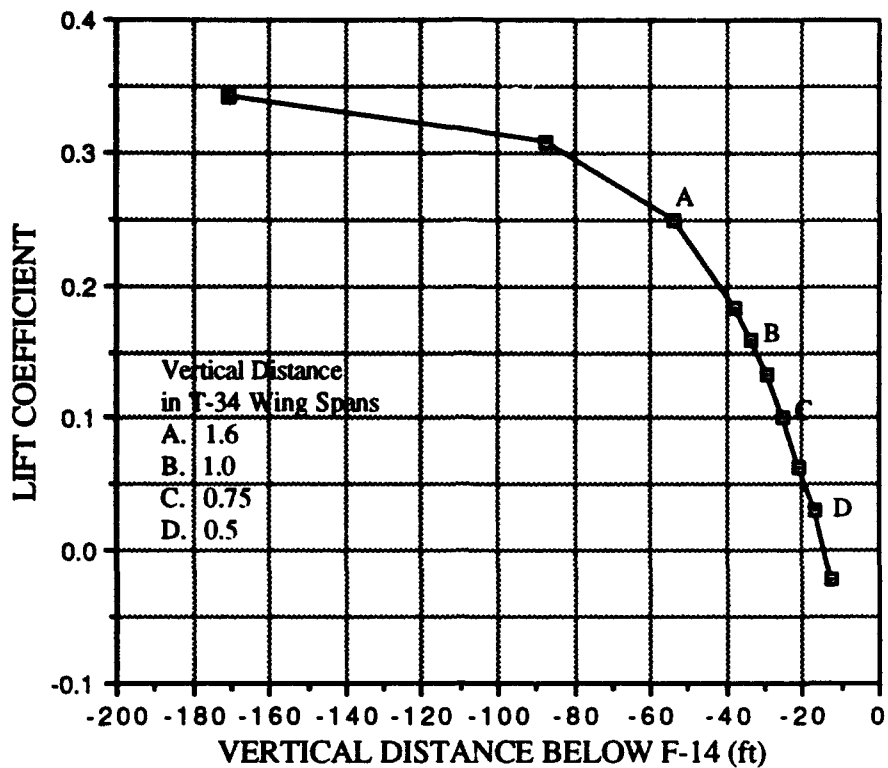


Figure 16. T-34 Lift Coefficient Versus Vertical Separation

The changes in lift on the T-34 are highlighted in Appendix A, Figures A14, A15 and A16. Figure A14 uses color to represent pressure coefficients on the T-34 wing and tail upper surfaces. The histogram to the right of the airplane geometry quantifies the representative colors. There is a large red band on the leading edge of the wing that represents a relatively strong suction peak. The colors transition to yellow, green, then dark blue at the trailing edge. Dark blue represents free-stream conditions for Figures A14, A15, and A16. Figure A15 displays the pressure coefficients on the T-34 when it is 37.5 feet or about a wing span beneath the F-14. The suction peak on the wing has decreased in magnitude and area as indicated by the smaller, narrower band of light red. Yellow has filled in for the red indicating less negative pressure coefficients. The lift coefficient at this flight condition was 0.183, indicating a loss of

approximately 48 percent of the T-34 lift. Figure A16 represents the pressure coefficients on the T-34 when it was 25 feet from the F-14. Traces of red are very faint, while the wing's leading edge is predominately yellow. At 25 feet, the T-34 had lost 71 percent of its lift. The loss in T-34 lift is highlighted best by a comparison of the T-34 wing leading edge in Figures A14 and A16.

The T-34 pitching moment was also affected as the vertical separation between the two airplanes decreased. In the cruise configuration and at one degree angle of attack, the modeled T-34 had a small (0.004), positive pitching moment coefficient. Figure 17 shows that as the T-34 approached the F-14, the

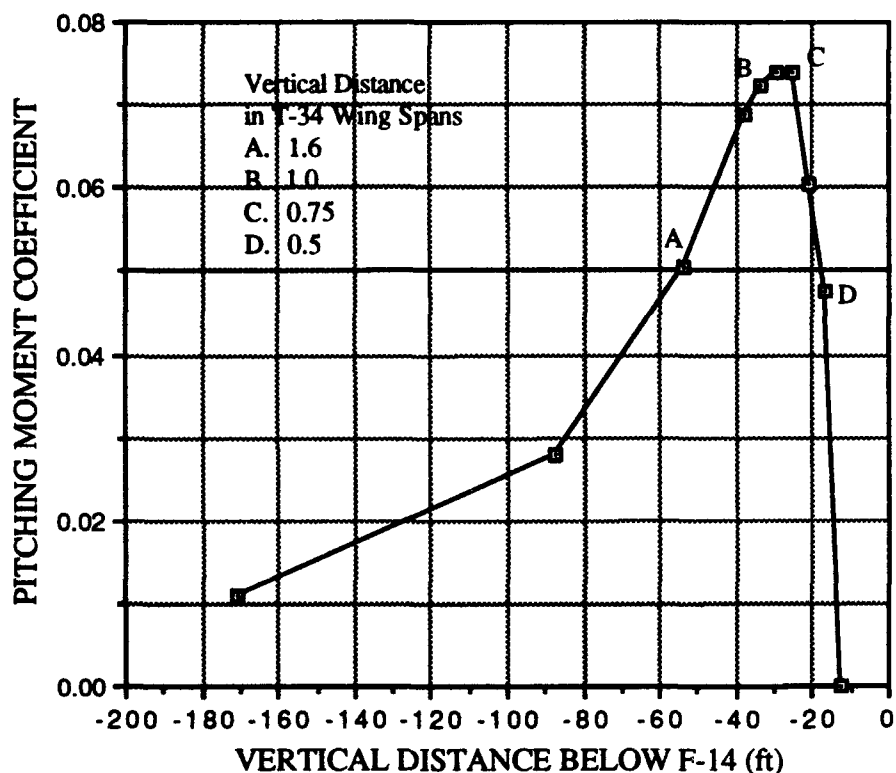


Figure 17. T-34 C_m (cg @ 0.25 mac) Versus Vertical Separation

T-34 pitching moment coefficient increased until the two airplanes were 25 feet, or 0.75 T-34 wing spans, away. The pitching moment coefficient then decreased with decreasing separation distance as shown in Figure 17. To the pilot, the

increases in nose-up pitching moment will increase push-stick forces and will require nose-down trim to zero these forces. Nose-down trim will then have to be decreased if the distance between the two airplanes becomes less than 25 feet.

The decrease in pitching moment coefficient at separation distances of less than 25 feet is probably due to local pressure effects of the F-14 fuselage. The reader should be aware, however, that distances directly below another airplane of less than 20 feet are not considered pertinent to most practical applications of formation flying.

The color display of pressure coefficients on the bottom of the T-34 tail also provided insight into the changes in pitching moment. Appendix A, Figure 17 shows the bottom of the T-34 tail when the airplane was beyond interference effects of other aircraft. The underside of the tail is predominantly yellow at the leading edge and blends to green and then blue toward the trailing edge. The histogram to the right of the figure indicates these pressures represent a small suction peak at the leading edge that tapers off to free-stream conditions at the trailing edge. Free-stream conditions are represented by dark blue in the figure. Figure A17 represents the tail of the T-34 model with a pitching moment coefficient of 0.004. Appendix A, Figure 18 shows the bottom of the tail when the T-34 model is 37.5 feet below the F-14. F-14 panel edges are white while T-34 panel edges are colored. A noticeable red band has developed along the lower leading edge, indicating a much stronger suction peak exists. The tail is generating more lift in the downward direction providing the model with a greater nose-up pitching moment. The suction peak increased further when the airplanes closed to 25 feet as shown in Appendix A, Figure A19. The downward

lift generated by the tail at this vertical distance produced the maximum nose-up pitching moment for the given test conditions as indicated in Figure 17.

A baseline pitching moment coefficient of 0.004 was established for the T-34 model at one degree angle of attack from Chapter III, Figure 6. As before, the differences between the pitching moment coefficients for each vertical distance and the baseline were used to determine the changes in elevator deflection to maintain trim at one degree angle of attack. Changes in elevator deflection for trim are presented in Figure 18. A positive change represents more

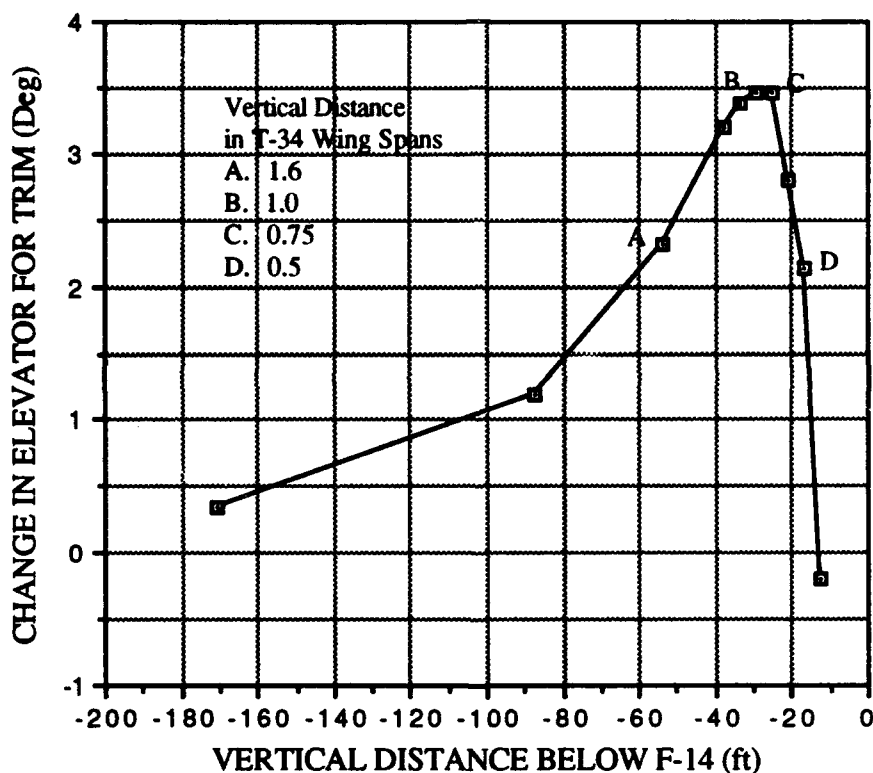


Figure 18. T-34 Change in Elevator Deflection Versus Vertical Separation

trailing-edge down. PMARC results indicated that a change of approximately 3.5 degrees in elevator deflection, more trailing-edge down, was required for trim as the T-34 approached to within 25 feet of the F-14. As the airplanes continued

to close, the nose-down trim changes from the baseline decreased to zero as shown in Figure 18. The T-34 formation pilot will need to change the trim 3.5 degrees (nose-down) for approaches within 25 feet of the F-14. The required nose-down trim will then decrease if the airplanes close further.

Streamlines provided a qualitative analysis of the aerodynamic disturbances between the F-14 and T-34. Appendix A, Figure A20 shows the streamlines around the T-34 when it is 33.33 feet or a wing span beneath the F-14. Appendix A, Figure A21 depicts the streamlines when the two airplanes are 16.67 feet away from each other. Streamlines were spaced 10 inches apart. A comparison of Figures A20 and A21 shows that as the two airplanes approach each other, the streamlines are deflected downward. There are six streamlines above the tail in Figure A20 while there are only five above the tail in Figure A21. The sixth streamline from the top in Figure A21 flows below the horizontal tail. Unfortunately, PMARC did not provide quantitative streamline deflection angles. This apparent downwash depicted by the streamlines decreased the tail's relative angle of attack, thereby contributing to the nose-up pitching moment.

2. Horizontal Separation

An investigation was made to determine the changes in lift and moment coefficients as the T-34 maintained altitude below the F-14 but changed position in the horizontal direction. The intent was to simulate a T-34 approaching the F-14 from behind with a closure rate that was too high for a proper rendezvous. A 25-foot step-down position was chosen because the maximum pitching moment coefficient was found at that separation distance from the previous study. Horizontal distances were chosen along the F-14's longitudinal axis. A positive

horizontal value represented the T-34 cg ahead of the F-14 cg, and a negative value behind.

The lift coefficient increased over a range of 0.3 as the T-34 position changed from 16.67 feet aft of the F-14 cg to a position 25 feet forward of the F-14 cg. Figure 19 shows the change in lift coefficient with horizontal distance from the F-14 cg. It is important to emphasize that the T-34 vertical separation

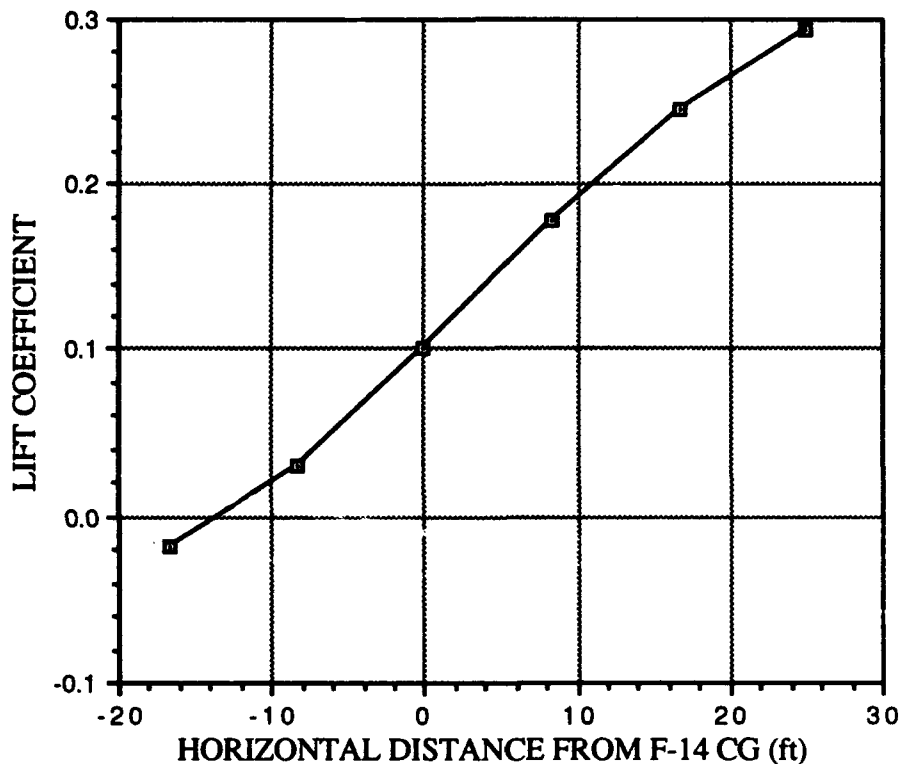


Figure 19. T-34 Lift Coefficient Versus Horizontal Distance from F-14 CG

from the F-14 remained fixed at 25 feet. This change in lift occurs from interference effects caused by the flow over the F-14. The flow is deflected downward as it comes off of the F-14's lifting surfaces. When the T-34 is aft of the F-14 cg, this downwash decreases the local angle of attack on the T-34 lifting surfaces, decreasing its overall lift. As the T-34 moves forward of the F-14 cg, it

eventually experiences the upwash that occurs ahead of the F-14 wing and fuselage. The upwash increases the local angle of attack on the T-34, increasing its lift. Local ambient pressure changes due to the T-34's proximity to the high-pressure side of the F-14 wing complicate the analysis, but nonetheless, the changes in lift of the T-34 as it flies along the longitudinal axis of the F-14 are profound. The T-34 formation pilot should be acutely aware of these potential changes and how they might affect vertical closure rates. Unanticipated closure rates toward the F-14 as the T-34 develops more lift may increase the probability of a collision.

The T-34 pitching moment coefficient also changed with horizontal separation as shown in Figure 20. A maximum nose-up pitching moment coefficient occurred 8.33 feet ahead of the F-14 cg. The pilot experiences a

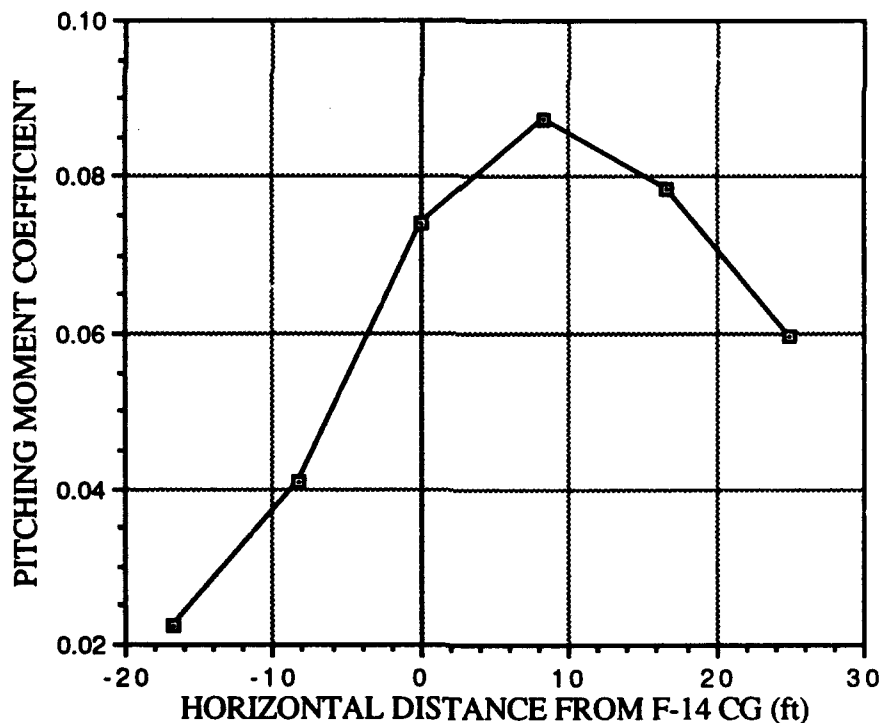


Figure 20. T-34 C_m (cg at 0.25 mac) Versus Horizontal Distance From F-14 CG

nose-up pitching moment throughout the longitudinal movement but the magnitude changes. The corresponding changes in elevator deflection for trim are presented in Figure 21. The data show that continuous elevator changes are required for trim and a maximum change of 4.12 deg. occurs at 8.33 feet forward of the F-14 cg position.

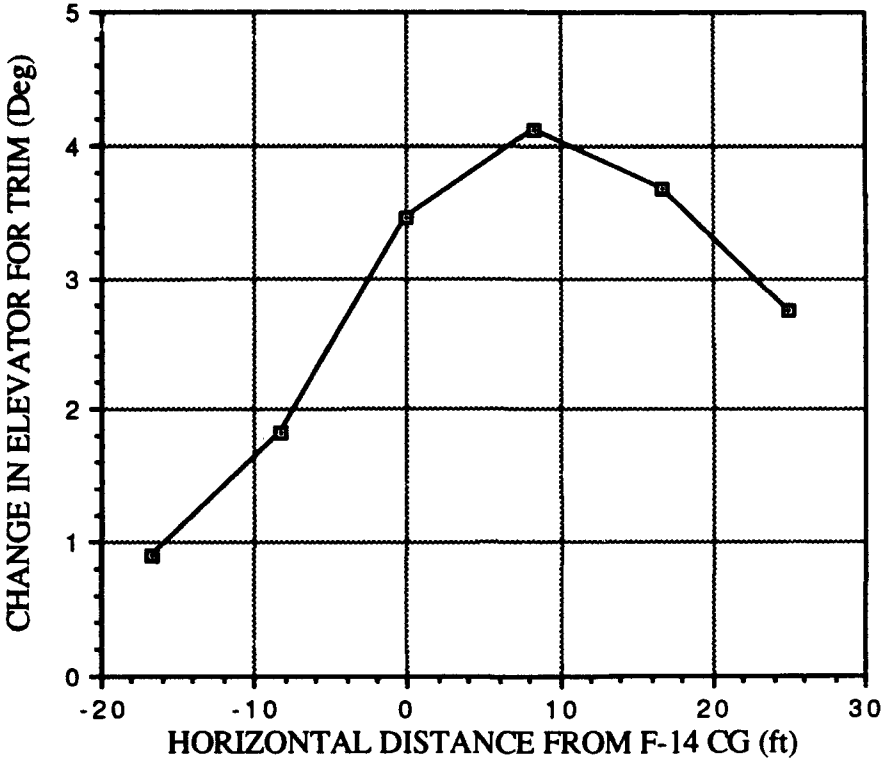


Figure 21. T-34 Change in Elevator Deflection Versus Horizontal Distance From F-14 CG

A follow-up study was conducted with the T-34 cg located 8.33 feet forward of the F-14 cg, where the maximum pitching moment coefficient discovered so far by the study was located. Vertical separation tests were performed to see if the T-34 pitching moment increased further. Lift and moment coefficient data are presented in Figures 22 and 23 respectively. The T-34 lift coefficient shown in Figure 22 does not decrease as appreciably as the lift

coefficient shown in Figure 16. This is probably due to the upwash from the F-14 wing. When the T-34 is 8.33 feet forward of the original test position, it is exposed more to the upwash of the F-14 wing. The direction of flow in the upwash is more uniform; therefore the changes in local angle of attack with vertical separation changes are not as high. Under the F-14 cg, however, the flow experiences more bending and perturbations, consequently having a greater effect on the T-34's angle of attack and subsequent lift.

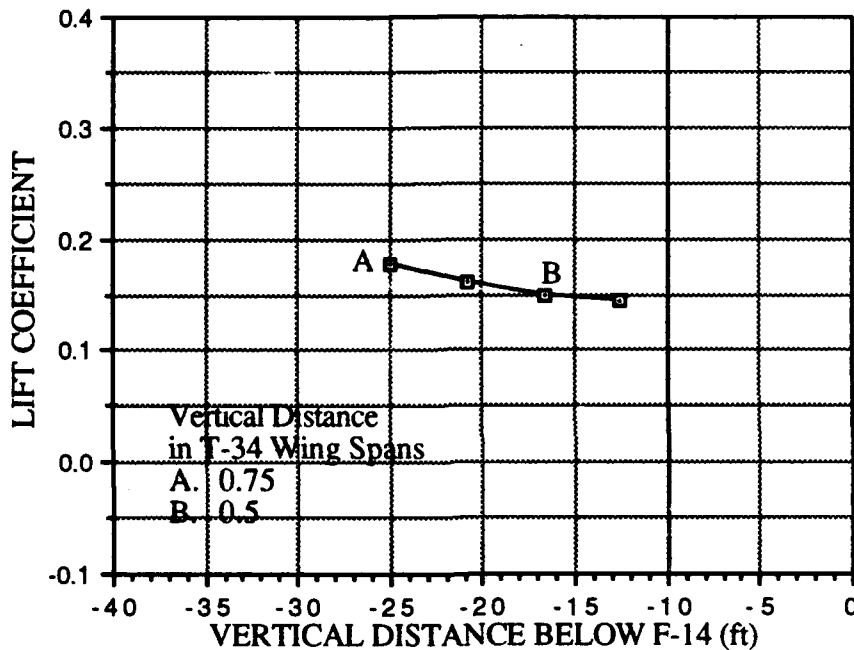


Figure 22. T-34 Lift Coefficient Versus Vertical Separation

A similar trend was noted with the T-34 pitching moment coefficient. The pitching moment did not decrease to zero as it had for the previous study. A new maximum pitching moment coefficient was obtained when the T-34 was 20.83 feet from the F-14 as shown in Figure 23. The change in elevator deflection required for trim was 4.47 degrees. It is important to emphasize that the scope of this study was limited and that a higher pitching moment may exist.

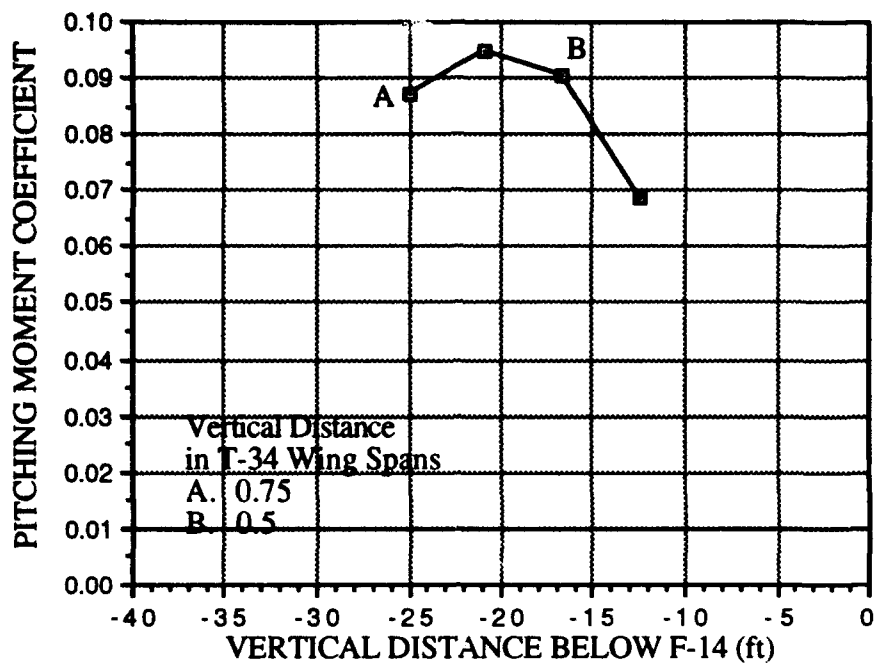


Figure 23. T-34 C_m (cg @ 0.25 mac) Versus Vertical Separation

3. F-14 Jet Intake Effects

PMARC provides a capability to prescribe normal velocities on groups of geometry panels. A brief investigation was conducted to see how the flow into the large F-14 jet intakes affected the lift and pitching moments on the T-34. A vertical separation study was conducted with the T-34 cg 8.33 feet forward of the F-14 cg. The location provided the maximum pitching moment discovered by this study and it placed the T-34 wing underneath the intakes. A flow velocity of Mach 0.3 was assumed at the face of the jet intakes. The changes in lift and pitching moment coefficients with vertical separation are shown in Figures 24 and 25 respectively. Data from Figures 22 and 23 are included to compare the effects with and with out jet intake considerations.

The data show that the flow into the jet intakes does influence the lift and pitching moment of the T-34. The influence is relatively small, however, as lift and pitching moments were increased by less than 5 percent. A new maximum

pitching moment was determined, however, at 20.83 feet below the F-14 with the T-34 cg 8.33 feet forward of the F-14 cg. In the presence of jet intake effects, a pitching moment of 0.0956 was realized on the T-34. The change in elevator deflection required for trim was 4.5 degrees.

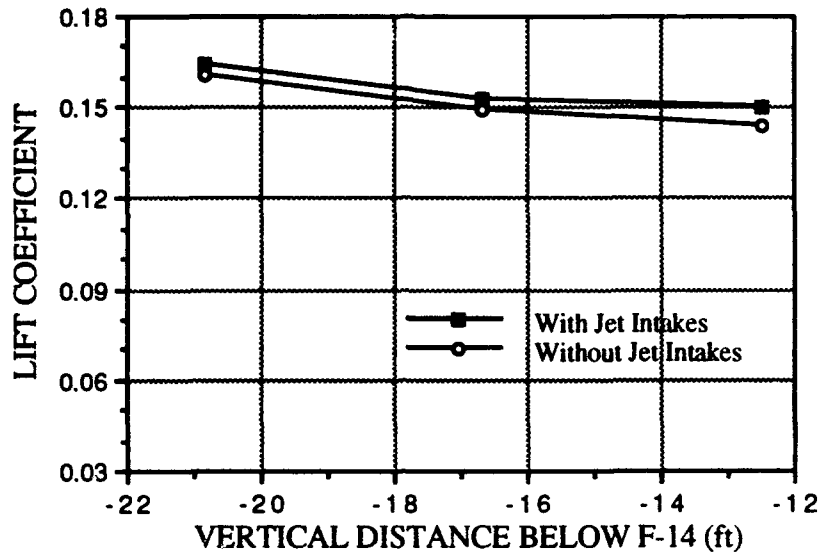


Figure 24. T-34 Lift Coefficient Versus Vertical Separation From Jet Intakes

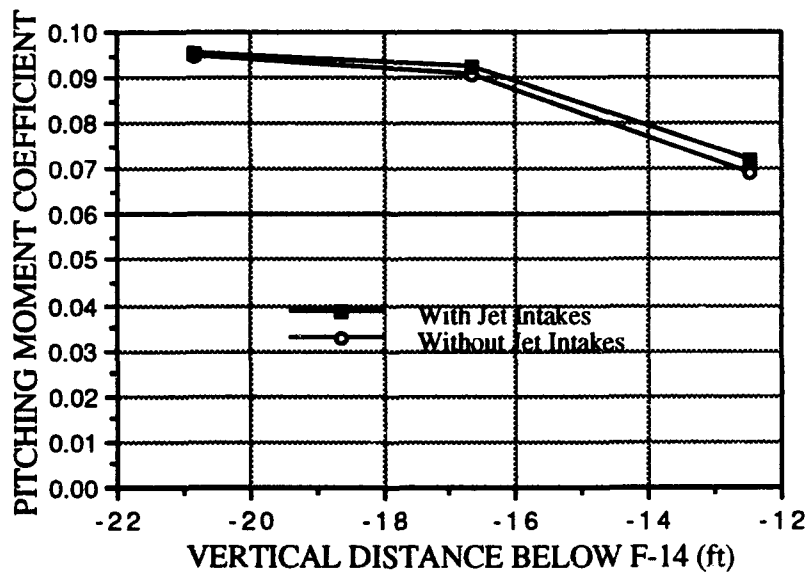


Figure 25. T-34 C_m (cg @ 0.25 mac) Versus Vertical Separation From Jet Intakes

V. CONCLUSIONS AND RECOMMENDATIONS

A. CONCLUSIONS

Airplanes flying in proximity to one another create mutual interference. PMARC studies have shown that this mutual interference affects the flow over each airplane, subsequently altering their aerodynamic characteristics. Significant changes in the lift and pitching moments of an airplane flying in formation underneath another were observed.

A T-34 flying beneath an F-14 will lose half of its lift as it closes to within one wing span. This loss of lift is accompanied by a nose-up pitching moment. The T-34 formation pilot is subsequently presented with confusing cues as he approaches the larger airplane. The loss of lift will correspond to a sensation of being pushed away by the F-14; yet as he gets closer, the T-34 will want to pitch up toward the F-14. This may cause the inexperienced or uninformed pilot to become disoriented. An appreciation of this mutual interference phenomenon combined with anticipated nose-down trim changes should help to avoid the possibility of a collision.

A T-34 will experience large changes in lift as it travels fore and aft underneath an F-14 with approximately one wing span of vertical separation. PMARC showed that as the T-34 moved from a point 25 feet aft of the F-14 cg to a point approximately 18 feet forward of the cg, the lift coefficient increased by 0.3. Combined with variations in nose-up pitching moments, unanticipated and possibly dangerous closure rates toward the F-14 may occur.

This study discovered that 9.5 degrees of elevator trim change were required as a T-34 wing and tail approached a large wing. A maximum of 4.5 degrees was

required for a T-34 as it approached an F-14. There are several issues that account for the relative discrepancy. The test conditions were identical except the AOA of the T-34 wing and tail was arbitrarily chosen at five degrees while the T-34 model AOA was established at one degree. This AOA difference varied the baseline pitching moments used to compute changes in elevator deflection. A case was conducted with the T-34 model at 5 degrees that showed a maximum of 7.5 degrees of elevator trim change was required underneath the F-14. Additionally, the flow disturbances created by the large wing were probably more effective than the F-14 on the T-34 tail. Downwash from the entire span of the large wing could impinge upon the T-34 tail creating a greater nose-up pitching moment. The F-14 fuselage prevented a significant portion of the downwash from interfering with the tail at the given test conditions.

Dissimilar airplanes in formation may experience aerodynamic interference. This phenomenon requires an increased awareness of the pilot to anticipate necessary trim and lift changes. A more thorough understanding of the effect one airplane has on another will increase the safety of formation flying.

B. RECOMMENDATIONS

1. Conduct further studies with complete geometry models. This will enable investigations into the changes in lateral and directional aerodynamic characteristics of formation aircraft. Geometries will not be confined to the XZ plane of symmetry; therefore, typical fleet formations such as parade and inflight refueling can be examined. There may be areas under the F-14 that provide more adverse effects than those revealed in this study.

2. Conduct further studies that include wing loading considerations for each airplane in the formation. This study assumed an F-14 that was "trimmed" in a

modified approach configuration. AOA and loading variations for the F-14 and T-34 were not addressed.

APPENDIX A PMARC/GVS FIGURES

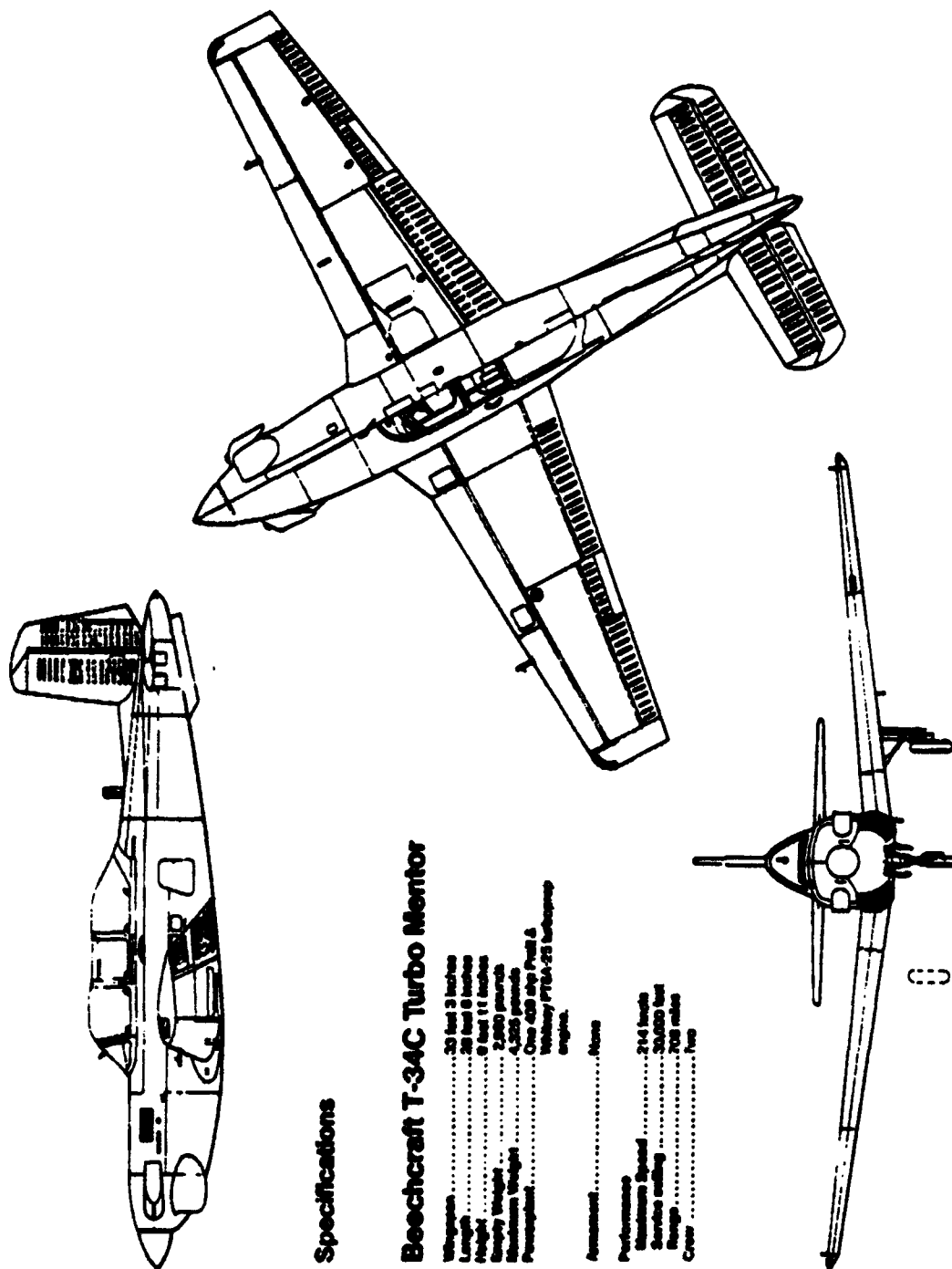


Figure A1 3-View Drawing of T-34

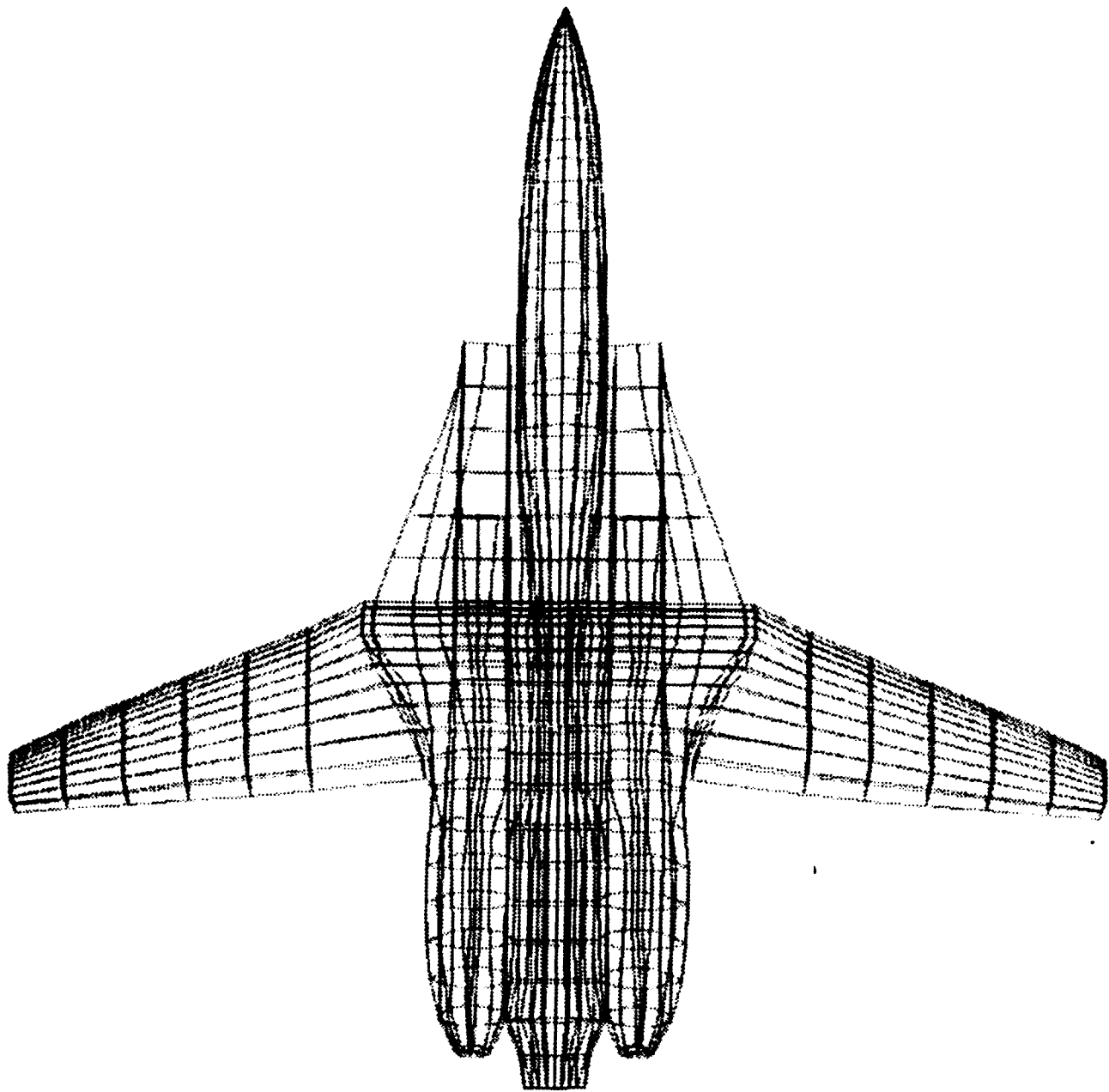


Figure A2 Tailless F-14 (Top View)

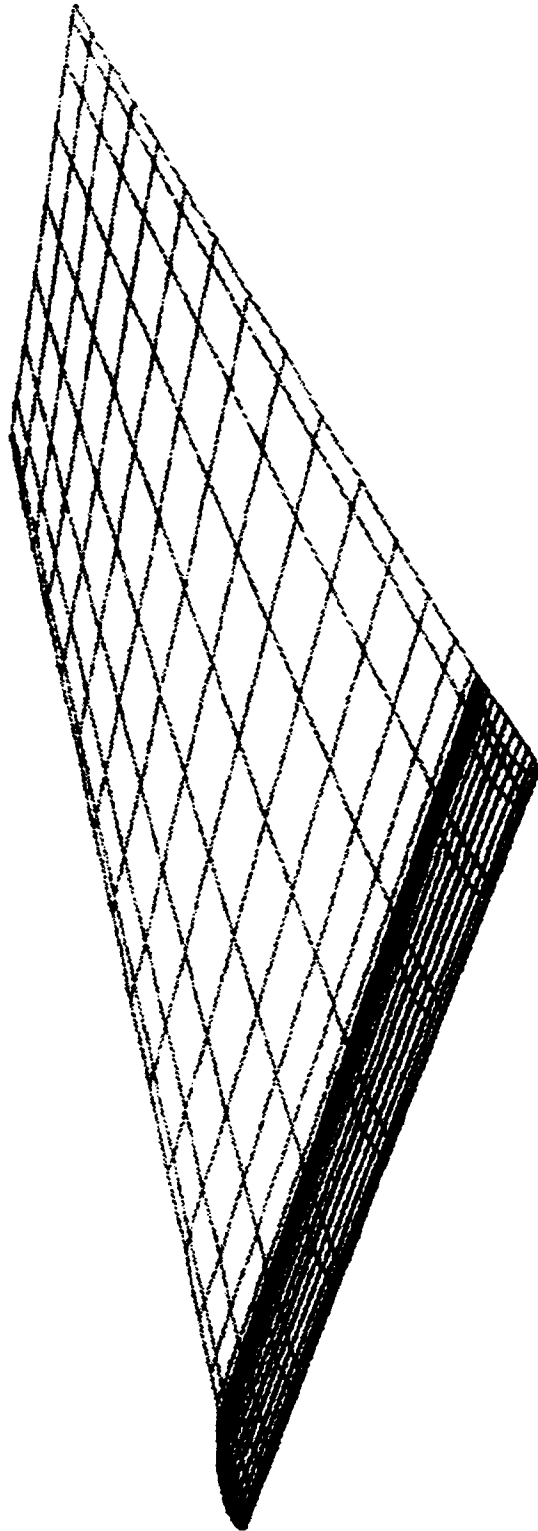


Figure A3 NACA 4415 Wing with Operator Defined Wake

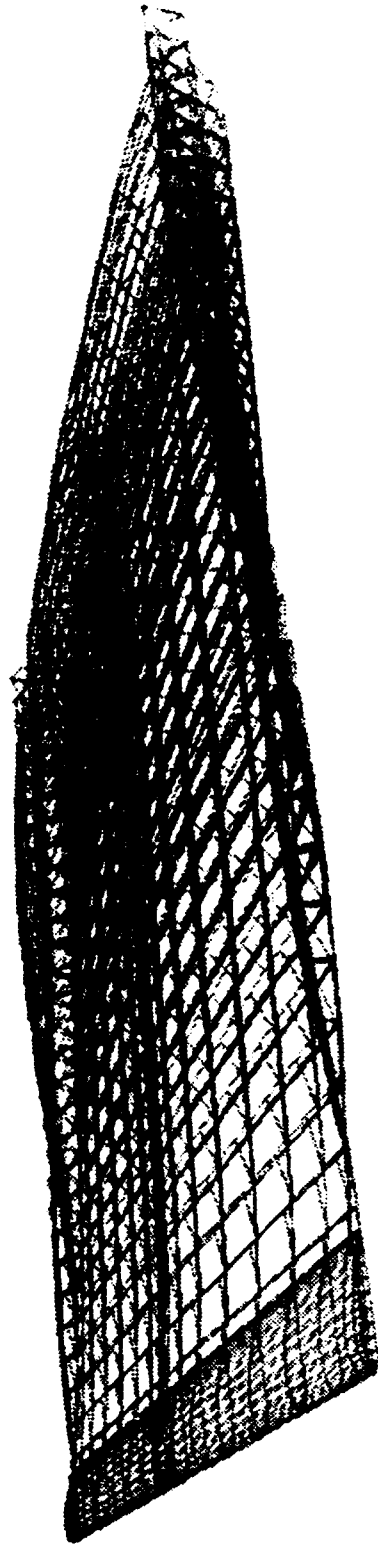


Figure A4 NACA 4415 Wing with PMARC Generated Wake

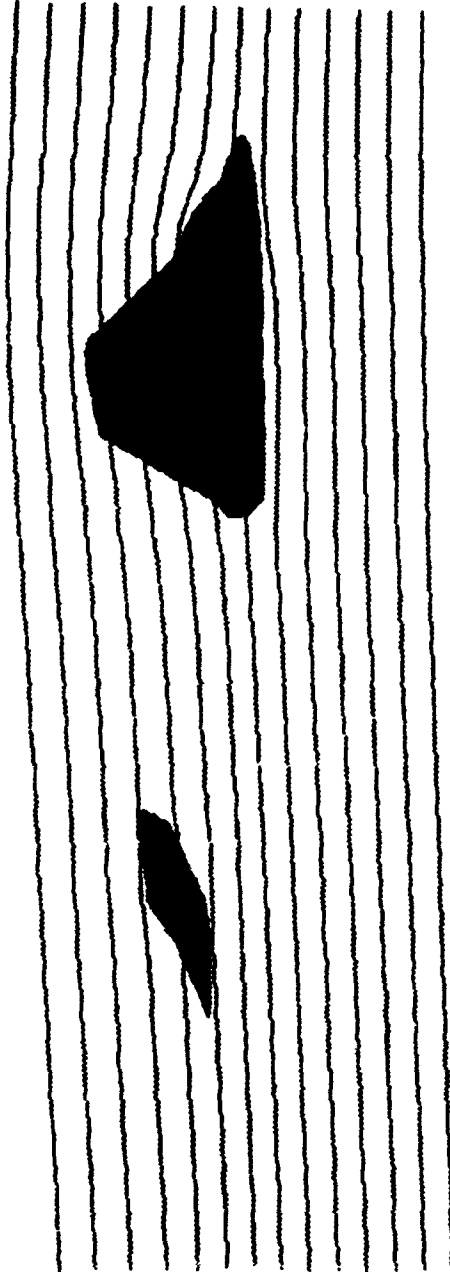


Figure A5 T-34 Wing and Tail with Streamlines at 5° AOA

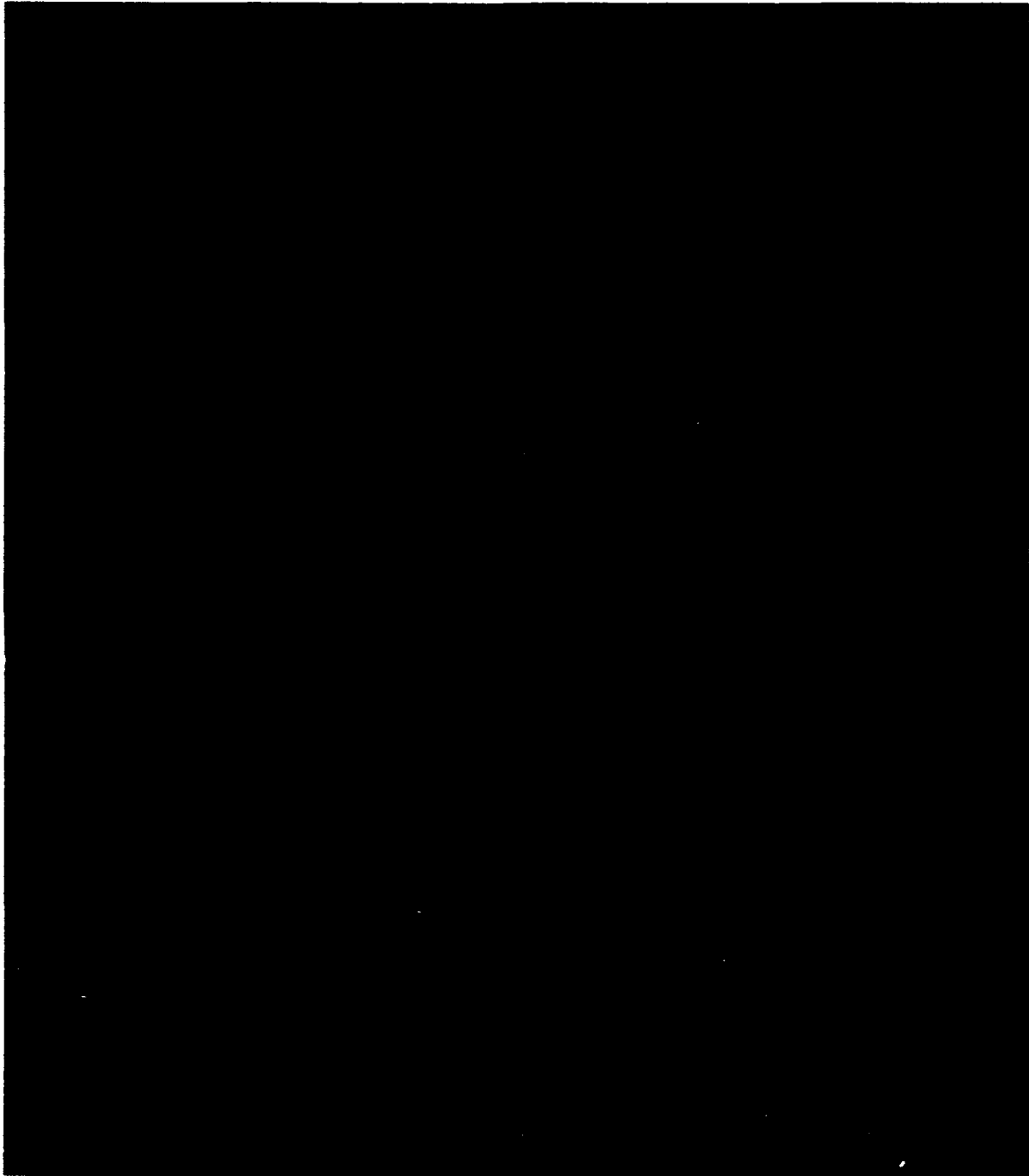


Figure A6 T-34 at 1° AOA with Streamlines

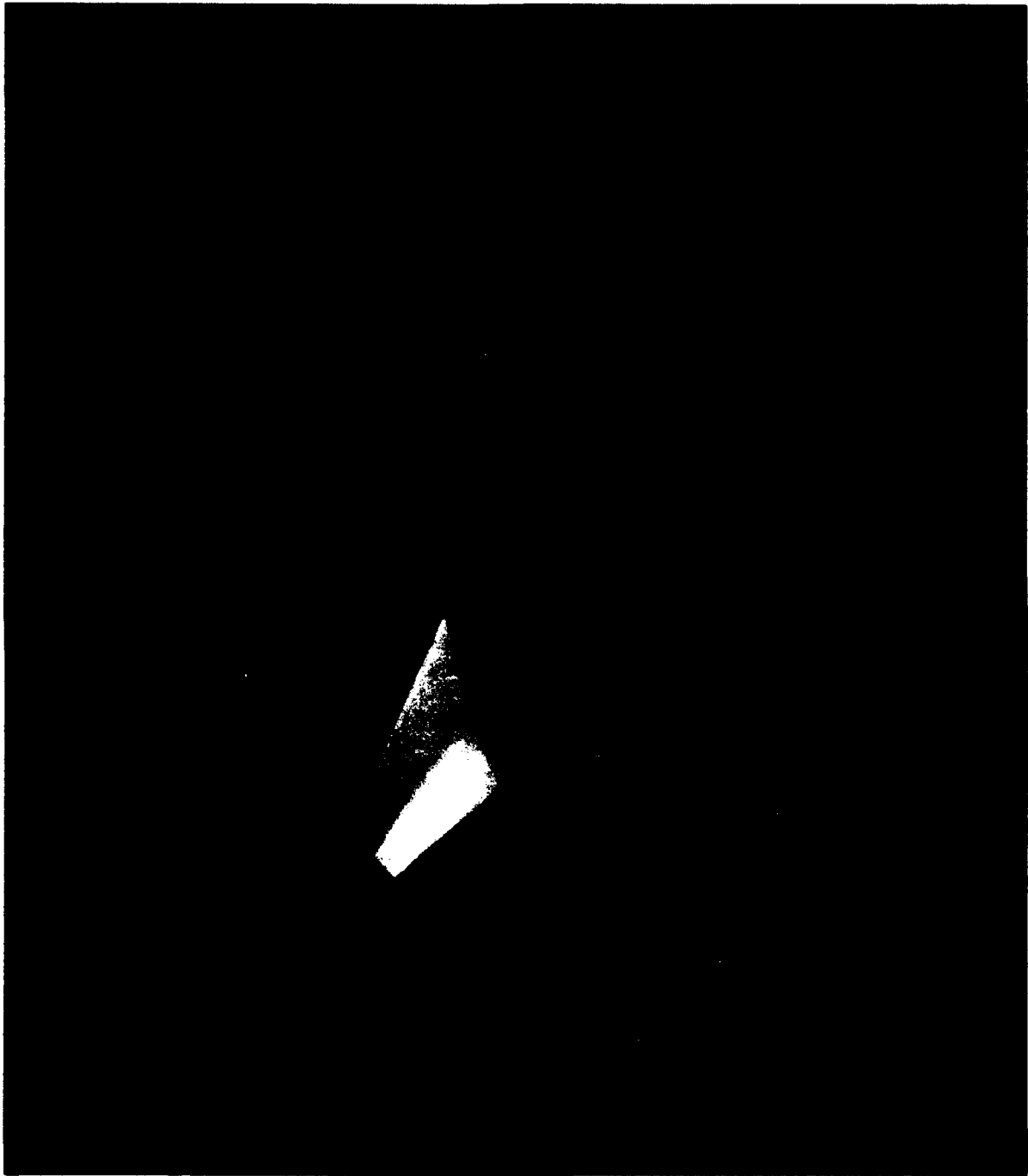


Figure A7 F-14 at 11° AOA

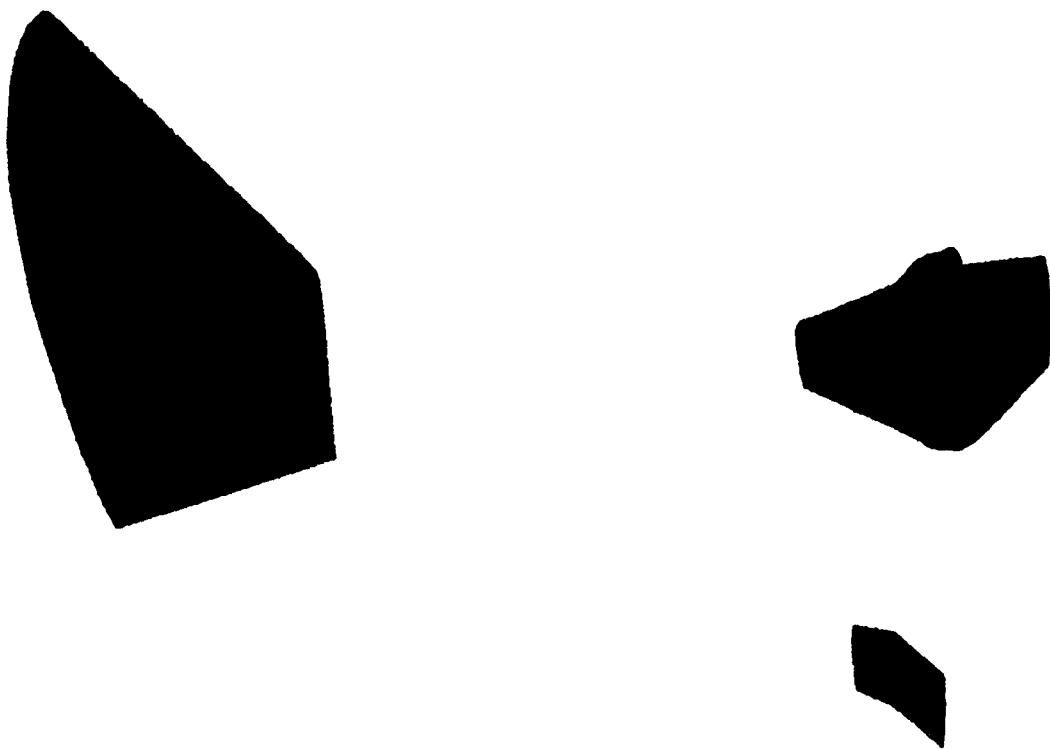


Figure A8 Large NACA 4415 Wing with T-34 Wing and Tail

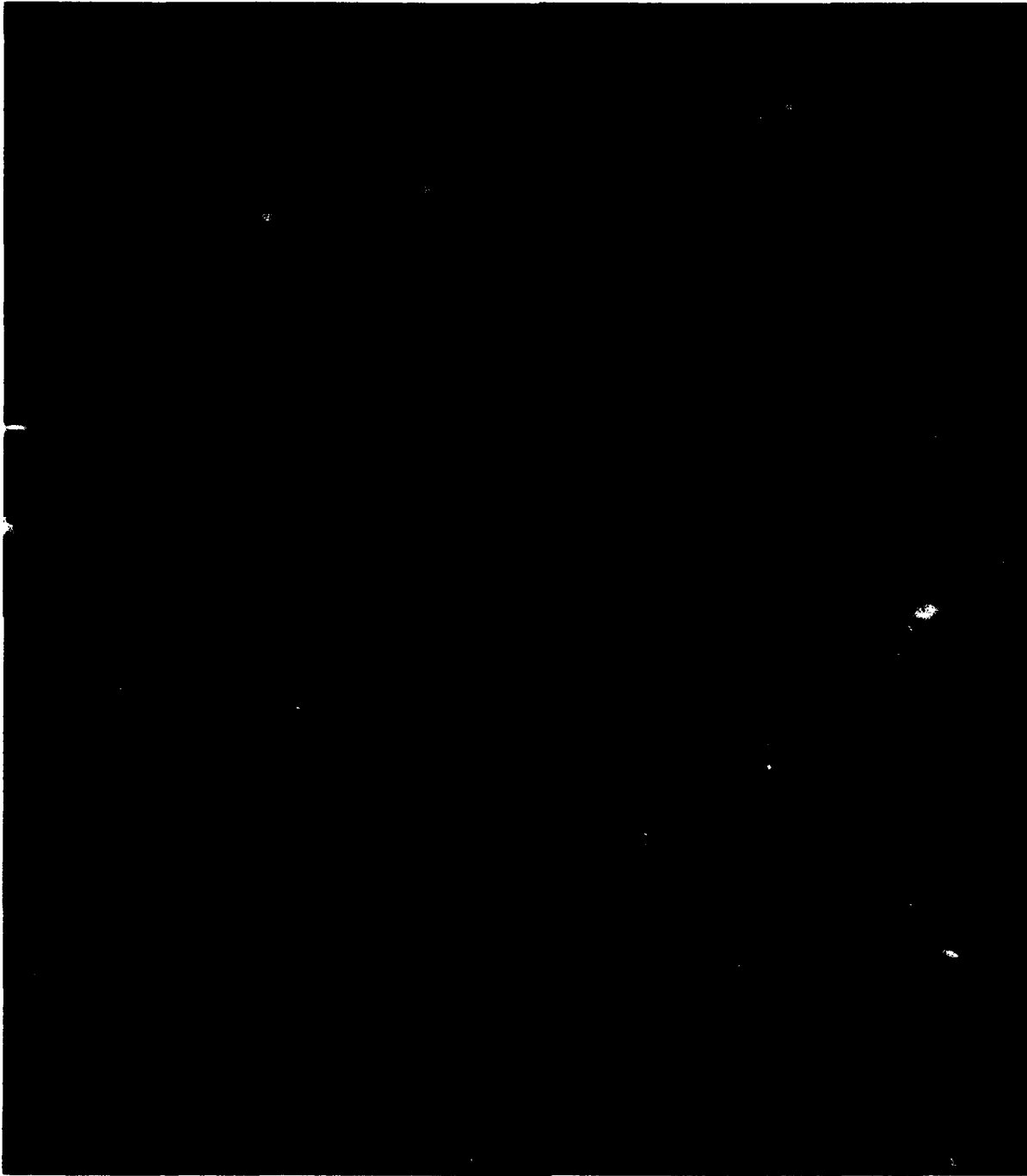


Figure A9 T-34 Wing and Tail Beyond Interference Effects

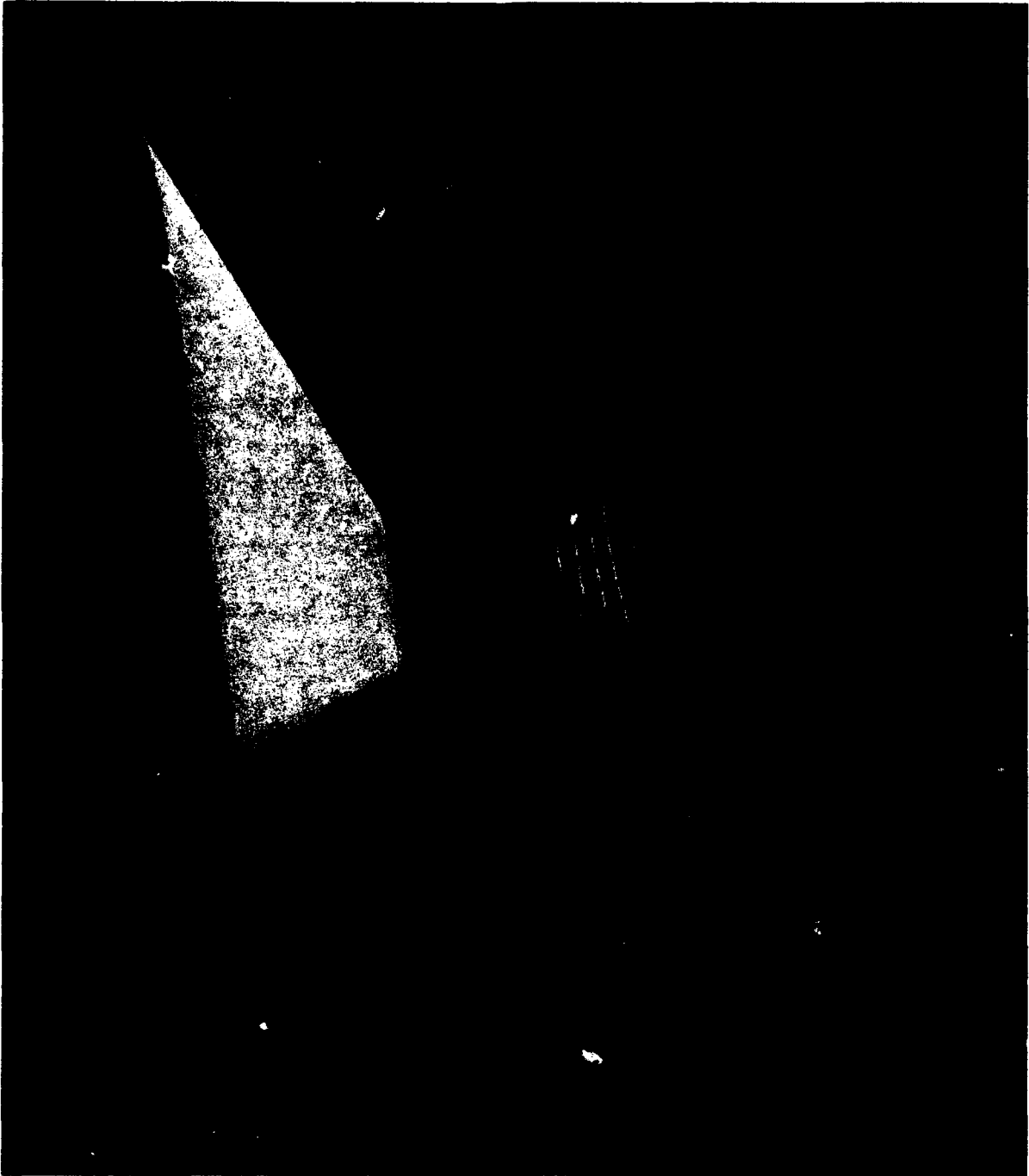


Figure A10 T-34 Wing and Tail 12.5 Feet Below Large Wing

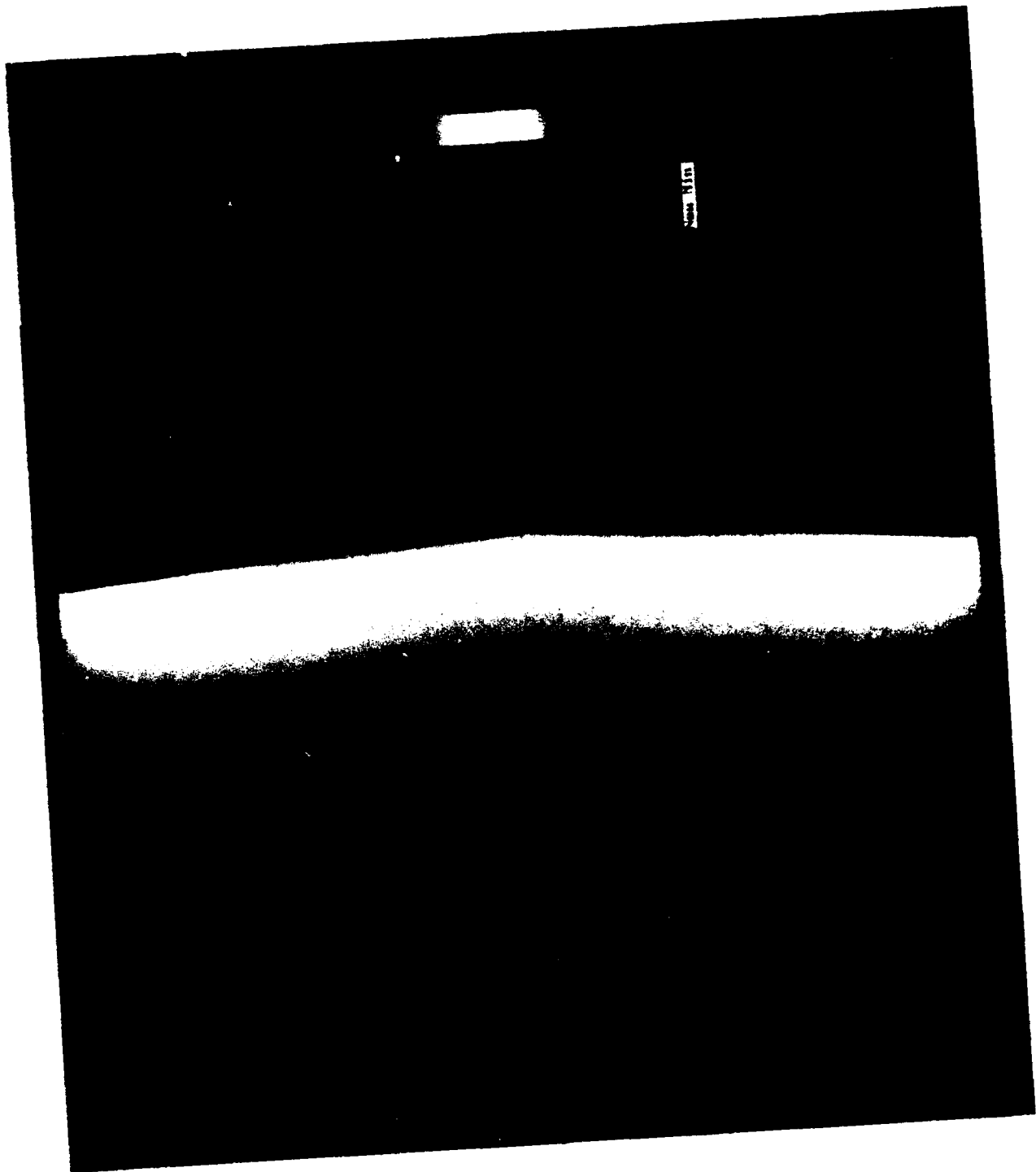


Figure A11 Pressure Coefficients on Bottom Surface of T-34 Tail When Beyond Interference Effects of Other Airplanes

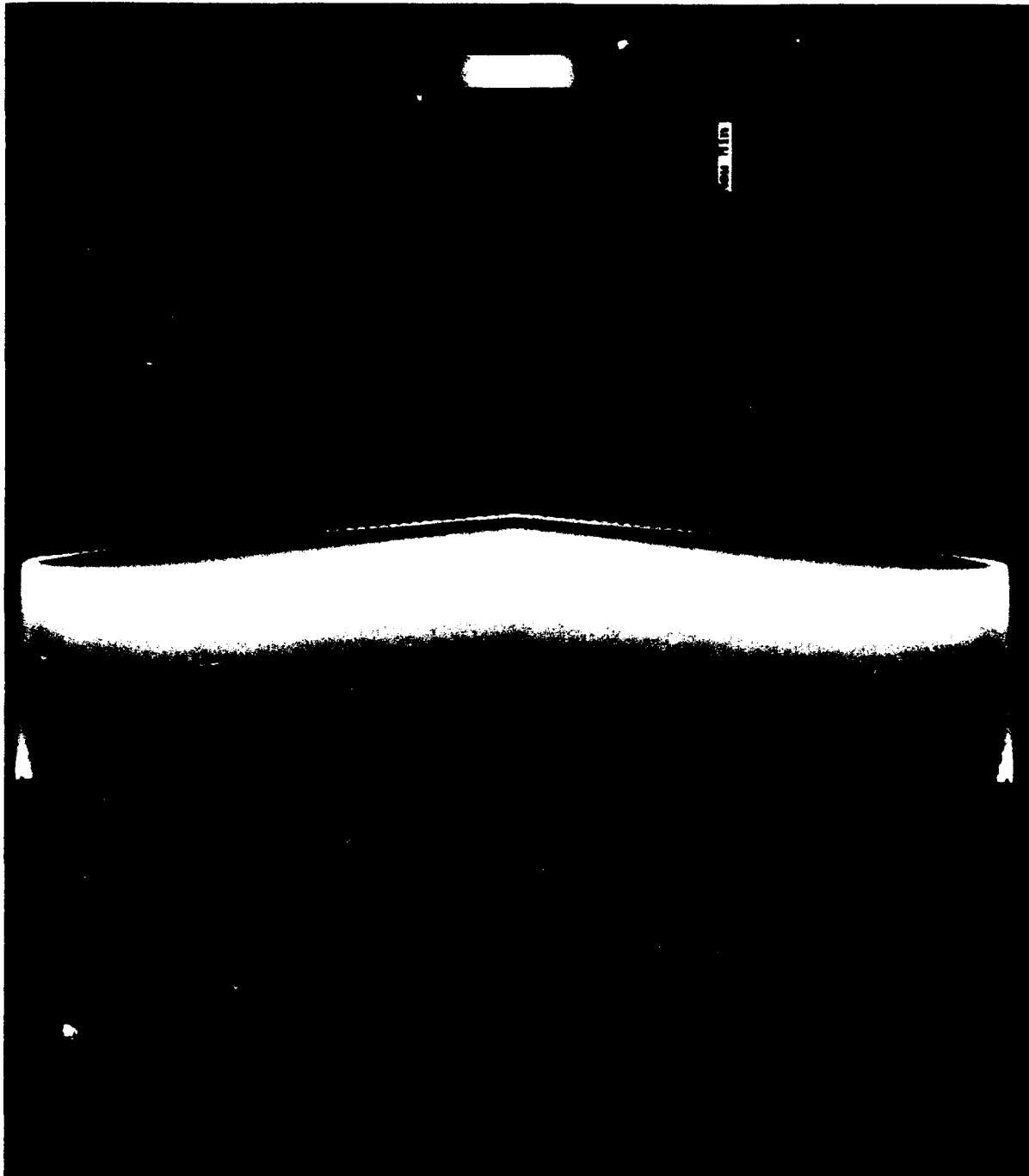


Figure A12 Pressure Coefficients on Bottom Surface of T-34 Tail When 8.33 Feet From Large Wing

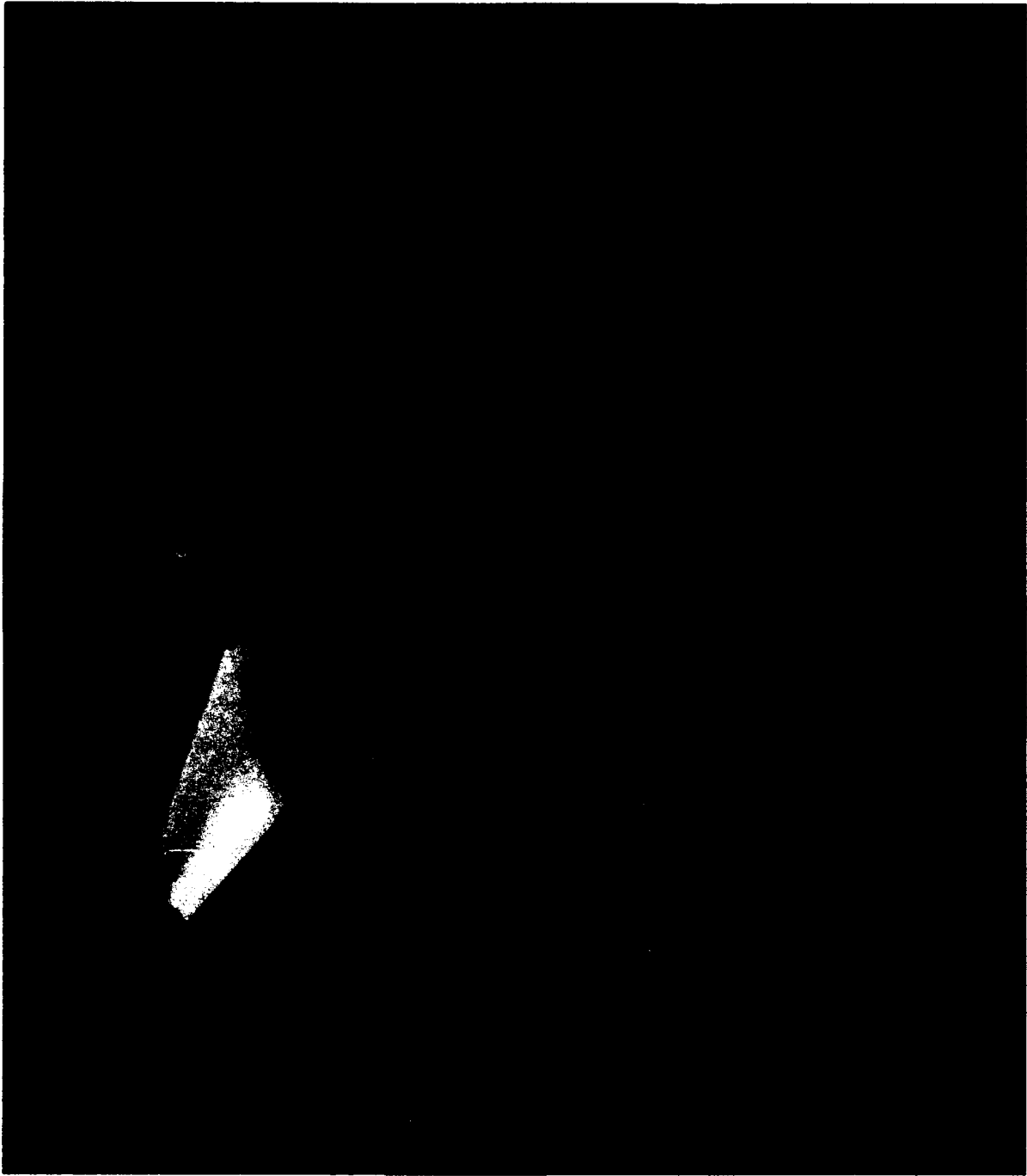


Figure A13 F-14 and T-34 in Proximity Test Case

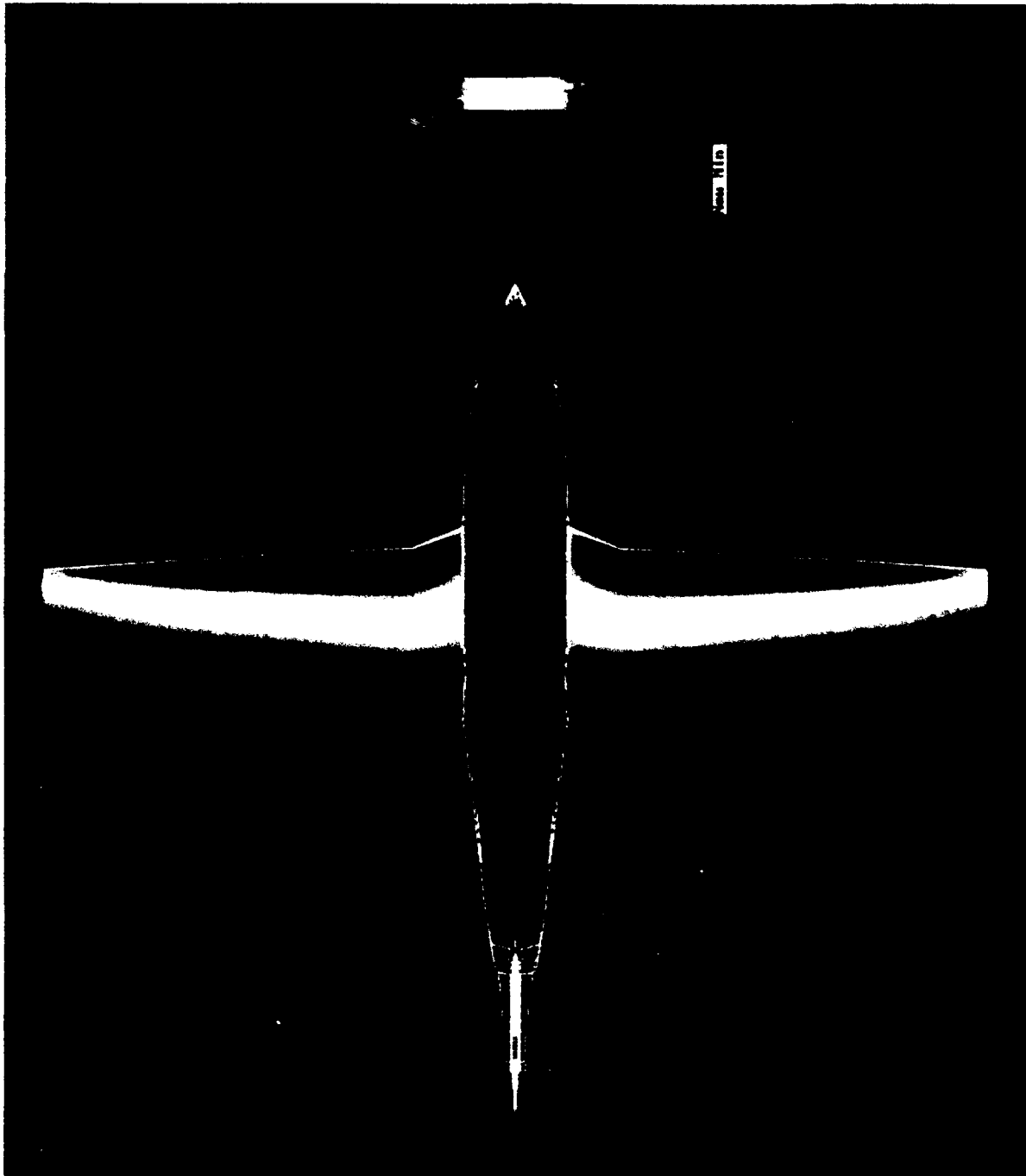


Figure A14 Pressure Coefficients on T-34 Wing and Tail When Beyond Interference Effects of Other Airplanes

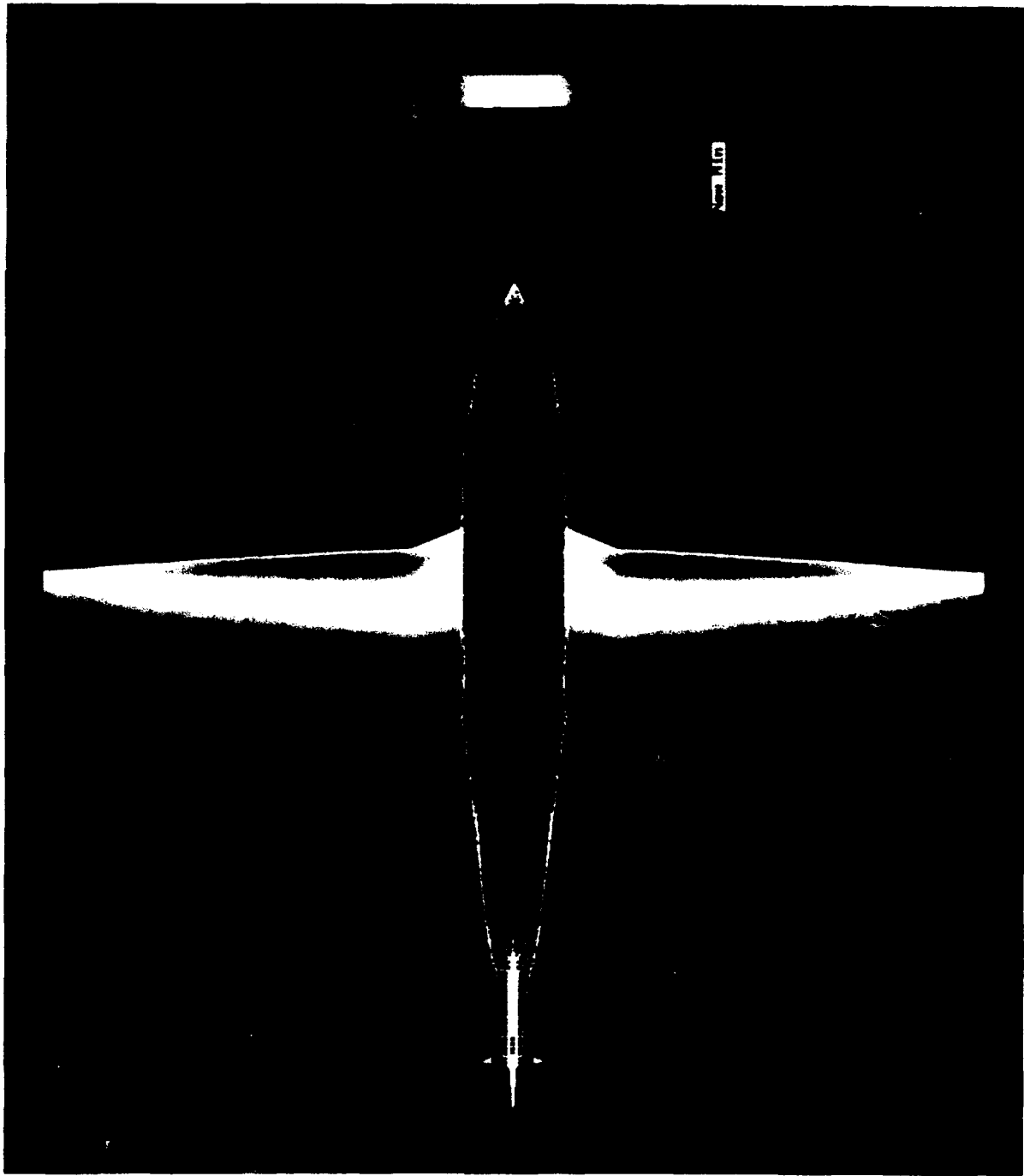
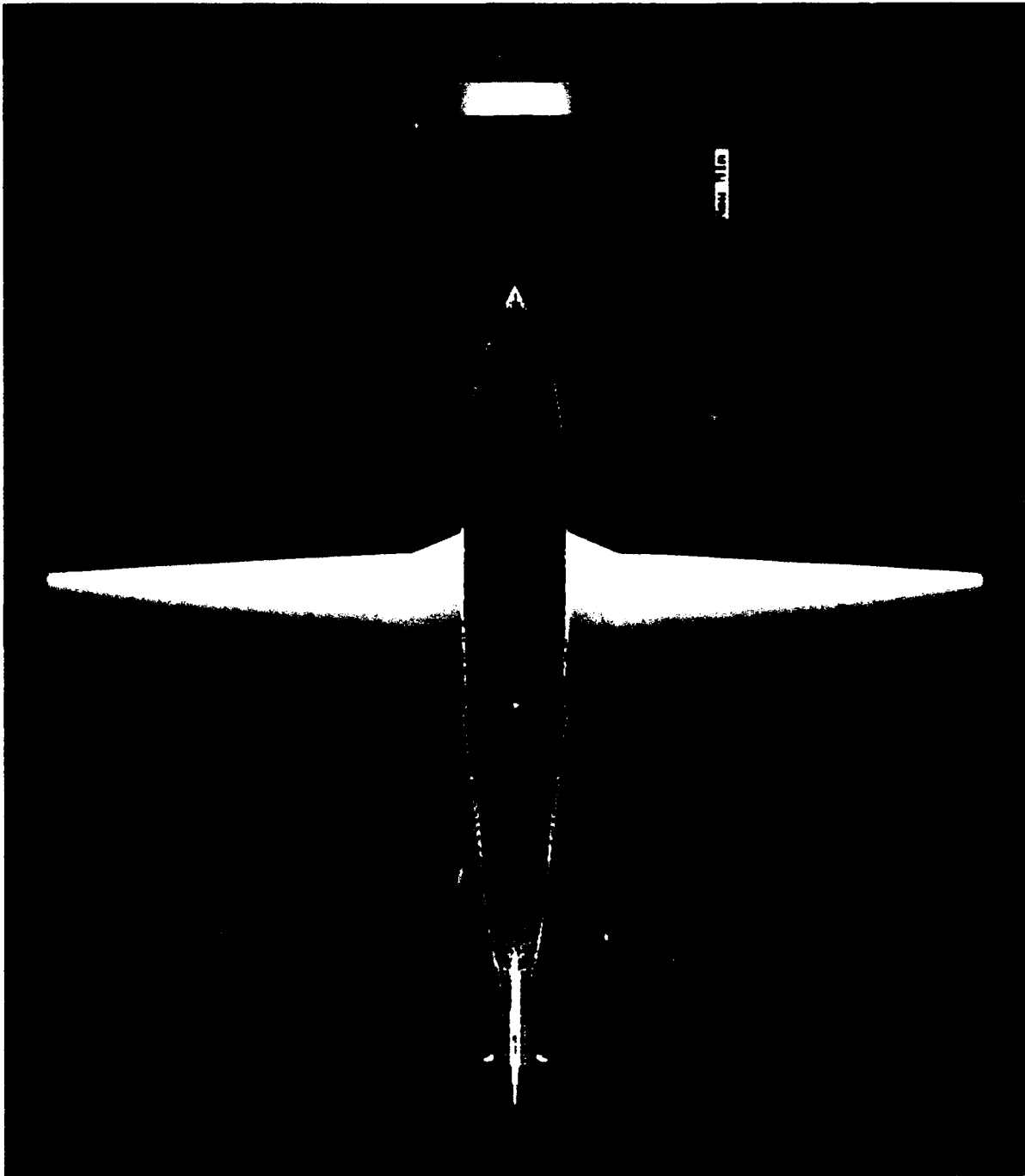


Figure A15 Pressure Coefficients on T-34 Wing and Tail When 37.5 Feet
Beneath the F-14



**Figure A16 Pressure Coefficients on T-34 Wing and Tail When 25 Feet
Beneath the F-14**

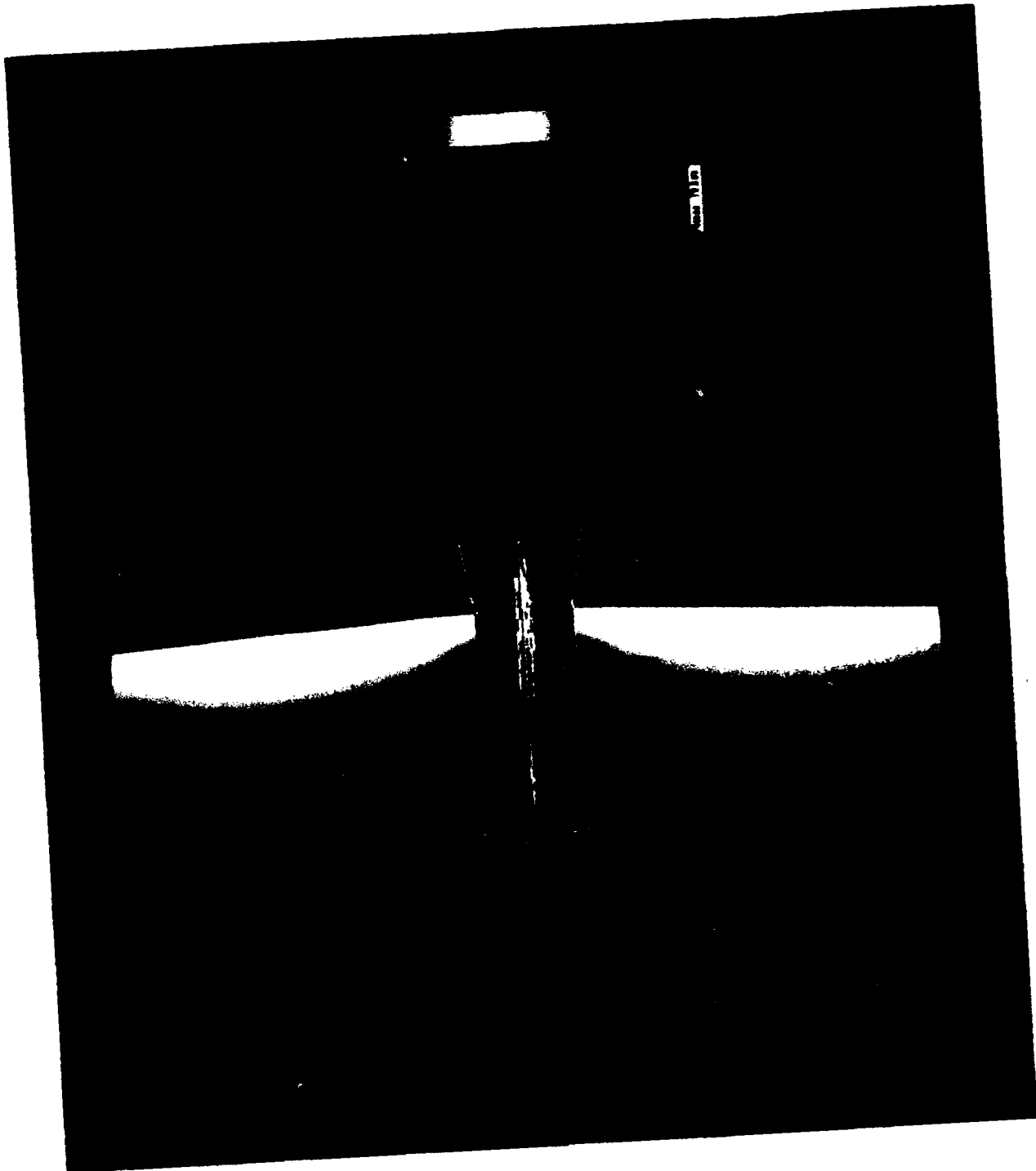
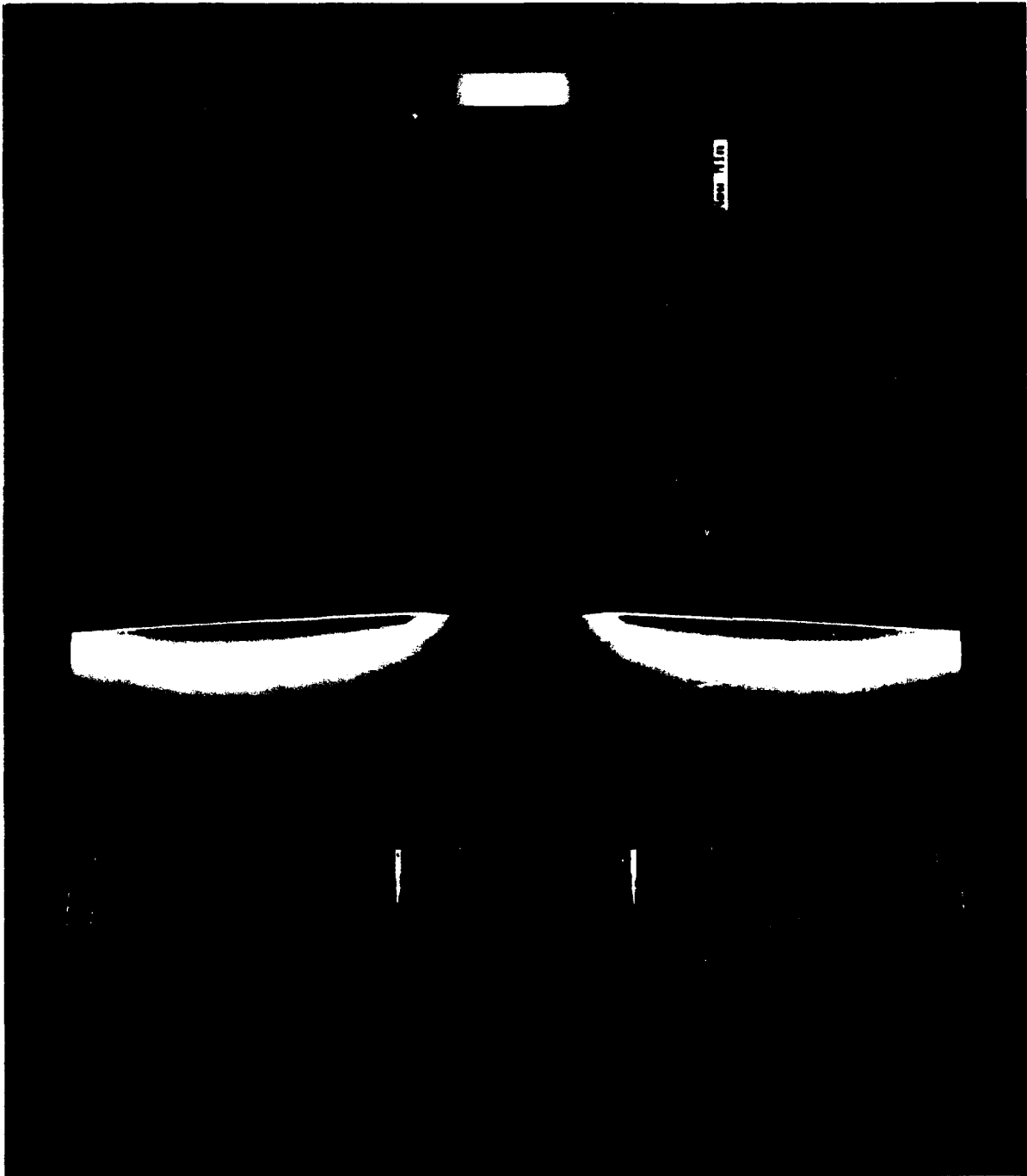
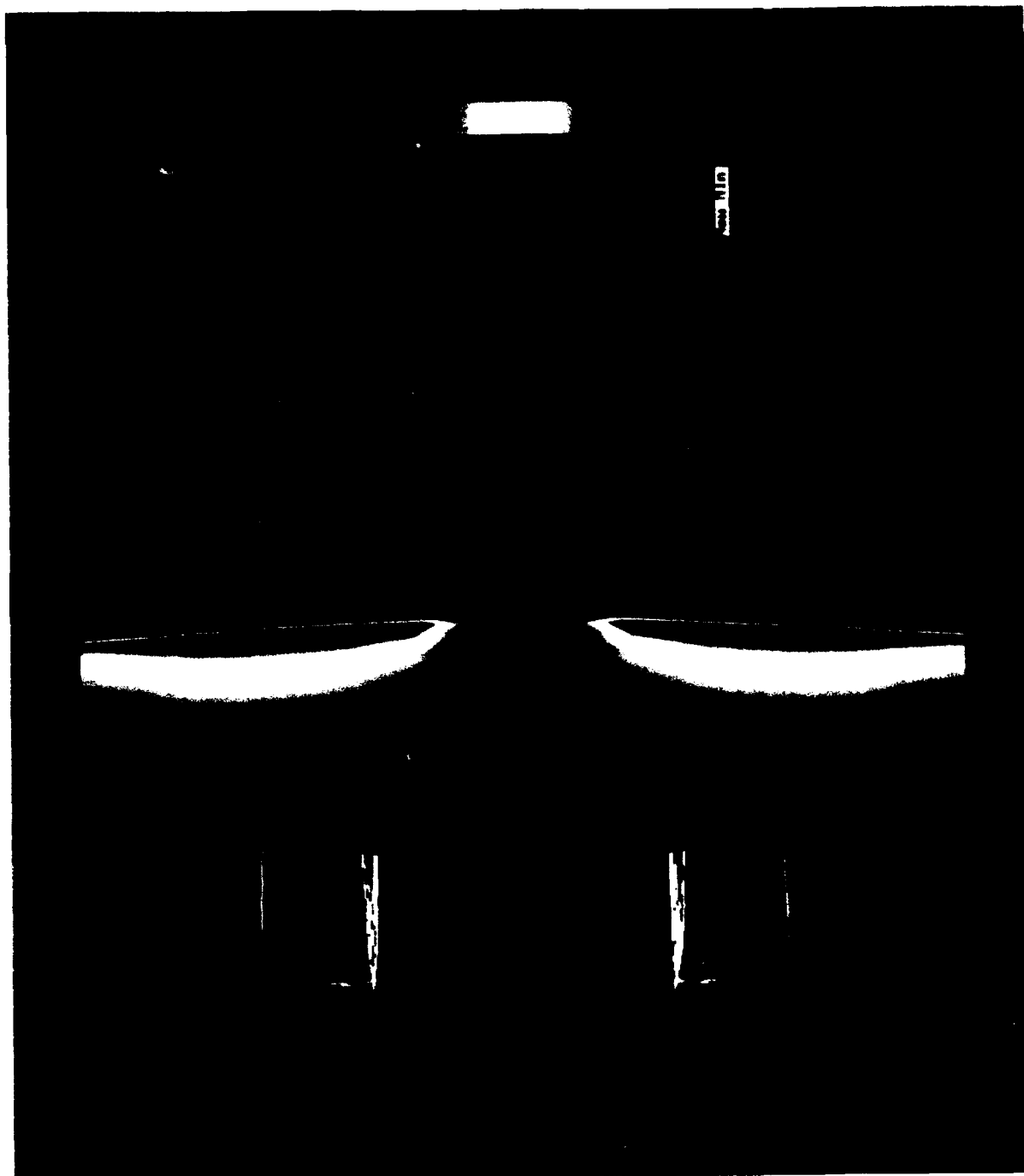


Figure A17 Pressure Coefficients on Bottom Surface of T-34 Tail When Beyond Interference Effects of Other Airplanes



**Figure A18 Pressure Coefficients on Bottom Surface of T-34 Tail When 37.5 Feet
Beneath the F-14**



**Figure A19 Pressure Coefficients on Bottom Surface of T-34 Tail When 25 Feet
Beneath the F-14**

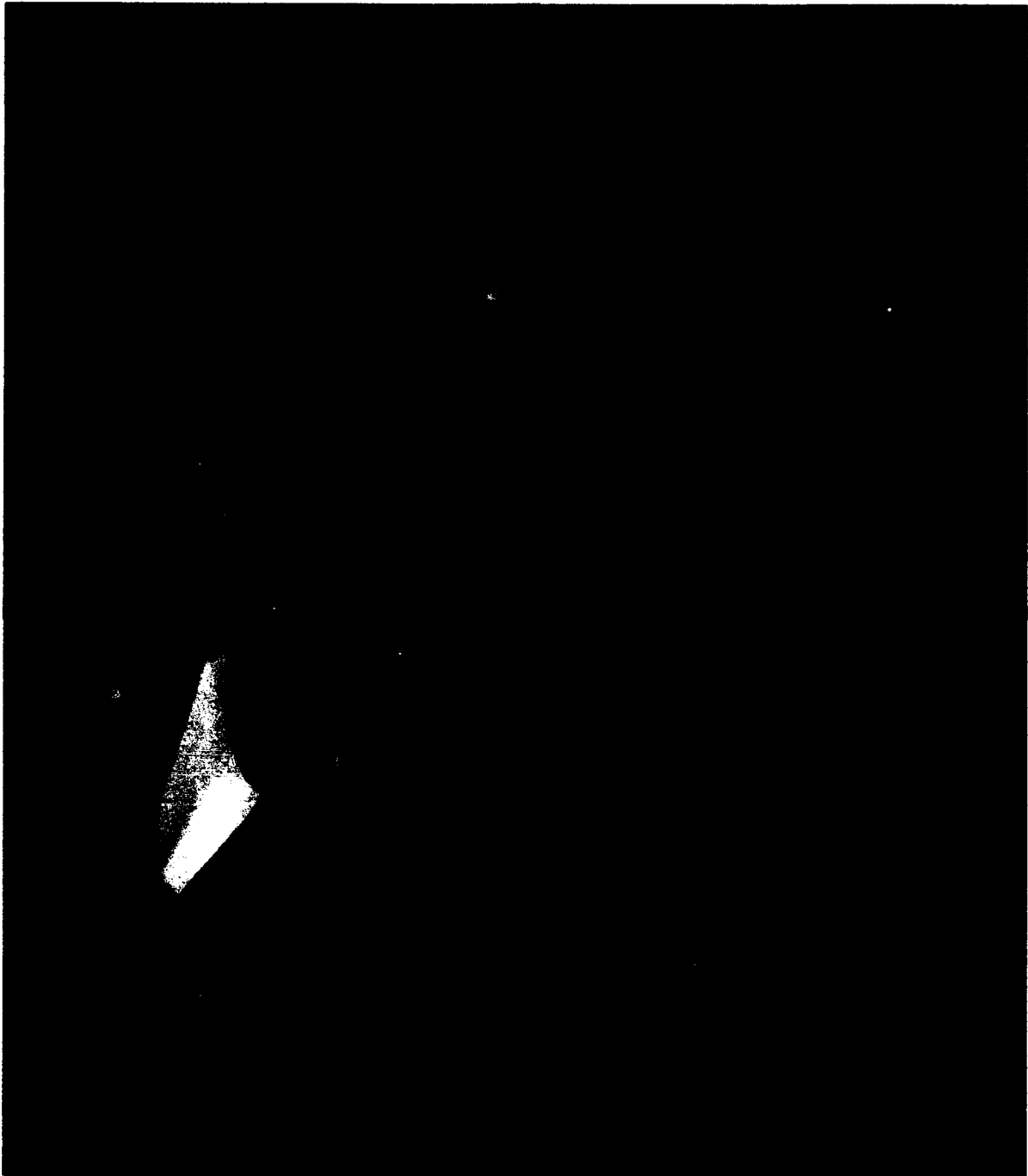


Figure A20 T-34 and Streamlines 33.33 Feet Beneath the F-14



Figure A21 T-34 and Streamlines 16.67 Feet Beneath the F-14

APPENDIX B PMARC F-14/T-34 INPUT

F14 AND T34

```

&BINP2 LSTINP=2, LSTOUT=1, LSTFRQ=1, LENRUN=0, &END
&BINP3 LSTGEO=1, LSTNAB=0, LSTWAK=3, LSTCPV=0, LSTJET=0, &END
&BINP4 MAXIT=250, SOLRES=0.0005, &END
&BINP5 NTSTPS=1, DTSTEP=0.5, &END
&BINP6 RSYM=0.0, RGPR=0.0, RFF=5.0, RCORE=0.05, &END
&BINP7 VINF=1.0, VSOUND=1116.0, UNIT=0, COMPOP=0.0, &END
&BINP8 ALDEG=0.0, YAWDEG=0.0, THEDOT=0.0, PSIDOT=0.0,
PHIDOT=0.0, &END
&BINP9 CBAR=65.028, SREF=25862.4, SSPAN=200.04,
RMPX=26.20, RMPY=0.00, RMPZ=0.00, &END
&BINP10 NORSET=0, NBCHGE=0, NCZONE=0,
NCZPAN=0, CZDUB=0.0, VREF=0.0, &END
&BINP11 NORPCH=0, NORF=0, NORL=0,
NOCF=0, NOCL=0, VNORM=0, &END
&BINP12 KPAN=0, KSIDE=0, NEWSID=0, &END

&ASEM1 ASEMZ=0.00, ASEMXY=0.00, ASEMZ=0.00,
ASCAL=1.00, ATHET=1.00, NODEA=0, &END
&ASEM2 APXX=0.0, APYY=0.0, APZZ=0.0,
AHXX=0.0, AHYY=1.0, AHZZ=0.0, &END

&ASEM1 ASEMZ=0.00, ASEMXY=0.00, ASEMZ=0.00,
ASCAL=1.00, ATHET=1.00, NODEA=0, &END
&ASEM2 APXX=0.0, APYY=0.0, APZZ=0.0,
AHXX=0.0, AHYY=1.0, AHZZ=0.0, &END

&ASEM1 ASEMZ=-511.00, ASEMXY=0.00, ASEMZ=2004.00,
ASCAL=1.00, ATHET=11.00, NODEA=0, &END
&ASEM2 APXX=0.0, APYY=0.0, APZZ=0.0,
AHXX=0.0, AHYY=1.0, AHZZ=0.0, &END

&ASEM1 ASEMZ=-511.00, ASEMXY=0.00, ASEMZ=2004.00,
ASCAL=1.00, ATHET=11.00, NODEA=5, &END
&ASEM2 APXX=0.0, APYY=0.0, APZZ=0.0,
AHXX=0.0, AHYY=1.0, AHZZ=0.0, &END

&COMP1 COMPC=0.00, COMPCY=0.00, COMPCZ=0.00,
CSCAL=1.00, CTHET=0.0, NODEC=0, &END
&COMP2 CPXX=0.0, CPYY=0.0, CPZZ=0.0,
CHXX=0.0, CHYY=1.0, CHZZ=0.0, &END

&COMP1 COMPC=0.00, COMPCY=0.00, COMPCZ=0.00,
CSCAL=1.00, CTHET=0.0, NODEC=5, &END
&COMP2 CPXX=0.0, CPYY=0.0, CPZZ=0.0,
CHXX=0.0, CHYY=1.0, CHZZ=0.0, &END

&PATCH1 IREV=0, IDPAT=2, MAKE=0, KCOMP=1, KASS=1, &END
T34 FUSELAGE FORWARD #1

```

```

&SECT1 STX=-99.38, STY=0.00, STZ=0.00, SCALE=1.0,
  ALF=0.0, THETA=0.0,
  INMODE=4, TNODS=0, TNPS=0, TINTS=0,
  0.0 0.0 25.388
  0.0 0.0 25.388
  0.0 0.0 25.388
  0.0 0.0 25.388
  0.0 0.0 25.388
  0.0 0.0 25.388
  0.0 0.0 25.388
  0.0 0.0 25.388
  0.0 0.0 25.388
&BPNODE TNODE=3, TNPC=12, TINTC=3,
&SECT1 STX=-81.359, STY=0.00, STZ=0.00, SCALE=1.0,
  ALF=0.0, THETA=0.00,
  INMODE=4, TNODS=2, TNPS=2, TINTS=0,
  0.0 0.0 16.926
  0.0 3.238 17.57
  0.0 5.98 19.404
  0.0 7.817 22.15
  0.0 8.462 25.388
  0.0 7.817 28.626
  0.0 5.98 31.371
  0.0 3.238 33.206
  0.0 0.0 33.85
&BPNODE TNODE=3, TNPC=12, TINTC=3,
&SECT1 STX=-61.7, STY=0.0, STZ=0.0, SCALE=1.0,
  ALF=0.0, THETA=0.0,
  INMODE=4, TNODS=2, TNPS=2, TINTS=0,
  0.0 0.0 5.46
  0.0 12.0 6.0
  0.0 15.8 10.0
  0.0 16.3 15.0
  0.0 16.926 21.84
  0.0 16.5 28.0
  0.0 15.0 34.3
  0.0 10.0 37.5
  0.0 0.0 38.22
&BPNODE TNODE=3, TNPC=12, TINTC=3,
&SECT1 STX=-44.23, STY=0.0, STZ=0.0, SCALE=1.0,
  ALF=0.0, THETA=0.0,
  INMODE=4, TNODS=2, TNPS=2, TINTS=0,
  0.0 0.0 0.0
  0.0 6.0 0.25
  0.0 12.0 0.5
  0.0 17.5 4.0
  0.0 19.4 9.0
  0.0 19.5 14.0
  0.0 19.657 19.11
  0.0 19.4 25.0
  0.0 19.2 31.0
  0.0 17.5 36.4
  0.0 13.0 38.35
  0.0 6.5 38.46

```

```

0.0 0.0 38.5
&BPNODE TNODE=3, TNPC=12, TINTC=3, &END
&SECT1 STX=-10.375, STY=0.0, STZ=0.0, SCALE=1.0,
ALF=0.0, THETA=0.0,
INMODE=4, TNODS=1, TNPS=2, TINTS=0, &END
0.0 0.0 -5.714
0.0 7.5 -5.1
0.0 15.0 -4.5
0.0 20.9 0.0
0.0 21.9 6.0
0.0 22.4 11.0
0.0 22.8 16.38
0.0 22.4 23.0
0.0 22.0 30.0
0.0 19.0 35.0
0.0 14.5 38.5
0.0 7.0 39.25
0.0 0.0 39.77
&BPNODE TNODE=3, TNPC=12, TINTC=3, &END
&SECT1 STX=0.0, STY=0.0, STZ=0.0, SCALE=1.0,
ALF=0.0, THETA=0.0,
INMODE=4, TNODS=3, TNPS=0, TINTS=0, &END
0.0 0.0 -5.714
0.0 5.5 -5.714
0.0 10.92 -5.714
0.0 15.0 -4.5
0.0 22.93 0.0
0.0 22.93 8.0
0.0 22.8 16.38
0.0 22.4 24.0
0.0 22.0 30.0
0.0 19.0 35.0
0.0 14.5 38.5
0.0 7.0 39.35
0.0 0.0 39.77
&BPNODE TNODE=3, TNPC=12, TINTC=3, &END
&PATCH1 IREV=0, IDPAT=1, MAKE=0, KCOMP=1, KASS=1, &END
T34 WING #2
&SECT1 STX=0.0, STY=22.93, STZ=0.0, SCALE=1.0,
ALF=0.0, THETA=0.0,
INMODE=4, TNODS=0, TNPS=0, TINTS=0, &END
88.457 0.0 0.0
84.03 0.0 -0.849
79.61 0.0 -1.513
70.766 0.0 -2.698
61.92 0.0 -3.724
53.07 0.0 -4.591
44.229 0.0 -5.254
35.383 0.0 -5.661
26.537 0.0 -5.714
22.114 0.0 -5.555
17.69 0.0 -5.21
13.269 0.0 -4.679

```

8.846	0.0	-3.954	
6.634	0.0	-3.485	
4.423	0.0	-2.910	
2.21	0.0	-2.123	
1.105	0.0	-1.451	
0.0	0.0	0.0	
&BPNODE	TNODE=2,	TNPC=15,	TINTC=0,
			&END
0.0	0.0	0.0	
1.105	0.0	3.176	
2.21	0.0	4.175	
4.423	0.0	5.511	
6.634	0.0	6.431	
8.846	0.0	7.112	
13.269	0.0	7.935	
17.69	0.0	8.315	
22.114	0.0	8.465	
26.537	0.0	8.448	
35.383	0.0	8.023	
44.229	0.0	7.236	
53.07	0.0	6.183	
61.92	0.0	4.918	
70.766	0.0	2.609	
79.61	0.0	1.911	
84.03	0.0	1.053	
88.457	0.0	0.0	
&BPNODE	TNODE=3,	TNPC=15,	TINTC=0,
			&END
&SECT1	STX=10.92,	STY=45.87,	STZ=2.1,
	SCALE=.84,		
	ALF=4.0,	THETA=0.0,	
	INMODE=0,	TNODS=2,	TNPS=0,
	TINTS=3,		&END
&SECT1	STX=21.84,	STY=202.0,	STZ=22.0,
	SCALE=1.0,		
	ALF=1.0,	THETA=0.0,	
	INMODE=4,	TNODS=3,	TNPS=10,
	TINTS=3,		&END
41.0	0.0	0.0	
38.95	0.0	-0.287	
36.9	0.0	-0.5	
32.8	0.0	-0.886	
28.7	0.0	-1.23	
24.6	0.0	-1.505	
20.5	0.0	-1.71	
16.4	0.0	-1.837	
12.3	0.0	-1.83	
10.25	0.0	-1.755	
8.2	0.0	-1.63	
6.15	0.0	-1.44	
4.1	0.0	-1.197	
3.08	0.0	-1.07	
2.05	0.0	-0.93	
1.03	0.0	-0.70	
0.51	0.0	-0.50	
0.0	0.0	0.0	
&BPNODE	TNODE=2,	TNPC=15,	TINTC=0,
			&END
0.0	0.0	0.0	
0.51	0.0	1.09	
1.03	0.0	1.48	

2.05	0.0	2.01	
3.08	0.0	2.38	
4.10	0.0	2.64	
6.15	0.0	2.95	
8.2	0.0	3.08	
10.25	0.0	3.116	
12.3	0.0	3.096	
16.4	0.0	2.93	
20.5	0.0	2.63	
24.6	0.0	2.24	
28.7	0.0	1.79	
32.8	0.0	1.26	
36.9	0.0	0.69	
38.95	0.0	0.38	
41.0	0.0	0.0	

&BPNODE TNODE=3, TNPC=15, TINTC=0, &END
&PATCH1 IREV=0, IDPAT=1, MAKE=2, KCOMP=1, KASS=2, &END
T34 WING TIP #3
&PATCH2 ITYP=1, TNODS=3, TNPS=2, TINTS=0, NPTTIP=0, &END
&PATCH1 IREV=0, IDPAT=2, MAKE=0, KCOMP=1, KASS=1, &END
T34 FUSELAGE UNDER WING #4
&SECT1 STX=0.0, STY=0.0, STZ=0.0, SCALE=1.0,
ALF=0.0, THETA=0.0,
INMODE=4, TNODS=0, TNPS=0, TINTS=0, &END
0.0 0.0 -5.714
0.0 10.92 -5.714
0.0 15.0 -5.5
0.0 22.93 0.0
&BPNODE TNODE=3, TNPC=0, TINTC=0, &END
&SECT1 STX=0.0, STY=0.0, STZ=0.0, SCALE=1.0,
ALF=0.0, THETA=0.0,
INMODE=4, TNODS=0, TNPS=3, TINTS=0, &END
6.634 0.0 -5.714
6.634 10.92 -5.714
6.634 18.57 -5.714
6.634 22.93 -3.485
&BPNODE TNODE=3, TNPC=0, TINTC=0, &END
&SECT1 STX=0.0, STY=0.0, STZ=0.0, SCALE=1.0,
ALF=0.0, THETA=0.0,
INMODE=4, TNODS=0, TNPS=0, TINTS=0, &END
8.846 0.0 -5.714
8.846 10.92 -5.714
8.846 18.57 -5.714
8.846 22.93 -3.954
&BPNODE TNODE=3, TNPC=0, TINTC=0, &END
&SECT1 STX=0.0, STY=0.0, STZ=0.0, SCALE=1.0,
ALF=0.0, THETA=0.0,
INMODE=4, TNODS=0, TNPS=0, TINTS=0, &END
13.269 0.0 -5.714
13.269 10.92 -5.714
13.269 18.57 -5.174
13.269 22.93 -4.679

```

&BPNODE TNODE=3, TNPC=0, TINTC=0, &END
&SECT1 STX=0.0, STY=0.0, STZ=0.0, SCALE=1.0,
  ALF=0.0, THETA=0.0,
  INMODE=4, TNODS=0, TNPS=0, TINTS=0, &END
  17.69 0.0 -5.714
  17.69 10.92 -5.714
  17.69 18.57 -5.714
  17.69 22.93 -5.21
&BPNODE TNODE=3, TNPC=0, TINTC=0, &END
&SECT1 STX=0.0, STY=0.0, STZ=0.0, SCALE=1.0,
  ALF=0.0, THETA=0.0,
  INMODE=4, TNODS=0, TNPS=0, TINTS=0, &END
  22.114 0.0 -5.714
  22.114 10.92 -5.714
  22.114 18.57 -5.714
  22.114 22.93 -5.555
&BPNODE TNODE=3, TNPC=0, TINTC=0, &END
&SECT1 STX=0.0, STY=0.0, STZ=0.0, SCALE=1.0,
  ALF=0.0, THETA=0.0,
  INMODE=4, TNODS=0, TNPS=0, TINTS=0, &END
  26.537 0.0 -5.714
  26.537 10.92 -5.714
  26.537 18.57 -5.714
  26.537 22.93 -5.714
&BPNODE TNODE=3, TNPC=0, TINTC=0, &END
&SECT1 STX=0.0, STY=0.0, STZ=0.0, SCALE=1.0,
  ALF=0.0, THETA=0.0,
  INMODE=4, TNODS=0, TNPS=0, TINTS=0, &END
  35.383 0.0 -5.661
  35.383 10.92 -5.661
  35.383 18.57 -5.661
  35.383 22.93 -5.661
&BPNODE TNODE=3, TNPC=0, TINTC=0, &END
&SECT1 STX=0.0, STY=0.0, STZ=0.0, SCALE=1.0,
  ALF=0.0, THETA=0.0,
  INMODE=4, TNODS=0, TNPS=0, TINTS=0, &END
  44.229 0.0 -5.254
  44.229 10.92 -5.254
  44.229 18.57 -5.254
  44.229 22.93 -5.254
&BPNODE TNODE=3, TNPC=0, TINTC=0, &END
&SECT1 STX=0.0, STY=0.0, STZ=0.0, SCALE=1.0,
  ALF=0.0, THETA=0.0,
  INMODE=4, TNODS=0, TNPS=0, TINTS=0, &END
  53.07 0.0 -4.591
  53.07 10.92 -4.591
  53.07 18.57 -4.591
  53.07 22.93 -4.591
&BPNODE TNODE=3, TNPC=0, TINTC=0, &END
&SECT1 STX=0.0, STY=0.0, STZ=0.0, SCALE=1.0,
  ALF=0.0, THETA=0.0,
  INMODE=4, TNODS=0, TNPS=0, TINTS=0, &END
  61.92 0.0 -3.724
  61.92 10.92 -3.724

```

```

61.92 18.57 -3.724
61.92 22.93 -3.724
&BPNODE TNODE=3, TNPC=0, TINTC=0, &END
&SECT1 STX=0.0, STY=0.0, STZ=0.0, SCALE=1.0,
ALF=0.0, THETA=0.0,
INMODE=4, TNODS=0, TNPS=0, TINTS=0, &END
70.766 0.0 -2.698
70.766 10.92 -2.698
70.766 18.57 -2.698
70.766 22.93 -2.698
&BPNODE TNODE=3, TNPC=0, TINTC=0, &END
&SECT1 STX=0.0, STY=0.0, STZ=0.0, SCALE=1.0,
ALF=0.0, THETA=0.0,
INMODE=4, TNODS=0, TNPS=0, TINTS=0, &END
79.61 0.0 -1.513
79.61 10.92 -1.513
79.61 18.57 -1.513
79.61 22.93 -1.513
&BPNODE TNODE=3, TNPC=0, TINTC=0, &END
&SECT1 STX=0.0, STY=0.0, STZ=0.0, SCALE=1.0,
ALF=0.0, THETA=0.0,
INMODE=4, TNODS=0, TNPS=0, TINTS=0, &END
84.03 0.0 -0.849
84.03 10.92 -0.849
84.03 18.57 -0.849
84.03 22.93 -0.849
&BPNODE TNODE=3, TNPC=0, TINTC=0, &END
&SECT1 STX=0.0, STY=0.0, STZ=0.0, SCALE=1.0,
ALF=0.0, THETA=0.0,
INMODE=4, TNODS=3, TNPS=0, TINTS=0, &END
88.457 0.0 0.0
88.457 10.92 0.0
88.457 18.57 0.0
88.457 22.93 0.0
&BPNODE TNODE=3, TNPC=0, TINTC=0, &END
&PATCH1 IREV=0, IDPAT=2, MAKE=0, KCOMP=1, KASS=1, &END
T34 UPPER MIDDLE FUSELAGE #5
&SECT1 STX=0.0, STY=0.0, STZ=0.0, SCALE=1.0,
ALF=0.0, THETA=0.0,
INMODE=4, TNODS=0, TNPS=0, TINTS=0, &END
0.0 22.93 0.0
0.0 22.93 13.1
0.0 22.38 16.38
0.0 22.0 30.0
0.0 20.0 36.0
0.0 14.5 39.0
0.0 0.0 39.77
&BPNODE TNODE=3, TNPC=9, TINTC=3, &END
&SECT1 STX=0.0, STY=0.0, STZ=0.0, SCALE=1.0,
ALF=0.0, THETA=0.0,
INMODE=4, TNODS=0, TNPS=3, TINTS=0, &END
6.634 22.93 6.431
6.634 22.93 25.1

```

```

6.634 21.00 32.22
6.634 6.55 39.9
6.634 4.0 40.0
6.634 2.0 41.0
6.634 0.0 41.498
&BPNODE TNODE=3, TNPC=9, TINTC=3, &END
&SECT1 STX=0.0, STY=0.0, STZ=0.0, SCALE=1.0,
ALF=0.0, THETA=0.0,
INMODE=4, TNODS=0, TNPS=0, TINTS=0, &END
8.846 22.93 7.112
8.846 22.93 25.1
8.846 21.00 32.22
8.846 11.47 36.58
8.846 6.0 41.498
8.846 2.0 43.136
8.846 0.0 44.775
&BPNODE TNODE=3, TNPC=9, TINTC=3, &END
&SECT1 STX=0.0, STY=0.0, STZ=0.0, SCALE=1.0,
ALF=0.0, THETA=0.0,
INMODE=4, TNODS=0, TNPS=0, TINTS=0, &END
13.269 22.93 7.935
13.269 22.93 25.1
13.269 21.00 32.22
13.269 14.46 36.038
13.269 6.0 43.68
13.269 2.0 46.96
13.269 0.0 49.416
&BPNODE TNODE=3, TNPC=9, TINTC=3, &END
&SECT1 STX=0.0, STY=0.0, STZ=0.0, SCALE=1.0,
ALF=0.0, THETA=0.0,
INMODE=4, TNODS=0, TNPS=0, TINTS=0, &END
17.69 22.93 8.315
17.69 22.93 25.1
17.69 21.00 32.22
17.69 15.28 36.038
17.69 6.5 48.05
17.69 2.0 51.6
17.69 0.0 54.0
&BPNODE TNODE=3, TNPC=9, TINTC=3, &END
&SECT1 STX=0.0, STY=0.0, STZ=0.0, SCALE=1.0,
ALF=0.0, THETA=0.0,
INMODE=4, TNODS=0, TNPS=0, TINTS=0, &END
22.114 22.93 8.465
22.114 22.93 25.1
22.114 21.00 32.22
22.114 15.28 36.038
22.114 7.0 49.69
22.114 2.0 53.51
22.114 0.0 56.79
&BPNODE TNODE=3, TNPC=9, TINTC=3, &END
&SECT1 STX=0.0, STY=0.0, STZ=0.0, SCALE=1.0,
ALF=0.0, THETA=0.0,
INMODE=4, TNODS=0, TNPS=0, TINTS=0, &END
26.537 22.93 8.448

```

26.537	22.93	25.1			
26.537	21.00	32.22			
26.537	15.28	36.038			
26.537	8.5	55.15			
26.537	2.0	57.33			
26.537	0.0	58.97			
&BPNODE	TNODE=3,	TNPC=9,	TINTC=3,	&END	
&SECT1	STX=0.0,	STY=0.0,	STZ=0.0,	SCALE=1.0,	
	ALF=0.0,	THETA=0.0,			
	INMODE=4,	TNODS=0,	TNPS=0,	TINTS=0,	&END
35.383	22.93	8.023			
35.383	22.93	25.1			
35.383	21.00	32.22			
35.383	15.28	36.038			
35.383	9.0	55.15			
35.383	2.0	57.33			
35.383	0.0	58.97			
&BPNODE	TNODE=3,	TNPC=9,	TINTC=3,	&END	
&SECT1	STX=0.0,	STY=0.0,	STZ=0.0,	SCALE=1.0,	
	ALF=0.0,	THETA=0.0,			
	INMODE=4,	TNODS=0,	TNPS=0,	TINTS=0,	&END
44.229	22.93	7.236			
44.229	22.93	25.1			
44.229	21.00	32.22			
44.229	15.28	36.038			
44.229	9.0	55.15			
44.229	2.0	57.33			
44.229	0.0	58.97			
&BPNODE	TNODE=3,	TNPC=9,	TINTC=3,	&END	
&SECT1	STX=0.0,	STY=0.0,	STZ=0.0,	SCALE=1.0,	
	ALF=0.0,	THETA=0.0,			
	INMODE=4,	TNODS=0,	TNPS=0,	TINTS=0,	&END
53.07	22.93	6.183			
53.07	22.93	25.1			
53.07	21.00	32.22			
53.07	15.28	36.038			
53.07	9.0	55.15			
53.07	2.0	57.33			
53.07	0.0	58.97			
&BPNODE	TNODE=3,	TNPC=9,	TINTC=3,	&END	
&SECT1	STX=0.0,	STY=0.0,	STZ=0.0,	SCALE=1.0,	
	ALF=0.0,	THETA=0.0,			
	INMODE=4,	TNODS=0,	TNPS=0,	TINTS=0,	&END
61.92	22.93	4.918			
61.92	22.93	25.1			
61.92	21.00	32.22			
61.92	15.28	36.038			
61.92	9.0	55.15			
61.92	2.0	57.33			
61.92	0.0	58.97			
&BPNODE	TNODE=3,	TNPC=9,	TINTC=3,	&END	
&SECT1	STX=0.0,	STY=0.0,	STZ=0.0,	SCALE=1.0,	
	ALF=0.0,	THETA=0.0,			
	INMODE=4,	TNODS=0,	TNPS=0,	TINTS=0,	&END

70.766	22.93	2.609	
70.766	22.93	25.1	
70.766	21.00	32.22	
70.766	15.28	36.038	
70.766	9.0	55.15	
70.766	2.0	57.33	
70.766	0.0	58.97	
&BPNODE	TNODE=3, TNPC=9, TINTC=3,		&END
&SECT1	STX=0.0, STY=0.0, STZ=0.0, SCALE=1.0,		
	ALF=0.0, THETA=0.0,		
	INMODE=4, TNODS=0, TNPS=0, TINTS=0,		&END
79.61	22.93	1.911	
79.61	22.93	25.1	
79.61	21.00	32.22	
79.61	15.28	36.038	
79.61	9.0	55.15	
79.61	2.0	57.33	
79.61	0.0	58.97	
&BPNODE	TNODE=3, TNPC=9, TINTC=3,		&END
&SECT1	STX=0.0, STY=0.0, STZ=0.0, SCALE=1.0,		
	ALF=0.0, THETA=0.0,		
	INMODE=4, TNODS=0, TNPS=0, TINTS=0,		&END
84.03	22.93	1.053	
84.03	22.93	25.1	
84.03	21.00	32.22	
84.03	15.28	36.038	
84.03	9.0	55.15	
84.03	2.0	57.33	
84.03	0.0	58.97	
&BPNODE	TNODE=3, TNPC=9, TINTC=3,		&END
&SECT1	STX=0.0, STY=0.0, STZ=0.0, SCALE=1.0,		
	ALF=0.0, THETA=0.0,		
	INMODE=4, TNODS=3, TNPS=0, TINTS=0,		&END
88.457	22.93	0.0	
88.457	22.93	5.0	
88.457	22.93	10.0	
88.457	22.93	15.0	
88.457	22.93	20.0	
88.457	22.93	25.1	
88.457	21.00	32.22	
88.457	15.28	36.038	
88.457	9.0	55.15	
88.457	2.0	57.33	
88.457	0.0	58.97	
&BPNODE	TNODE=3, TNPC=9, TINTC=3,		&END
&PATCH1	IREV=0, IDPAT=2, MAKE=0, KCOMP=1, KASS=1,		&END
	T34 AFT FUESELAGE #6		
&SECT1	STX=0.0, STY=0.0, STZ=0.0, SCALE=1.0,		
	ALF=0.0, THETA=0.0,		
	INMODE=4, TNODS=0, TNPS=0, TINTS=0,		&END
88.457	0.0	0.0	
88.457	10.92	0.0	
88.457	18.57	0.0	

88.457	22.93	0.0			
88.457	22.93	5.0			
88.457	22.93	10.0			
88.457	22.93	15.0			
88.547	22.93	20.0			
88.457	22.93	25.1			
88.457	18.0	34.0			
88.457	15.28	36.038			
88.457	9.0	55.15			
88.457	4.0	57.33			
88.457	0.0	58.97			
&BPNODE	TNODE=3,	TNPC=12,	TINTC=3,	&END	
&SECT1	STX=0.0,	STY=0.0,	STZ=0.0,	SCALE=1.0,	
	ALF=0.0,	THETA=0.0,			
	INMODE=4,	TNODS=2,	TNPS=2,	TINTS=3,	&END
119.58	0.0	2.73			
119.58	10.92	2.73			
119.58	18.02	2.73			
119.58	18.02	21.30			
119.58	18.02	33.85			
119.58	14.74	39.31			
119.58	10.92	43.00			
119.58	0.0	48.05			
&BPNODE	TNODE=3,	TNPC=12,	TINTC=3,	&END	
&SECT1	STX=0.0,	STY=0.0,	STZ=0.0,	SCALE=1.0,	
	ALF=0.0,	THETA=0.0,			
	INMODE=4,	TNODS=2,	TNPS=2,	TINTS=3,	&END
127.77	0.0	4.37			
127.77	10.92	4.37			
127.77	16.93	4.37			
127.77	16.93	21.3			
127.77	16.93	33.85			
127.77	14.74	39.31			
127.77	10.37	42.04			
127.77	0.0	45.87			
&BPNODE	TNODE=3,	TNPC=12,	TINTC=3,	&END	
&SECT1	STX=0.0,	STY=0.0,	STZ=0.0,	SCALE=1.0,	
	ALF=0.0,	THETA=0.0,			
	INMODE=4,	TNODS=2,	TNPS=2,	TINTS=3,	&END
146.88	0.0	7.64			
146.88	10.92	7.64			
146.88	14.74	7.64			
146.88	14.74	21.3			
146.88	14.74	33.85			
146.88	13.00	38.5			
146.88	8.74	40.41			
146.88	0.0	44.22			
&BPNODE	TNODE=3,	TNPC=12,	TINTC=3,	&END	
&SECT1	STX=0.0,	STY=0.0,	STZ=0.0,	SCALE=1.0,	
	ALF=0.0,	THETA=0.0,			
	INMODE=4,	TNODS=2,	TNPS=2,	TINTS=3,	&END
179.64	0.0	13.3			
179.64	3.0	13.3			
179.64	7.00	13.3			

179.64	10.0	13.3	
179.64	11.3	13.3	
179.64	11.3	21.3	
179.64	11.3	27.84	
179.64	11.3	32.21	
179.64	5.46	38.22	
179.64	2.27	40.41	
179.64	0.0	46.96	
&BPNODE TNODE=3, TNPC=12, TINTC=3,			&END
&SECT1 STX=0.0, STY=0.0, STZ=0.0, SCALE=1.0,			
ALF=0.0, THETA=0.0,			
INMODE=4, TNODS=3, TNPS=0, TINTS=3,			&END
181.83	0.0	13.65	
181.83	3.0	13.65	
181.83	7.00	13.65	
181.83	9.0	13.65	
181.83	10.0	13.65	
181.83	10.5	13.65	
181.83	10.92	13.65	
181.83	10.92	14.5	
181.83	10.92	16.0	
181.83	10.92	21.3	
181.83	10.92	27.84	
181.83	10.92	32.216	
181.83	5.00	37.17	
181.83	2.6	39.86	
181.83	0.0	47.50	
&BPNODE TNODE=3, TNPC=12, TINTC=3,			&END
&PATCH1 IREV=0, IDPAT=1, MAKE=0, KCOMP=1, KASS=1,			&END
T34 HORIZONTAL TAIL #7			
&SECT1 STX=0.0, STY=0.0, STZ=0.0, SCALE=1.0,			
ALF=0.0, THETA=0.0,			
INMODE=4, TNODS=0, TNPS=0, TINTS=3,			&END
234.795	8.74	32.216	
230.645	8.74	31.816	
226.495	8.74	31.490	
222.345	8.74	31.202	
218.195	8.74	30.953	
214.045	8.74	30.751	
209.895	8.74	30.610	
205.745	8.74	30.556	
203.670	8.74	30.572	
201.595	8.74	30.629	
199.520	8.74	30.737	
197.445	8.74	30.921	
196.408	8.74	31.054	
195.370	8.74	31.233	
194.332	8.74	31.493	
193.814	8.74	31.692	
193.295	8.74	32.216	
&BPNODE TNODE=2, TNPC=15, TINTC=3,			&END
193.295	8.74	32.216	
193.814	8.74	32.740	

194.332 8.74 32.939
195.370 8.74 33.199
196.408 8.74 33.378
197.445 8.74 33.511
199.520 8.74 33.695
201.595 8.74 33.803
203.670 8.74 33.860
205.745 8.74 33.870
209.895 8.74 33.822
214.045 8.74 33.681
218.195 8.74 33.479
222.345 8.74 33.230
226.495 8.74 32.942
230.645 8.74 32.616
234.795 8.74 32.216

&BPNODE TNODE=3, TNPC=15, TINTC=3, &END

&SECT1 STX=0.0, STY=0.0, STZ=0.0, SCALE=1.0,

ALF=0.0, THETA=0.0,

INMODE=4, TNODS=3, TNPS=7, TINTS=3, &END

231.517 73.168 32.216
229.797 73.168 32.031
228.077 73.168 31.884
224.637 73.168 31.614
221.197 73.168 31.376
217.757 73.168 31.169
214.317 73.168 31.002
210.877 73.168 30.885
207.437 73.168 30.840
205.717 73.168 30.853
203.997 73.168 30.900
202.277 73.168 30.990
200.557 73.168 31.142
199.697 73.168 31.253
198.837 73.168 31.401
197.977 73.168 31.616
197.289 73.168 31.781
197.117 73.168 32.216

&BPNODE TNODE=2, TNPC=15, TINTC=3, &END

197.117 73.168 32.216
197.289 73.168 32.650
197.977 73.168 32.816
198.837 73.168 33.031
199.697 73.168 33.179
200.557 73.168 33.290
202.277 73.168 33.442
203.997 73.168 33.532
205.717 73.168 33.579
207.437 73.168 33.592
210.877 73.168 33.547
214.317 73.168 33.430
217.757 73.168 33.263
221.197 73.168 33.056
224.637 73.168 32.818
228.077 73.168 32.548

```

229.797  73.168  32.400
231.517  73.168  32.216
&BPNODE TNODE=3, TNPC=15, TINTC=3,                                &END

&PATCH1 IREV=0, IDPAT=1, MAKE=7, KCOMP=1, KASS=2,                &END
T34 HORIZONTAL TAIL TIP #8
&PATCH2 ITYP=1, TNODS=3, TNPS=2, TINTS=0, NPTTIP=0,            &END

&PATCH1 IREV=0, IDPAT=2, MAKE=0, KCOMP=1, KASS=1,                &END
T34 FUSELAGE UNDER TAIL #9
&SECT1 STX=0.0, STY=0.0, STZ=0.0, SCALE=1.0,
ALF=0.0, THETA=0.0,
INMODE=4, TNODS=0, TNPS=0, TINTS=0,                                &END
181.83   0.0   13.65
181.83   10.92  13.65
181.83   10.92  25.0
181.83   10.92  27.84
181.83   10.92  32.216
&BPNODE TNODE=3, TNPC=0, TINTC=0,                                &END
&SECT1 STX=0.0, STY=0.0, STZ=0.0, SCALE=1.0,
ALF=0.0, THETA=0.0,
INMODE=4, TNODS=2, TNPS=6, TINTS=0,                                &END
193.295  0.0   15.83
193.295  8.74  15.83
193.295  8.74  25.0
193.295  8.74  27.84
193.295  8.74  32.216
&BPNODE TNODE=3, TNPC=0, TINTC=0,                                &END
&SECT1 STX=0.0, STY=0.0, STZ=0.0, SCALE=1.0,
ALF=0.0, THETA=0.0,
INMODE=4, TNODS=0, TNPS=0, TINTS=0,                                &END
194.332  0.0   16.00
194.332  8.14  16.00
194.332  8.14  25.0
194.332  8.74  27.84
194.332  8.74  31.493
&BPNODE TNODE=3, TNPC=0, TINTC=0,                                &END
&SECT1 STX=0.0, STY=0.0, STZ=0.0, SCALE=1.0,
ALF=0.0, THETA=0.0,
INMODE=4, TNODS=0, TNPS=0, TINTS=0,                                &END
195.370  0.0   16.10
195.370  7.94  16.10
195.370  7.94  25.0
195.370  8.74  27.84
195.370  8.74  31.233
&BPNODE TNODE=3, TNPC=0, TINTC=0,                                &END
&SECT1 STX=0.0, STY=0.0, STZ=0.0, SCALE=1.0,
ALF=0.0, THETA=0.0,
INMODE=4, TNODS=0, TNPS=0, TINTS=0,                                &END
197.445  0.0   16.381
197.445  7.34  16.381
197.445  7.34  25.0
197.445  8.74  27.84
197.445  8.74  30.921

```

```

&BPNODE TNODE=3, TNPC=0, TINTC=0, &END
&SECT1 STX=0.0, STY=0.0, STZ=0.0, SCALE=1.0,
  ALF=0.0, THETA=0.0,
  INMODE=4, TNODS=0, TNPS=0, TINTS=0, &END
199.520 0.0 16.654
199.520 7.04 16.654
199.520 7.04 25.0
199.520 8.74 27.84
199.520 8.74 30.737
&BPNODE TNODE=3, TNPC=0, TINTC=0, &END
&SECT1 STX=0.0, STY=0.0, STZ=0.0, SCALE=1.0,
  ALF=0.0, THETA=0.0,
  INMODE=4, TNODS=0, TNPS=0, TINTS=0, &END
201.595 0.0 16.93
201.595 6.74 16.93
201.595 6.74 25.0
201.595 8.74 27.84
201.595 8.74 30.629
&BPNODE TNODE=3, TNPC=0, TINTC=0, &END
&SECT1 STX=0.0, STY=0.0, STZ=0.0, SCALE=1.0,
  ALF=0.0, THETA=0.0,
  INMODE=4, TNODS=0, TNPS=0, TINTS=0, &END
203.67 0.0 17.473
203.67 6.44 17.473
203.67 6.44 25.0
203.67 8.74 27.84
203.67 8.74 30.572
&BPNODE TNODE=3, TNPC=0, TINTC=0, &END
&SECT1 STX=0.0, STY=0.0, STZ=0.0, SCALE=1.0,
  ALF=0.0, THETA=0.0,
  INMODE=4, TNODS=0, TNPS=0, TINTS=0, &END
205.745 0.0 18.02
205.745 6.14 18.02
205.745 6.14 25.0
205.745 8.74 27.84
205.745 8.74 30.556
&BPNODE TNODE=3, TNPC=0, TINTC=0, &END
&SECT1 STX=0.0, STY=0.0, STZ=0.0, SCALE=1.0,
  ALF=0.0, THETA=0.0,
  INMODE=4, TNODS=0, TNPS=0, TINTS=0, &END
209.895 0.0 18.9
209.895 5.84 18.9
209.895 5.84 25.0
209.895 8.74 27.84
209.895 8.74 30.61
&BPNODE TNODE=3, TNPC=0, TINTC=0, &END
&SECT1 STX=0.0, STY=0.0, STZ=0.0, SCALE=1.0,
  ALF=0.0, THETA=0.0,
  INMODE=4, TNODS=0, TNPS=0, TINTS=0, &END
214.045 0.0 19.11
214.045 5.54 19.11
214.045 5.54 25.0
214.045 8.74 27.84
214.045 8.74 30.751

```

```

&BPNODE TNODE=3, TNPC=0, TINTC=0,                                &END
&SECT1 STX=0.0, STY=0.0, STZ=0.0, SCALE=1.0,
  ALF=0.0, THETA=0.0,
  INMODE=4, TNODS=0, TNPS=0, TINTS=0,                            &END
218.195  0.0  20.48
218.195  5.24 20.48
218.195  5.24 25.0
218.195  8.74 27.84
218.195  8.74 30.953
&BPNODE TNODE=3, TNPC=0, TINTC=0,                                &END
&SECT1 STX=0.0, STY=0.0, STZ=0.0, SCALE=1.0,
  ALF=0.0, THETA=0.0,
  INMODE=4, TNODS=0, TNPS=0, TINTS=0,                            &END
222.345  0.0  21.30
222.345  4.94 21.30
222.345  4.94 25.0
222.345  8.74 27.84
222.345  8.74 31.202
&BPNODE TNODE=3, TNPC=0, TINTC=0,                                &END
&SECT1 STX=0.0, STY=0.0, STZ=0.0, SCALE=1.0,
  ALF=0.0, THETA=0.0,
  INMODE=4, TNODS=0, TNPS=0, TINTS=0,                            &END
226.495  0.0  21.84
226.495  4.64 21.84
226.495  4.64 25.0
226.495  8.74 27.84
226.495  8.74 31.49
&BPNODE TNODE=3, TNPC=0, TINTC=0,                                &END
&SECT1 STX=0.0, STY=0.0, STZ=0.0, SCALE=1.0,
  ALF=0.0, THETA=0.0,
  INMODE=4, TNODS=0, TNPS=0, TINTS=0,                            &END
230.645  0.0  22.67
230.645  4.34 22.67
230.645  4.34 25.0
230.645  5.74 27.84
230.645  8.74 31.816
&BPNODE TNODE=3, TNPC=0, TINTC=0,                                &END
&SECT1 STX=0.0, STY=0.0, STZ=0.0, SCALE=1.0,
  ALF=0.0, THETA=0.0,
  INMODE=4, TNODS=0, TNPS=0, TINTS=0,                            &END
232.72   0.0  23.04
232.72   4.04 23.04
232.72   4.04 25.0
232.72   5.74 27.84
232.72   8.74 31.993
&BPNODE TNODE=3, TNPC=0, TINTC=0,                                &END
&SECT1 STX=0.0, STY=0.0, STZ=0.0, SCALE=1.0,
  ALF=0.0, THETA=0.0,
  INMODE=4, TNODS=0, TNPS=0, TINTS=0,                            &END
234.795  0.0  23.95
234.795  3.74 23.95
234.795  3.74 25.0
234.795  4.74 27.84
234.795  8.74 32.181

```

```

&BPNODE TNODE=3, TNPC=0, TINTC=0, &END
&SECT1 STX=0.0, STY=0.0, STZ=0.0, SCALE=1.0,
    ALF=0.0, THETA=0.0,
    INMODE=4, TNODS=3, TNPS=0, TINTS=0, &END
    235.5 0.0 23.95
    235.5 0.0 24.1
    235.5 0.0 25.0
    235.5 0.0 27.84
    235.5 0.0 32.181
&BPNODE TNODE=3, TNPC=0, TINTC=0, &END

&PATCH1 IREV=0, IDPAT=2, MAKE=0, KCOMP=1, KASS=1, &END
    T34 VERTICAL TAIL #10
&SECT1 STX=0.0, STY=0.0, STZ=0.0, SCALE=1.0,
    ALF=0.0, THETA=0.0,
    INMODE=4, TNODS=2, TNPS=0, TINTS=3, &END
    181.83 0.0 47.5
    198.76 0.0 98.83
    198.76 0.0 98.83
&BPNODE TNODE=3, TNPC=0, TINTC=3, &END
&SECT1 STX=0.0, STY=0.0, STZ=0.0, SCALE=1.0,
    ALF=0.0, THETA=0.0,
    INMODE=4, TNODS=2, TNPS=0, TINTS=3, &END
    182.47 0.49 47.5
    199.22 0.35 98.83
    199.22 0.0 98.83
&BPNODE TNODE=3, TNPC=0, TINTC=3, &END
&SECT1 STX=0.0, STY=0.0, STZ=0.0, SCALE=1.0,
    ALF=0.0, THETA=0.0,
    INMODE=4, TNODS=2, TNPS=0, TINTS=3, &END
    183.12 0.67 47.5
    199.69 0.48 98.83
    199.69 0.0 98.83
&BPNODE TNODE=3, TNPC=0, TINTC=3, &END
&SECT1 STX=0.0, STY=0.0, STZ=0.0, SCALE=1.0,
    ALF=0.0, THETA=0.0,
    INMODE=4, TNODS=2, TNPS=0, TINTS=3, &END
    184.41 0.92 47.5
    200.62 0.66 98.83
    200.62 0.0 98.83
&BPNODE TNODE=3, TNPC=0, TINTC=3, &END
&SECT1 STX=0.0, STY=0.0, STZ=0.0, SCALE=1.0,
    ALF=0.0, THETA=0.0,
    INMODE=4, TNODS=2, TNPS=0, TINTS=3, &END
    185.69 1.08 47.5
    201.54 0.78 98.83
    201.54 0.0 98.83
&BPNODE TNODE=3, TNPC=0, TINTC=3, &END
&SECT1 STX=0.0, STY=0.0, STZ=0.0, SCALE=1.0,
    ALF=0.0, THETA=0.0,
    INMODE=4, TNODS=2, TNPS=0, TINTS=3, &END
    186.98 1.21 47.5
    202.47 0.87 98.83
    202.47 0.0 98.83

```

```

&BPNODE TNODE=3, TNPC=0, TINTC=3, &END
&SECT1 STX=0.0, STY=0.0, STZ=0.0, SCALE=1.0,
  ALF=0.0, THETA=0.0,
  INMODE=4, TNODS=2, TNPS=0, TINTS=3, &END
  189.56 1.38 47.5
  204.33 0.99 98.83
  204.33 0.0 98.83
&BPNODE TNODE=3, TNPC=0, TINTC=3, &END
&SECT1 STX=0.0, STY=0.0, STZ=0.0, SCALE=1.0,
  ALF=0.0, THETA=0.0,
  INMODE=4, TNODS=2, TNPS=0, TINTS=3, &END
  192.13 1.48 47.5
  206.18 1.06 98.83
  206.18 0.0 98.83
&BPNODE TNODE=3, TNPC=0, TINTC=3, &END
&SECT1 STX=0.0, STY=0.0, STZ=0.0, SCALE=1.0,
  ALF=0.0, THETA=0.0,
  INMODE=4, TNODS=2, TNPS=0, TINTS=3, &END
  194.71 1.53 47.5
  208.04 1.0 98.83
  208.04 0.0 98.83
&BPNODE TNODE=3, TNPC=0, TINTC=3, &END
&SECT1 STX=0.0, STY=0.0, STZ=0.0, SCALE=1.0,
  ALF=0.0, THETA=0.0,
  INMODE=4, TNODS=2, TNPS=0, TINTS=3, &END
  197.28 1.55 47.5
  209.89 1.11 98.83
  209.89 0.0 98.83
&BPNODE TNODE=3, TNPC=0, TINTC=3, &END
&SECT1 STX=0.0, STY=0.0, STZ=0.0, SCALE=1.0,
  ALF=0.0, THETA=0.0,
  INMODE=4, TNODS=2, TNPS=0, TINTS=3, &END
  202.43 1.49 47.5
  213.60 1.08 98.83
  213.60 0.0 98.83
&BPNODE TNODE=3, TNPC=0, TINTC=3, &END
&SECT1 STX=0.0, STY=0.0, STZ=0.0, SCALE=1.0,
  ALF=0.0, THETA=0.0,
  INMODE=4, TNODS=2, TNPS=0, TINTS=3, &END
  207.58 1.36 47.5
  217.31 0.98 98.83
  217.31 0.0 98.83
&BPNODE TNODE=3, TNPC=0, TINTC=3, &END
&SECT1 STX=0.0, STY=0.0, STZ=0.0, SCALE=1.0,
  ALF=0.0, THETA=0.0,
  INMODE=4, TNODS=2, TNPS=0, TINTS=3, &END
  212.73 1.18 47.5
  221.02 0.85 98.83
  221.02 0.0 98.83
&BPNODE TNODE=3, TNPC=0, TINTC=3, &END
&SECT1 STX=0.0, STY=0.0, STZ=0.0, SCALE=1.0,
  ALF=0.0, THETA=0.0,
  INMODE=4, TNODS=2, TNPS=0, TINTS=3, &END
  217.88 0.94 47.5

```

```

224.73  0.68  98.83
224.73  0.0   98.83
&BPNODE TNODE=3, TNPC=0, TINTC=3, &END
&SECT1  STX=0.0, STY=0.0, STZ=0.0, SCALE=1.0,
      ALF=0.0, THETA=0.0,
      INMODE=4, TNODS=2, TNPS=0, TINTS=3, &END
223.03  0.68  47.5
228.44  0.49  98.83
228.44  0.0   98.83
&BPNODE TNODE=3, TNPC=0, TINTC=3, &END
&SECT1  STX=0.0, STY=0.0, STZ=0.0, SCALE=1.0,
      ALF=0.0, THETA=0.0,
      INMODE=4, TNODS=2, TNPS=0, TINTS=3, &END
228.18  0.37  47.5
232.15  0.27  98.83
232.15  0.0   98.83
&BPNODE TNODE=3, TNPC=0, TINTC=3, &END
&SECT1  STX=0.0, STY=0.0, STZ=0.0, SCALE=1.0,
      ALF=0.0, THETA=0.0,
      INMODE=4, TNODS=2, TNPS=0, TINTS=3, &END
230.76  0.21  47.5
234.01  0.15  98.83
234.01  0.0   98.83
&BPNODE TNODE=3, TNPC=0, TINTC=3, &END
&SECT1  STX=0.0, STY=0.0, STZ=0.0, SCALE=1.0,
      ALF=0.0, THETA=0.0,
      INMODE=4, TNODS=3, TNPS=0, TINTS=3, &END
233.33  0.0   47.5
235.86  0.0   98.83
235.86  0.0   98.83
&BPNODE TNODE=3, TNPC=0, TINTC=3, &END

&PATCH1 IREV=0, IDPAT=2, MAKE=0, KCOMP=1, KASS=1. &END
      T34 FUS BTWN HOR AND VERT TAIL 1HV #11
&SECT1  STX=0.0, STY=0.0, STZ=0.0, SCALE=1.0,
      ALF=0.0, THETA=0.0,
      INMODE=4, TNODS=0, TNPS=0, TINTS=0, &END
181.83  10.92  32.216
181.83  5.00  37.17
181.83  2.6   39.86
181.83  0.0   47.5
&BPNODE TNODE=3, TNPC=0, TINTC=0, &END
&SECT1  STX=0.0, STY=0.0, STZ=0.0, SCALE=1.0,
      ALF=0.0, THETA=0.0,
      INMODE=4, TNODS=0, TNPS=0, TINTS=0, &END
182.47  10.68  32.216
182.47  5.0   37.07
182.47  2.55  39.44
182.47  0.49  47.5
&BPNODE TNODE=3, TNPC=0, TINTC=0, &END
&SECT1  STX=0.0, STY=0.0, STZ=0.0, SCALE=1.0,
      ALF=0.0, THETA=0.0,
      INMODE=4, TNODS=0, TNPS=0, TINTS=0, &END
183.12  10.44  32.216

```

```

183.12    5.0    36.97
183.12    2.50   39.02
183.12    0.67   47.5
&BPNODE TNODE=3, TNPC=0, TINTC=0,                                &END
&SECT1 STX=0.0, STY=0.0, STZ=0.0, SCALE=1.0,
    ALF=0.0, THETA=0.0,
    INMODE=4, TNODS=0, TNPS=0, TINTS=0,                            &END
184.41    10.20  32.216
184.41     5.0   36.87
184.41     2.45  38.6
184.41     0.92  47.5
&BPNODE TNODE=3, TNPC=0, TINTC=0,                                &END
&SECT1 STX=0.0, STY=0.0, STZ=0.0, SCALE=1.0,
    ALF=0.0, THETA=0.0,
    INMODE=4, TNODS=0, TNPS=0, TINTS=0,                            &END
185.69     9.96  32.216
185.69     5.0   36.77
185.69     2.40  38.4
185.69     1.08  47.5
&BPNODE TNODE=3, TNPC=0, TINTC=0,                                &END
&SECT1 STX=0.0, STY=0.0, STZ=0.0, SCALE=1.0,
    ALF=0.0, THETA=0.0,
    INMODE=4, TNODS=0, TNPS=0, TINTS=0,                            &END
186.98     9.72  32.216
186.98     5.0   36.67
186.98     2.38  38.18
186.98     1.21  47.5
&BPNODE TNODE=3, TNPC=0, TINTC=0,                                &END
&SECT1 STX=0.0, STY=0.0, STZ=0.0, SCALE=1.0,
    ALF=0.0, THETA=0.0,
    INMODE=4, TNODS=0, TNPS=0, TINTS=0,                            &END
189.56     9.48  32.216
189.56     5.0   36.57
189.56     2.35  37.76
189.56     1.38  47.5
&BPNODE TNODE=3, TNPC=0, TINTC=0,                                &END
&SECT1 STX=0.0, STY=0.0, STZ=0.0, SCALE=1.0,
    ALF=0.0, THETA=0.0,
    INMODE=4, TNODS=0, TNPS=0, TINTS=0,                            &END
192.13     9.24  32.216
192.13     4.5   36.37
192.13     2.32  37.34
192.13     1.48  47.5
&BPNODE TNODE=3, TNPC=0, TINTC=0,                                &END
&SECT1 STX=0.0, STY=0.0, STZ=0.0, SCALE=1.0,
    ALF=0.0, THETA=0.0,
    INMODE=4, TNODS=3, TNPS=0, TINTS=0,                            &END
193.295    8.74  32.216
193.295    4.00  36.17
193.295    2.3   36.92
193.295    1.5   47.5
&BPNODE TNODE=3, TNPC=0, TINTC=0,                                &END
&PATCH1 IREV=0, IDPAT=2, MAKE=0, KCOMP=1, KASS=1,                &END

```

```

T34 FUS BTWN HOR AND VERT TAIL 2H #12
&SECT1 STX=0.0, STY=0.0, STZ=0.0, SCALE=1.0,
  ALF=0.0, THETA=0.0,
  INMODE=4, TNODS=0, TNPS=0, TINTS=0,
  193.295 8.74 32.216
  193.295 4.0 36.17
  193.295 2.3 36.92
  193.295 1.6 38.0
&BPNODE TNODE=3, TNPC=0, TINTC=0,
&SECT1 STX=0.0, STY=0.0, STZ=0.0, SCALE=1.0,
  ALF=0.0, THETA=0.0,
  INMODE=4, TNODS=0, TNPS=0, TINTS=0,
  193.814 8.74 32.74
  193.814 4.0 36.0
  193.814 2.3 36.82
  193.814 1.6 38.0
&BPNODE TNODE=3, TNPC=0, TINTC=0,
&SECT1 STX=0.0, STY=0.0, STZ=0.0, SCALE=1.0,
  ALF=0.0, THETA=0.0,
  INMODE=4, TNODS=0, TNPS=0, TINTS=0,
  194.332 8.74 32.939
  194.332 4.0 35.9
  194.332 2.3 36.72
  194.332 1.6 38.0
&BPNODE TNODE=3, TNPC=0, TINTC=0,
&SECT1 STX=0.0, STY=0.0, STZ=0.0, SCALE=1.0,
  ALF=0.0, THETA=0.0,
  INMODE=4, TNODS=0, TNPS=0, TINTS=0,
  195.37 8.74 33.199
  195.37 4.0 35.8
  195.37 2.3 36.62
  195.37 1.6 38.0
&BPNODE TNODE=3, TNPC=0, TINTC=0,
&SECT1 STX=0.0, STY=0.0, STZ=0.0, SCALE=1.0,
  ALF=0.0, THETA=0.0,
  INMODE=4, TNODS=0, TNPS=0, TINTS=0,
  196.408 8.74 33.378
  196.408 4.0 35.7
  196.408 2.3 36.52
  196.408 1.6 38.0
&BPNODE TNODE=3, TNPC=0, TINTC=0,
&SECT1 STX=0.0, STY=0.0, STZ=0.0, SCALE=1.0,
  ALF=0.0, THETA=0.0,
  INMODE=4, TNODS=0, TNPS=0, TINTS=0,
  197.445 8.74 33.511
  197.445 4.0 35.6
  197.445 2.3 36.42
  197.445 1.6 38.0
&BPNODE TNODE=3, TNPC=0, TINTC=0,
&SECT1 STX=0.0, STY=0.0, STZ=0.0, SCALE=1.0,
  ALF=0.0, THETA=0.0,
  INMODE=4, TNODS=0, TNPS=0, TINTS=0,
  199.520 8.74 33.695
  199.52 4.0 35.5

```

```

199.52  2.3  36.32
199.52  1.6  38.0
&BPNODE TNODE=3, TNPC=0, TINTC=0, &END
&SECT1 STX=0.0, STY=0.0, STZ=0.0, SCALE=1.0,
  ALF=0.0, THETA=0.0,
  INMODE=4, TNODS=0, TNPS=0, TINTS=0, &END
201.595  8.74  33.803
201.595  4.0  35.4
201.595  2.3  36.22
201.595  1.6  38.0
&BPNODE TNODE=3, TNPC=0, TINTC=0, &END
&SECT1 STX=0.0, STY=0.0, STZ=0.0, SCALE=1.0,
  ALF=0.0, THETA=0.0,
  INMODE=4, TNODS=0, TNPS=0, TINTS=0, &END
203.67  8.74  33.86
203.67  4.0  35.3
203.67  2.3  36.12
203.67  1.6  38.0
&BPNODE TNODE=3, TNPC=0, TINTC=0, &END
&SECT1 STX=0.0, STY=0.0, STZ=0.0, SCALE=1.0,
  ALF=0.0, THETA=0.0,
  INMODE=4, TNODS=0, TNPS=0, TINTS=0, &END
205.745  8.74  33.87
205.745  4.0  35.2
205.745  2.3  36.02
205.745  1.6  38.0
&BPNODE TNODE=3, TNPC=0, TINTC=0, &END
&SECT1 STX=0.0, STY=0.0, STZ=0.0, SCALE=1.0,
  ALF=0.0, THETA=0.0,
  INMODE=4, TNODS=0, TNPS=0, TINTS=0, &END
209.895  8.74  33.822
209.895  4.0  35.1
209.895  2.3  35.92
209.895  1.6  38.0
&BPNODE TNODE=3, TNPC=0, TINTC=0, &END
&SECT1 STX=0.0, STY=0.0, STZ=0.0, SCALE=1.0,
  ALF=0.0, THETA=0.0,
  INMODE=4, TNODS=0, TNPS=0, TINTS=0, &END
214.045  8.74  33.681
214.045  4.0  35.0
214.045  2.3  35.82
214.045  1.6  38.0
&BPNODE TNODE=3, TNPC=0, TINTC=0, &END
&SECT1 STX=0.0, STY=0.0, STZ=0.0, SCALE=1.0,
  ALF=0.0, THETA=0.0,
  INMODE=4, TNODS=0, TNPS=0, TINTS=0, &END
218.195  8.74  33.479
218.195  4.0  34.9
218.195  2.3  35.72
218.195  1.6  38.0
&BPNODE TNODE=3, TNPC=0, TINTC=0, &END
&SECT1 STX=0.0, STY=0.0, STZ=0.0, SCALE=1.0,
  ALF=0.0, THETA=0.0,
  INMODE=4, TNODS=0, TNPS=0, TINTS=0, &END

```

```

222.345  8.74  33.23
222.345  4.0   34.8
222.345  2.3   35.62
222.345  1.6   38.0
&BPNODE TNODE=3, TNPC=0, TINTC=0, &END
&SECT1 STX=0.0, STY=0.0, STZ=0.0, SCALE=1.0,
  ALF=0.0, THETA=0.0,
  INMODE=4, TNODS=0, TNPS=0, TINTS=0, &END
226.495  8.74  32.942
226.495  4.0   34.7
226.495  2.3   35.52
226.495  1.6   38.0
&BPNODE TNODF=3, TNPC=0, TINTC=0, &END
&SECT1 STX=0.0, STY=0.0, STZ=0.0, SCALE=1.0,
  ALF=0.0, THETA=0.0,
  INMODE=4, TNODS=0, TNPS=0, TINTS=0, &END
230.645  8.74  32.616
230.645  4.0   34.6
230.645  2.3   35.42
230.645  1.6   38.0
&BPNODE TNODE=3, TNPC=0, TINTC=0, &END
&SECT1 STX=0.0, STY=0.0, STZ=0.0, SCALE=1.0,
  ALF=0.0, THETA=0.0,
  INMODE=4, TNODS=0, TNPS=0, TINTS=0, &END
232.72   8.74  32.439
232.72   4.0   34.5
232.72   2.3   35.32
232.72   1.6   38.0
&BPNODE TNODE=3, TNPC=0, TINTC=0, &END
&SECT1 STX=0.0, STY=0.0, STZ=0.0, SCALE=1.0,
  ALF=0.0, THETA=0.0,
  INMODE=4, TNODS=0, TNPS=0, TINTS=0, &END
234.795  8.74  32.216
234.795  4.0   34.4
234.795  2.3   35.22
234.795  1.6   38.0
&BPNODE TNODE=3, TNPC=0, TINTC=0, &END
&SECT1 STX=0.0, STY=0.0, STZ=0.0, SCALE=1.0,
  ALF=0.0, THETA=0.0,
  INMODE=4, TNODS=3, TNPS=0, TINTS=0, &END
235.2    0.0   32.216
235.2    0.0   34.4
235.2    0.0   35.12
234.0    0.0   38.0
&BPNODE TNODE=3, TNPC=0, TINTC=0, &END

&PATCH1 IREV=0, IDPAT=2, MAKE=0, KCOMP=1, KASS=1, &END
  T34 FUS BTWN HOR AND VERT TAIL 3V #13
&SECT1 STX=0.0, STY=0.0, STZ=0.0, SCALE=1.0,
  ALF=0.0, THETA=0.0,
  INMODE=4, TNODS=0, TNPS=0, TINTS=0, &END
193.295  1.6   38.0
193.295  1.5   47.5
&BPNODE TNODE=3, TNPC=0, TINTC=0, &END

```

```

&SECT1 STX=0.0, STY=0.0, STZ=0.0, SCALE=1.0,
      ALF=0.0, THETA=0.0,
      INMODE=4, TNODS=0, TNPS=0, TINTS=0,
      194.71  1.6  38.0
      194.71  1.53  47.5
&BPNODE TNODE=3, TNPC=0, TINTC=0,
&SECT1 STX=0.0, STY=0.0, STZ=0.0, SCALE=1.0,
      ALF=0.0, THETA=0.0,
      INMODE=4, TNODS=0, TNPS=0, TINTS=0,
      197.28  1.6  38.0
      197.28  1.55  47.5
&BPNODE TNODE=3, TNPC=0, TINTC=0,
&SECT1 STX=0.0, STY=0.0, STZ=0.0, SCALE=1.0,
      ALF=0.0, THETA=0.0,
      INMODE=4, TNODS=0, TNPS=0, TINTS=0,
      202.43  1.6  38.0
      202.43  1.49  47.5
&BPNODE TNODE=3, TNPC=0, TINTC=0,
&SECT1 STX=0.0, STY=0.0, STZ=0.0, SCALE=1.0,
      ALF=0.0, THETA=0.0,
      INMODE=4, TNODS=0, TNPS=0, TINTS=0,
      207.58  1.6  38.0
      207.58  1.36  47.5
&BPNODE TNODE=3, TNPC=0, TINTC=0,
&SECT1 STX=0.0, STY=0.0, STZ=0.0, SCALE=1.0,
      ALF=0.0, THETA=0.0,
      INMODE=4, TNODS=0, TNPS=0, TINTS=0,
      212.73  1.6  38.0
      212.73  1.18  47.5
&BPNODE TNODE=3, TNPC=0, TINTC=0,
&SECT1 STX=0.0, STY=0.0, STZ=0.0, SCALE=1.0,
      ALF=0.0, THETA=0.0,
      INMODE=4, TNODS=0, TNPS=0, TINTS=0,
      217.88  1.6  38.0
      217.88  0.94  47.5
&BPNODE TNODE=3, TNPC=0, TINTC=0,
&SECT1 STX=0.0, STY=0.0, STZ=0.0, SCALE=1.0,
      ALF=0.0, THETA=0.0,
      INMODE=4, TNODS=0, TNPS=0, TINTS=0,
      223.03  1.6  38.0
      223.03  0.68  47.5
&BPNODE TNODE=3, TNPC=0, TINTC=0,
&SECT1 STX=0.0, STY=0.0, STZ=0.0, SCALE=1.0,
      ALF=0.0, THETA=0.0,
      INMODE=4, TNODS=0, TNPS=0, TINTS=0,
      228.18  1.6  38.0
      228.18  0.37  47.5
&BPNODE TNODE=3, TNPC=0, TINTC=0,
&SECT1 STX=0.0, STY=0.0, STZ=0.0, SCALE=1.0,
      ALF=0.0, THETA=0.0,
      INMODE=4, TNODS=0, TNPS=0, TINTS=0,
      230.76  1.6  38.0
      230.76  0.21  47.5
&BPNODE TNODE=3, TNPC=0, TINTC=0,

```

```

&SECT1 STX=0.0, STY=0.0, STZ=0.0, SCALE=1.0,
      ALF=0.0, THETA=0.0,
      INMODE=4, TNODS=0, TNPS=0, TINTS=0,
      233.33 1.6 38.0
      233.33 0.0 47.5
&BPNODE TNODE=3, TNPC=0, TINTC=0,
&SECT1 STX=0.0, STY=0.0, STZ=0.0, SCALE=1.0,
      ALF=0.0, THETA=0.0,
      INMODE=4, TNODS=3, TNPS=0, TINTS=0,
      234.0 0.0 38.0
      234.0 0.0 47.5
&BPNODE TNODE=3, TNPC=0, TINTC=0,

&PATCH1 IREV=0, IDPAT= 2, MAKE= 0, KCOMP= 2, KASS= 3, &END
F14 NOSE CONE #14
&SECT1 STX= 0.0000, STY= 0.0000, STZ= 0.0000, SCALE= 1.0000,
      ALF= 0.0, THETA= 0.0,
      INMODE= 4, TNODS= 0, TNPS= 0, TINTS= 0,
      93.00000 0.00000 131.50000
      93.00000 0.00000 131.50000
      93.00000 0.00000 131.50000
      93.00000 0.00000 131.50000
      93.00000 0.00000 131.50000
      93.00000 0.00000 131.50000
      93.00000 0.00000 131.50000
      93.00000 0.00000 131.50000
      93.00000 0.00000 131.50000
&BPNODE TNODE= 3, TNPC= 0, TINTC= 0,
&SECT1 STX= 0.0000, STY= 0.0000, STZ= 0.0000, SCALE= 1.0000,
      ALF= 0.0, THETA= 0.0,
      INMODE= 4, TNODS= 0, TNPS= 0, TINTS= 0,
      103.00000 0.00000 127.41701
      103.00000 2.13000 127.99400
      103.00000 3.87900 129.38200
      103.00000 4.68200 131.45700
      103.00000 4.63300 133.66901
      103.00000 4.04400 135.14101
      103.00000 2.96900 136.28101
      103.00000 1.57700 136.91800
      103.00000 0.00000 137.08299
&BPNODE TNODE= 3, TNPC= 0, TINTC= 0,
&SECT1 STX= 0.0000, STY= 0.0000, STZ= 0.0000, SCALE= 1.0000,
      ALF= 0.0, THETA= 0.0,
      INMODE= 4, TNODS= 0, TNPS= 0, TINTS= 0,
      116.23801 0.00000 123.50900
      116.23801 4.28500 124.68500
      116.23801 7.77400 127.46800
      116.23801 9.54400 131.54401
      116.23801 9.51700 135.97501
      116.23801 8.28300 138.98700
      116.23801 6.04300 141.30400
      116.23801 3.21400 142.77800

```

```

116.23801 0.00000 143.25700
&BPNODE TNODE= 3, TNPC= 0, TINTC= 0, &END
&SECT1 STX= 0.0000, STY= 0.0000, STZ= 0.0000, SCALE= 1.0000,
ALF= 0.0, THETA= 0.0,
INMODE= 4, TNODS= 0, TNPS= 0, TINTS= 0, &END
133.02400 0.00000 120.12601
133.02400 6.51000 121.62900
133.02400 11.79000 125.72900
133.02400 14.50300 131.82800
133.02400 14.48400 138.50101
133.02400 12.63100 143.14600
133.02400 9.20500 146.74001
133.02400 4.91000 149.18500
133.02400 0.00000 150.00800
&BPNODE TNODE= 3, TNPC= 0, TINTC= 0, &END
&SECT1 STX= 0.0000, STY= 0.0000, STZ= 0.0000, SCALE= 1.0000,
ALF= 0.0, THETA= 0.0,
INMODE= 4, TNODS= 0, TNPS= 0, TINTS= 0, &END
153.68600 0.00000 117.67900
153.68600 8.73900 119.05800
153.68600 15.82700 124.28101
153.68600 19.35200 132.37300
153.68600 19.28300 141.22099
153.68600 16.89700 147.56000
153.68600 12.34600 152.53600
153.68600 6.61300 156.03900
153.68600 0.00000 157.18800
&BPNODE TNODE= 3, TNPC= 0, TINTC= 0, &END
&SECT1 STX= 0.0000, STY= 0.0000, STZ= 0.0000, SCALE= 1.0000,
ALF= 0.0, THETA= 0.0,
INMODE= 4, TNODS= 0, TNPS= 0, TINTS= 0, &END
178.57300 0.00000 117.08900
178.57300 10.37500 118.23801
178.57300 19.10200 123.87100
178.57300 23.54800 133.21300
178.57300 23.30400 143.62100
178.57300 20.45399 151.51801
178.57300 15.28600 158.09599
178.57300 8.22000 162.42900
178.57300 0.00000 163.96500
&BPNODE TNODE= 3, TNPC= 0, TINTC= 0, &END
&SECT1 STX= 0.0000, STY= 0.0000, STZ= 0.0000, SCALE= 1.0000,
ALF= 0.0, THETA= 0.0,
INMODE= 4, TNODS= 0, TNPS= 0, TINTS= 0, &END
208.05000 0.00000 118.00000
208.05000 11.66900 118.07700
208.05000 21.59200 123.72800
208.05000 26.31100 134.23700
208.05000 26.10600 145.88000
208.05000 23.01401 155.58600
208.05000 17.26601 163.95900
208.05000 9.82200 170.55701
208.05000 0.00000 172.95399
&BPNODE TNODE= 3, TNPC= 0, TINTC= 0, &END

```

```

&SECT1 STX= 0.0000, STY= 0.0000, STZ= 0.0000, SCALE= 1.0000,
  ALF= 0.0, THETA= 0.0,
  INMODE= 4, TNODS= 0, TNPS= 0, TINTS= 0, &END
242.50500 0.00000 118.53799
242.50500 12.89300 118.53799
242.50500 24.25000 124.16200
242.50500 29.02000 135.87700
242.50500 27.78101 148.71400
242.50500 23.29300 161.87100
242.50500 16.32100 173.58900
242.50500 12.03400 186.30701
242.50500 0.00000 192.42900
&BPNODE TNODE= 3, TNPC= 0, TINTC= 0, &END
&SECT1 STX= 0.0000, STY= 0.0000, STZ= 0.0000, SCALE= 1.0000,
  ALF= 0.0, THETA= 0.0,
  INMODE= 4, TNODS= 0, TNPS= 0, TINTS= 0, &END
282.34595 0.00000 119.48500
282.34595 14.21600 119.48500
282.34595 26.76700 124.61500
282.34595 30.03900 138.00000
282.34595 28.83099 152.14200
282.34595 24.04201 166.91901
282.34595 16.33200 179.94299
282.34595 13.20600 194.35699
282.34595 0.00000 201.38699
&BPNODE TNODE= 3, TNPC= 0, TINTC= 0, &END
&SECT1 STX= 0.0000, STY= 0.0000, STZ= 0.0000, SCALE= 1.0000,
  ALF= 0.0, THETA= 0.0,
  INMODE= 4, TNODS= 3, TNPS= 0, TINTS= 0, &END
328.00000 0.00000 121.00000
328.00000 14.86000 121.00000
328.00000 28.51601 125.18899
328.00000 30.58900 139.50000
328.00000 29.24100 154.28600
328.00000 25.38100 168.91600
328.00000 17.39000 181.56599
328.00000 12.95200 195.45200
328.00000 0.00000 202.50000
&BPNODE TNODE= 3, TNPC= 0, TINTC= 0, &END

&PATCH1 IREV=0, IDPAT= 2, MAKE= 0, KCOMP= 2, KASS= 3, &END
  F14 INLET REGION FORWARD #15
&SECT1 STX= 0.0000, STY= 0.0000, STZ= 0.0000, SCALE= 1.0000,
  ALF= 0.0, THETA= 0.0,
  INMODE= 4, TNODS= 0, TNPS= 0, TINTS= 0, &END
328.00000 0.00000 121.00000
328.00000 14.86000 121.00000
328.00000 28.51601 125.18899
328.00000 30.58900 139.50000
328.00000 29.24100 154.28600
328.00000 37.00000 154.70000
328.00000 66.20000 159.70000
328.00000 66.20000 159.70000
328.00000 66.20000 159.70000

```

```

328.00000  51.61000  157.39999
328.00000  37.00000  154.70000
328.00000  29.24100  154.28600
328.00000  25.38100  168.91600
328.00000  17.39000  181.56599
328.00000  12.95200  195.45200
328.00000   0.00000  202.50000
&BPNODE TNODE=  3, TNPC=  0, TINTC=  0, &END
&SECT1 STX=  0.0000, STY=  0.0000, STZ=  0.0000, SCALE=  1.0000,
ALF=  0.0, THETA=  0.0,
INMODE=  4, TNODS=  0, TNPS=  0, TINTS=  0, &END
357.08691   0.00000  122.01800
357.08691  14.14000  122.01800
357.08691  27.86501  124.20000
357.08691  31.13400  137.08099
357.08691  30.26401  151.18201
357.08691  37.00000  152.22800
357.08691  67.61800  157.86400
357.08691  69.50101  158.76900
357.08691  70.54401  160.34000
357.08691  54.00101  161.64700
357.08691  35.98199  159.46300
357.08691  28.72700  158.54500
357.08691  24.83299  171.10201
357.08691  17.64301  182.00000
357.08691  11.81700  193.49899
357.08691   0.00000  198.79100
&BPNODE TNODE=  3, TNPC=  0, TINTC=  0, &END
&SECT1 STX=  0.0000, STY=  0.0000, STZ=  0.0000, SCALE=  1.0000,
ALF=  0.0, THETA=  0.0,
INMODE=  4, TNODS=  0, TNPS=  0, TINTS=  0, &END
386.17505   0.00000  123.24699
386.17505  12.78800  123.24699
386.17505  25.44200  123.75900
386.17505  30.56300  133.70799
386.17505  30.07500  146.43800
386.17505  37.04900  147.28700
386.17505  68.82201  154.23399
386.17505  75.02901  156.59399
386.17505  80.02100  160.00200
386.17505  58.87100  165.02200
386.17505  34.87601  162.34599
386.17505  27.45100  161.24699
386.17505  24.01199  171.91400
386.17505  17.36400  180.76601
386.17505  10.32100  189.32600
386.17505   0.00000  193.44000
&BPNODE TNODE=  3, TNPC=  0, TINTC=  0, &END
&SECT1 STX=  0.0000, STY=  0.0000, STZ=  0.0000, SCALE=  1.0000,
ALF=  0.0, THETA=  0.0,
INMODE=  4, TNODS=  0, TNPS=  0, TINTS=  0, &END
415.26294   0.00000  124.44099
415.26294  11.16300  124.44099
415.26294  22.29300  124.55701

```

```

415.26294 29.54201 130.31599
415.26294 29.44800 141.43401
415.26294 37.09000 142.61800
415.26294 69.68401 150.79601
415.26294 81.52000 154.37601
415.26294 91.67900 159.97301
415.26294 65.19400 167.75000
415.26294 34.42599 163.95200
415.26294 26.56400 162.25700
415.26294 22.86800 171.35600
415.26294 16.87900 178.78200
415.26294 9.18000 184.71300
415.26294 0.00000 187.72400
&BPNODE TNODE= 3, TNPC= 0, TINTC= 0, &END
&SECT1 STX= 0.0000, STY= 0.0000, STZ= 0.0000, SCALE= 1.0000,
ALF= 0.0, THETA= 0.0,
INMODE= 4, TNODS= 3, TNPS= 0, TINTS= 0, &END
444.35107 0.00000 125.88400
444.35107 8.36100 125.88400
444.35107 16.71700 125.90199
444.35107 24.23399 127.19800
444.35107 27.81599 132.70300
444.35107 37.41299 134.37399
444.35107 70.11400 147.76100
444.35107 87.96400 152.57401
444.35107 103.00700 160.05800
444.35107 71.23000 170.03200
444.35107 34.35699 165.24200
444.35107 24.38800 162.92799
444.35107 20.74600 170.36200
444.35107 15.17400 176.36000
444.35107 7.97000 180.43201
444.35107 0.00000 182.50600
&BPNODE TNODE= 3, TNPC= 0, TINTC= 0, &END

&PATCH1 IREV=0, IDPAT= 2, MAKE= 0, KCOMP= 2, KASS= 3, &END
F14 INLET SIDE OUT #16
&SECT1 STX= 0.0000, STY= 0.0000, STZ= 0.0000, SCALE= 1.0000,
ALF= 0.0, THETA= 0.0,
INMODE= 4, TNODS= 0, TNPS= 0, TINTS= 0, &END
328.00000 66.20000 159.70000
328.00000 66.20000 159.70000
328.00000 66.20000 159.70000
328.00000 66.20000 159.70000
328.00000 66.20000 159.70000
328.00000 66.20000 159.70000
&BPNODE TNODE= 3, TNPC= 0, TINTC= 0, &END
&SECT1 STX= 0.0000, STY= 0.0000, STZ= 0.0000, SCALE= 1.0000,
ALF= 0.0, THETA= 0.0,
INMODE= 4, TNODS= 0, TNPS= 0, TINTS= 0, &END
357.08691 66.61800 157.86400
357.08691 66.82899 153.14799
357.08691 67.16499 148.43700
357.08691 68.16499 148.43700

```

```

357.08691 67.82899 153.14799
357.08691 67.61800 157.86400
&BPNODE TNODE= 3, TNPC= 0, TINTC= 0, &END
&SECT1 STX= 0.0000, STY= 0.0000, STZ= 0.0000, SCALE= 1.0000,
ALF= 0.0, THETA= 0.0,
INMODE= 4, TNODS= 0, TNPS= 0, TINTS= 0, &END
386.17505 67.82201 154.23399
386.17505 68.60899 145.74001
386.17505 69.13699 137.22099
386.17505 70.13699 137.22099
386.17505 69.60899 145.74001
386.17505 68.82201 154.23399
&BPNODE TNODE= 3, TNPC= 0, TINTC= 0, &END
&SECT1 STX= 0.0000, STY= 0.0000, STZ= 0.0000, SCALE= 1.0000,
ALF= 0.0, THETA= 0.0,
INMODE= 4, TNODS= 0, TNPS= 0, TINTS= 0, &END
415.26294 68.68401 150.79601
415.26294 70.55299 138.46600
415.26294 71.10500 126.01199
415.26294 72.10500 126.01199
415.26294 71.55299 138.46600
415.26294 69.68401 150.79601
&BPNODE TNODE= 3, TNPC= 0, TINTC= 0, &END
&SECT1 STX= 0.0000, STY= 0.0000, STZ= 0.0000, SCALE= 1.0000,
ALF= 0.0, THETA= 0.0,
INMODE= 4, TNODS= 3, TNPS= 0, TINTS= 0, &END
444.35107 69.11400 147.76100
444.35107 71.67500 131.95000
444.35107 70.13499 117.03900
444.35107 71.13499 117.03900
444.35107 72.67500 131.95000
444.35107 70.11400 147.76100
&BPNODE TNODE= 3, TNPC= 0, TINTC= 0, &END
&PATCH1 IREV= 0, IDPAT= 2, MAKE= 0, KCOMP= 2, KASS= 3, &END
F14 INLET FACE #17
&SECT1 STX= 0.0000, STY= 0.0000, STZ= 0.0000, SCALE= 1.0000,
ALF= 0.0, THETA= 0.0,
INMODE= 4, TNODS= 0, TNPS= 0, TINTS= 0, &END
444.35107 45.38000 112.40401
444.35107 39.77499 122.21201
444.35107 37.41299 134.37399
&BPNODE TNODE= 3, TNPC= 0, TINTC= 0, &END
&SECT1 STX= 0.0000, STY= 0.0000, STZ= 0.0000, SCALE= 1.0000,
ALF= 0.0, THETA= 0.0,
INMODE= 4, TNODS= 0, TNPS= 0, TINTS= 0, &END
444.35107 58.25800 114.72200
444.35107 56.22500 127.08101
444.35107 53.76349 141.06750
&BPNODE TNODE= 3, TNPC= 0, TINTC= 0, &END
&SECT1 STX= 0.0000, STY= 0.0000, STZ= 0.0000, SCALE= 1.0000,
ALF= 0.0, THETA= 0.0,
INMODE= 4, TNODS= 3, TNPS= 0, TINTS= 0, &END
444.35107 71.13499 117.03900

```

```

444.35107 72.67500 131.95000
444.35107 70.11400 147.76100
&BPNODE TNODE= 3, TNPC= 0, TINTC= 0, &END

&PATCH1 IREV= 0, IDPAT= 2, MAKE= 0, KCOMP= 2, KASS= 4, &END
F14 INLET REGION AFT #18
&SECT1 STX= 0.0000, STY= 0.0000, STZ= 0.0000, SCALE= 1.0000,
ALF= 0.0, THETA= 0.0,
INMODE= 4, TNODS= 0, TNPS= 0, TINTS= 0, &END
444.35107 0.00000 125.88400
444.35107 8.36100 125.88400
444.35107 16.71700 125.90199
444.35107 24.23399 127.19800
444.35107 27.81599 132.70300
444.35107 37.41299 134.37399
444.35107 39.77499 122.21201
444.35107 45.38000 112.40401
444.35107 58.25800 114.72200
444.35107 71.13499 117.03900
444.35107 72.67500 131.95000
444.35107 70.11400 147.76100
444.35107 87.96400 152.57401
444.35107 103.00700 160.05800
444.35107 71.23000 170.03200
444.35107 34.35699 165.24200
444.35107 24.38800 162.92799
444.35107 20.74600 170.36200
444.35107 15.17400 176.36000
444.35107 7.97000 180.43201
444.35107 0.00000 182.50600
&BPNODE TNODE= 3, TNPC= 0, TINTC= 0, &END
&SECT1 STX= 0.0000, STY= 0.0000, STZ= 0.0000, SCALE= 1.0000,
ALF= 0.0, THETA= 0.0,
INMODE= 4, TNODS= 0, TNPS= 0, TINTS= 0, &END
473.43799 0.00000 127.17400
473.43799 6.60500 127.17400
473.43799 13.21100 127.17400
473.43799 19.81500 127.17400
473.43799 26.34599 127.86700
473.43799 38.01900 128.03999
473.43799 40.06000 116.52699
473.43799 47.74100 109.59900
473.43799 58.27699 111.42300
473.43799 68.81300 113.24600
473.43799 73.53500 127.91299
473.43799 70.76700 144.75900
473.43799 94.41499 151.69299
473.43799 114.50301 159.95900
473.43799 77.30400 171.36800
473.43799 34.08701 166.06700
473.43799 22.09900 163.22701
473.43799 18.43300 169.16000
473.43799 13.36900 173.84801
473.43799 6.88200 176.34300

```

```

473.43799 0.00000 177.56500
&BPNODE TNODE= 3, TNPC= 0, TINTC= 0, &END
&SECT1 STX= 0.0000, STY= 0.0000, STZ= 0.0000, SCALE= 1.0000,
ALF= 0.0, THETA= 0.0,
INMODE= 4, TNODS= 3, TNPS= 0, TINTS= 0, &END
502.52588 0.00000 128.58400
502.52588 6.71300 128.58400
502.52588 13.42700 128.58400
502.52588 20.14000 128.58400
502.52588 26.85300 128.58400
502.52588 35.79401 128.58400
502.52588 38.81200 114.92200
502.52588 49.58400 108.03599
502.52588 58.37900 109.60500
502.52588 67.17300 111.17300
502.52588 73.88800 125.70500
502.52588 71.30099 142.89500
502.52588 100.27901 151.67700
502.52588 124.46500 161.01900
502.52588 82.08000 171.69000
502.52588 34.00000 166.54100
502.52588 18.95100 163.46100
502.52588 15.44200 167.86800
502.52588 10.95000 171.23801
502.52588 5.61800 173.00200
502.52588 0.00000 173.55099
&BPNODE TNODE= 3, TNPC= 0, TINTC= 0, &END

&PATCH1 IREV= 0, IDPAT= 2, MAKE= 0, KCOMP= 2, KASS= 3, &END
F14 UPPER WING ROOT REGION #19
&SECT1 STX= 0.0000, STY= 0.0000, STZ= 0.0000, SCALE= 1.0000,
ALF= 0.0, THETA= 0.0,
INMODE= 4, TNODS= 0, TNPS= 0, TINTS= 0, &END
502.52588 124.46500 161.01900
502.52588 82.08000 171.69000
502.52588 34.00000 166.54100
502.52588 18.95100 163.46100
502.52588 15.44200 167.86800
502.52588 10.95000 171.23801
502.52588 5.61800 173.00200
502.52588 0.00000 173.55099
&BPNODE TNODE= 3, TNPC= 0, TINTC= 0, &END
&SECT1 STX= 0.0000, STY= 0.0000, STZ= 0.0000, SCALE= 1.0000,
ALF= 0.0, THETA= 0.0,
INMODE= 4, TNODS= 0, TNPS= 0, TINTS= 0, &END
506.24194 125.32700 163.75900
506.24194 81.28200 171.63800
506.24194 34.00000 166.56799
506.24194 18.58299 163.50200
506.24194 15.08500 167.72501
506.24194 10.66200 170.94000
506.24194 5.46700 172.64600
506.24194 0.00000 173.18201
&BPNODE TNODE= 3, TNPC= 0, TINTC= 0, &END

```

```

&SECT1 STX= 0.0000, STY= 0.0000, STZ= 0.0000, SCALE= 1.0000,
  ALF= 0.0, THETA= 0.0,
  INMODE= 4, TNODS= 0, TNPS= 0, TINTS= 0, &END
  511.12305 126.10500 165.30200
  511.12305 80.66299 171.57500
  511.12305 34.00000 166.60400
  511.12305 18.09801 163.55600
  511.12305 14.61600 167.53500
  511.12305 10.28500 170.54800
  511.12305 5.27000 172.17799
  511.12305 0.00000 172.69800
&BPNODE TNODE= 3, TNPC= 0, TINTC= 0, &END
&SECT1 STX= 0.0000, STY= 0.0000, STZ= 0.0000, SCALE= 1.0000,
  ALF= 0.0, THETA= 0.0,
  INMODE= 4, TNODS= 0, TNPS= 0, TINTS= 0, &END
  517.27002 125.32400 166.69701
  517.27002 79.91299 171.49200
  517.27002 34.00000 166.64900
  517.27002 17.48801 163.62300
  517.27002 14.02900 167.29401
  517.27002 9.81600 170.05200
  517.27002 5.02500 171.58800
  517.27002 0.00000 172.08800
&BPNODE TNODE= 3, TNPC= 0, TINTC= 0, &END
&SECT1 STX= 0.0000, STY= 0.0000, STZ= 0.0000, SCALE= 1.0000,
  ALF= 0.0, THETA= 0.0,
  INMODE= 4, TNODS= 0, TNPS= 0, TINTS= 0, &END
  524.79297 124.90900 167.69901
  524.79297 79.59300 171.37601
  524.79297 34.00000 166.70000
  524.79297 16.80499 163.73300
  524.79297 13.33400 166.98900
  524.79297 9.26200 169.44200
  524.79297 4.73600 170.86900
  524.79297 0.00000 171.35400
&BPNODE TNODE= 3, TNPC= 0, TINTC= 0, &END
&SECT1 STX= 0.0000, STY= 0.0000, STZ= 0.0000, SCALE= 1.0000,
  ALF= 0.0, THETA= 0.0,
  INMODE= 4, TNODS= 0, TNPS= 0, TINTS= 0, &END
  533.80591 119.49400 168.57700
  533.80591 76.75900 170.82401
  533.80591 34.00000 166.70000
  533.80591 16.88800 164.22900
  533.80591 12.89000 166.42300
  533.80591 8.89900 168.67799
  533.80591 4.54500 170.05299
  533.80591 0.00000 170.65100
&BPNODE TNODE= 3, TNPC= 0, TINTC= 0, &END
&SECT1 STX= 0.0000, STY= 0.0000, STZ= 0.0000, SCALE= 1.0000,
  ALF= 0.0, THETA= 0.0,
  INMODE= 4, TNODS= 0, TNPS= 0, TINTS= 0, &END
  544.42896 112.61700 168.84599
  544.42896 73.29201 170.20599
  544.42896 34.00000 166.70000

```

```

544.42896 16.98599 164.81300
544.42896 12.76300 165.47501
544.42896 8.76700 167.63000
544.42896 4.48000 169.06100
544.42896 0.00000 169.82201
&BPNODE TNODE= 3, TNPC= 0, TINTC= 0, &END
&SECT1 STX= 0.0000, STY= 0.0000, STZ= 0.0000, SCALE= 1.0000,
ALF= 0.0, THETA= 0.0,
INMODE= 4, TNODS= 0, TNPS= 0, TINTS= 0, &END
556.78906 103.03000 168.47600
556.78906 68.48599 169.35800
556.78906 34.00000 166.50700
556.78906 17.53900 164.55299
556.78906 13.06700 164.62100
556.78906 8.87000 166.45799
556.78906 4.53400 167.91400
556.78906 0.00000 168.62100
&BPNODE TNODE= 3, TNPC= 0, TINTC= 0, &END
&SECT1 STX= 0.0000, STY= 0.0000, STZ= 0.0000, SCALE= 1.0000,
ALF= 0.0, THETA= 0.0,
INMODE= 4, TNODS= 0, TNPS= 0, TINTS= 0, &END
571.02002 98.51700 167.31900
571.02002 66.23199 168.46899
571.02002 34.00000 166.25301
571.02002 18.25101 164.09599
571.02002 13.56100 163.64900
571.02002 9.12400 165.07001
571.02002 4.66700 166.58400
571.02002 0.00000 167.19800
&BPNODE TNODE= 3, TNPC= 0, TINTC= 0, &END
&SECT1 STX= 0.0000, STY= 0.0000, STZ= 0.0000, SCALE= 1.0000,
ALF= 0.0, THETA= 0.0,
INMODE= 4, TNODS= 0, TNPS= 0, TINTS= 0, &END
587.26099 90.91499 165.54300
587.26099 62.46899 166.91200
587.26099 34.00000 165.23100
587.26099 18.91000 163.79601
587.26099 14.11600 163.38200
587.26099 9.40000 164.08900
587.26099 4.77400 165.39900
587.26099 0.00000 165.93100
&BPNODE TNODE= 3, TNPC= 0, TINTC= 0, &END
&SECT1 STX= 0.0000, STY= 0.0000, STZ= 0.0000, SCALE= 1.0000,
ALF= 0.0, THETA= 0.0,
INMODE= 4, TNODS= 0, TNPS= 0, TINTS= 0, &END
605.66089 85.64600 163.09500
605.66089 60.12300 165.03700
605.66089 34.40401 163.97600
605.66089 19.48100 163.31700
605.66089 14.57800 163.09000
605.66089 9.70100 163.18401
605.66089 4.88800 164.12300
605.66089 0.00000 164.51500
&BPNODE TNODE= 3, TNPC= 0, TINTC= 0, &END

```

```

&SECT1 STX= 0.0000, STY= 0.0000, STZ= 0.0000, SCALE= 1.0000,
      ALF= 0.0, THETA= 0.0,
      INMODE= 4, TNODS= 3, TNPS= 0, TINTS= 0, &END
      626.37207 85.03799 159.84200
      626.37207 61.09300 162.53000
      626.37207 35.88400 162.79300
      626.37207 19.77699 162.28101
      626.37207 14.82800 162.26500
      626.37207 9.88100 162.31300
      626.37207 4.94700 162.65100
      626.37207 0.00000 162.73900

```

```

&BPNODE TNODE= 3, TNPC= 0, TINTC= 0, &END

```

```

&PATCH1 IREV= 0, IDPAT= 2, MAKE= 0, KCOMP= 2, KASS= 3, &END
F14 LOWER WING ROOT REGION #20

```

```

&SECT1 STX= 0.0000, STY= 0.0000, STZ= 0.0000, SCALE= 1.0000,
      ALF= 0.0, THETA= 0.0,
      INMODE= 4, TNODS= 0, TNPS= 0, TINTS= 0, &END
      502.52588 0.00000 128.58400
      502.52588 6.71300 128.58400
      502.52588 13.42700 128.58400
      502.52588 20.14000 128.58400
      502.52588 26.85300 128.58400
      502.52588 35.79401 128.58400
      502.52588 38.81200 114.92200
      502.52588 49.58400 108.03599
      502.52588 58.37900 109.60500
      502.52588 67.17300 111.17300
      502.52588 73.88800 125.70500
      502.52588 71.30099 142.89500
      502.52588 100.27901 151.67700
      502.52588 124.46500 161.01900

```

```

&BPNODE TNODE= 3, TNPC= 0, TINTC= 0, &END

```

```

&SECT1 STX= 0.0000, STY= 0.0000, STZ= 0.0000, SCALE= 1.0000,
      ALF= 0.0, THETA= 0.0,
      INMODE= 4, TNODS= 0, TNPS= 0, TINTS= 0, &END
      506.24194 0.00000 128.77600
      506.24194 6.85700 128.77499
      506.24194 13.71400 128.77600
      506.24194 20.57001 128.77499
      506.24194 27.42700 128.77600
      506.24194 35.52000 128.77600
      506.24194 38.66901 114.88300
      506.24194 49.77600 107.85800
      506.24194 58.33099 109.37199
      506.24194 66.88600 110.88600
      506.24194 73.89600 125.42999
      506.24194 71.37000 142.69000
      506.24194 99.88100 151.27299
      506.24194 124.81900 158.46100

```

```

&BPNODE TNODE= 3, TNPC= 0, TINTC= 0, &END

```

```

&SECT1 STX= 0.0000, STY= 0.0000, STZ= 0.0000, SCALE= 1.0000,
      ALF= 0.0, THETA= 0.0,
      INMODE= 4, TNODS= 0, TNPS= 0, TINTS= 0, &END

```

511.12305	0.00000	129.02699			
511.12305	7.04500	129.02699			
511.12305	14.09000	129.02699			
511.12305	21.13499	129.02699			
511.12305	28.18100	129.02699			
511.12305	35.16200	129.02699			
511.12305	38.48100	114.82600			
511.12305	50.02699	107.62500			
511.12305	58.26801	109.06700			
511.12305	66.50999	110.50999			
511.12305	73.90700	125.06500			
511.12305	71.46001	142.42101			
511.12305	100.25700	151.17101			
511.12305	125.66400	157.50500			
&BPNODE	TNODE= 3,	TNPC= 0,	TINTC= 0,	&END	
&SECT1	STX= 0.0000,	STY= 0.0000,	STZ= 0.0000,	SCALE= 1.0000,	
	ALF= 0.0,	THETA= 0.0,			
INMODE=	4,	TNODS= 0,	TNPS= 0,	TINTS= 0,	&END
517.27002	0.00000	129.34300			
517.27002	7.28200	129.34300			
517.27002	14.56500	129.34300			
517.27002	21.84700	129.34300			
517.27002	29.13000	129.34300			
517.27002	34.70900	129.34300			
517.27002	38.24600	114.74300			
517.27002	50.34300	107.33099			
517.27002	58.18900	108.68300			
517.27002	66.03500	110.03500			
517.27002	73.92101	124.59801			
517.27002	71.57300	142.08200			
517.27002	100.91600	151.13200			
517.27002	126.83701	156.89799			
&BPNODE	TNODE= 3,	TNPC= 0,	TINTC= 0,	&END	
&SECT1	STX= 0.0000,	STY= 0.0000,	STZ= 0.0000,	SCALE= 1.0000,	
	ALF= 0.0,	THETA= 0.0,			
INMODE=	4,	TNODS= 0,	TNPS= 0,	TINTS= 0,	&END
524.79297	0.00000	129.73000			
524.79297	7.53800	129.73000			
524.79297	15.07700	129.73000			
524.79297	22.61501	129.73000			
524.79297	30.15401	129.73000			
524.79297	34.15401	129.73000			
524.79297	37.97600	114.60400			
524.79297	50.78200	106.96700			
524.79297	58.10699	108.20799			
524.79297	65.43201	109.44800			
524.79297	73.92799	123.99100			
524.79297	71.73300	141.64799			
524.79297	99.69501	150.14700			
524.79297	127.78599	156.44701			
&BPNODE	TNODE= 3,	TNPC= 0,	TINTC= 0,	&END	
&SECT1	STX= 0.0000,	STY= 0.0000,	STZ= 0.0000,	SCALE= 1.0000,	
	ALF= 0.0,	THETA= 0.0,			
INMODE=	4,	TNODS= 0,	TNPS= 0,	TINTS= 0,	&END

533.80591	0.00000	130.18500			
533.80591	7.36300	130.18500			
533.80591	14.72500	130.18500			
533.80591	22.08800	130.18500			
533.80591	29.45100	130.18500			
533.80591	33.45100	130.18500			
533.80591	37.89000	114.10400			
533.80591	52.02200	106.47099			
533.80591	58.21001	107.56700			
533.80591	64.39800	108.66299			
533.80591	73.77800	122.91701			
533.80591	72.22900	140.86301			
533.80591	97.58800	149.31599			
533.80591	123.47000	156.09300			
&BPNODE	TNODE= 3,	TNPC= 0,	TINTC= 0,	&END	
&SECT1	STX= 0.0000,	STY= 0.0000,	STZ= 0.0000,	SCALE= 1.0000,	
	ALF= 0.0,	THETA= 0.0,			
INMODE=	4,	TNODS= 0,	TNPS= 0,	TINTS= 0,	&END
544.42896	0.00000	130.72099			
544.42896	7.15600	130.72099			
544.42896	14.31100	130.72099			
544.42896	21.46700	130.72099			
544.42896	28.62300	130.72099			
544.42896	32.62199	130.72099			
544.42896	37.80200	113.51100			
544.42896	53.48399	105.88600			
544.42896	58.33200	106.81200			
544.42896	63.17999	107.73700			
544.42896	73.59801	121.63600			
544.42896	72.81300	139.93700			
544.42896	96.19501	148.75200			
544.42896	119.92999	155.97301			
&BPNODE	TNODE= 3,	TNPC= 0,	TINTC= 0,	&END	
&SECT1	STX= 0.0000,	STY= 0.0000,	STZ= 0.0000,	SCALE= 1.0000,	
	ALF= 0.0,	THETA= 0.0,			
INMODE=	4,	TNODS= 0,	TNPS= 0,	TINTS= 0,	&END
556.78906	0.00000	131.26199			
556.78906	6.98000	131.26199			
556.78906	13.96100	131.26199			
556.78906	20.94099	131.26199			
556.78906	27.92200	131.26199			
556.78906	31.92200	131.26199			
556.78906	37.06799	114.24300			
556.78906	51.88901	105.68401			
556.78906	56.86600	106.33400			
556.78906	61.84399	106.98300			
556.78906	73.58701	120.44900			
556.78906	73.59399	139.18300			
556.78906	92.73500	147.60600			
556.78906	111.56599	156.15401			
&BPNODE	TNODE= 3,	TNPC= 0,	TINTC= 0,	&END	
&SECT1	STX= 0.0000,	STY= 0.0000,	STZ= 0.0000,	SCALE= 1.0000,	
	ALF= 0.0,	THETA= 0.0,			
INMODE=	4,	TNODS= 0,	TNPS= 0,	TINTS= 0,	&END

571.02002	0.00000	131.87199			
571.02002	6.79000	131.87199			
571.02002	13.58000	131.87199			
571.02002	20.37000	131.87199			
571.02002	27.16000	131.87199			
571.02002	31.16000	131.87199			
571.02002	36.14500	115.22900			
571.02002	49.50000	105.53200			
571.02002	54.91000	105.85100			
571.02002	60.31900	106.17000			
571.02002	73.61099	119.09300			
571.02002	74.50800	138.37000			
571.02002	89.76401	146.58200			
571.02002	103.62601	156.68201			
&BPNODE	TNODE= 3,	TNPC= 0,	TINTC= 0,	&END	
&SECT1	STX= 0.0000,	STY= 0.0000,	STZ= 0.0000,	SCALE= 1.0000,	
	ALF= 0.0,	THETA= 0.0,			
INMODE=	4,	TNODS= 0,	TNPS= 0,	TINTS= 0,	&END
587.26099	0.00000	132.66299			
587.26099	6.62200	132.66299			
587.26099	13.24500	132.66299			
587.26099	19.86700	132.66299			
587.26099	26.49001	132.66299			
587.26099	30.59200	132.66299			
587.26099	35.68700	115.52299			
587.26099	49.50999	104.99001			
587.26099	54.75500	105.11200			
587.26099	60.00000	105.23500			
587.26099	74.04100	117.84700			
587.26099	75.72000	137.17999			
587.26099	88.18300	144.52100			
587.26099	95.70599	157.50301			
&BPNODE	TNODE= 3,	TNPC= 0,	TINTC= 0,	&END	
&SECT1	STX= 0.0000,	STY= 0.0000,	STZ= 0.0000,	SCALE= 1.0000,	
	ALF= 0.0,	THETA= 0.0,			
INMODE=	4,	TNODS= 0,	TNPS= 0,	TINTS= 0,	&END
605.66089	0.00000	133.58299			
605.66089	6.48500	133.58299			
605.66089	12.97000	133.58299			
605.66089	19.45399	133.58299			
605.66089	25.93900	133.58299			
605.66089	30.09900	133.58299			
605.66089	35.38600	115.67400			
605.66089	50.00000	104.39900			
605.66089	55.00000	104.39900			
605.66089	60.00000	104.39900			
605.66089	74.45799	116.80099			
605.66089	76.94299	135.99800			
605.66089	87.76500	144.20599			
605.66089	88.13400	158.54201			
&BPNODE	TNODE= 3,	TNPC= 0,	TINTC= 0,	&END	
&SECT1	STX= 0.0000,	STY= 0.0000,	STZ= 0.0000,	SCALE= 1.0000,	
	ALF= 0.0,	THETA= 0.0,			
INMODE=	4,	TNODS= 3,	TNPS= 0,	TINTS= 0,	&END

626.37207	0.00000	134.61800
626.37207	6.42900	134.61800
626.37207	12.85900	134.61800
626.37207	19.28799	134.61800
626.37207	25.71700	134.61900
626.37207	29.72900	134.61900
626.37207	35.17200	116.06100
626.37207	50.00000	104.02901
626.37207	55.00000	104.02901
626.37207	60.00000	104.02901
626.37207	74.50000	116.35699
626.37207	77.83000	135.25800
626.37207	86.06300	145.53000
626.37207	85.03799	159.84200

&BPNODE TNODE= 3, TNPC= 0, TINTC= 0, &END

&PATCH1 IREV= 0, IDPAT= 2, MAKE= 0, KCOMP= 2, KASS= 3, &END
F14 FUSELAGE AFT OF WING TE #21

&SECT1 STX= 0.0000, STY= 0.0000, STZ= 0.0000, SCALE= 1.0000,
ALF= 0.0, THETA= 0.0,

INMODE= 4, TNODS= 0, TNPS= 0, TINTS= 0, &END

626.37207	0.00000	134.61800
626.37207	6.42900	134.61800
626.37207	12.85900	134.61800
626.37207	19.28799	134.61800
626.37207	25.71700	134.61900
626.37207	29.72900	134.61900
626.37207	35.17200	116.06100
626.37207	50.00000	104.02901
626.37207	55.00000	104.02901
626.37207	60.00000	104.02901
626.37207	74.50000	116.35699
626.37207	77.83000	135.25800
626.37207	86.06300	145.53000
626.37207	85.03799	159.84200
626.37207	61.09300	162.53000
626.37207	35.88400	162.79300
626.37207	19.77699	162.28101
626.37207	14.82800	162.26500
626.37207	9.88100	162.31300
626.37207	4.94700	162.65100
626.37207	0.00000	162.73900

&BPNODE TNODE= 3, TNPC= 0, TINTC= 0, &END

&SECT1 STX= 0.0000, STY= 0.0000, STZ= 0.0000, SCALE= 1.0000,

ALF= 0.0, THETA= 0.0,

INMODE= 4, TNODS= 0, TNPS= 0, TINTS= 0, &END

654.75000	0.00000	136.39200
654.75000	6.42500	136.39200
654.75000	12.85000	136.39200
654.75000	19.27499	136.39200
654.75000	25.70000	136.39200
654.75000	29.11800	136.39200
654.75000	35.95200	115.55800
654.75000	54.14500	104.38400

654.75000	58.86800	105.27000			
654.75000	63.59000	106.15601			
654.75000	75.65900	117.25400			
654.75000	79.38300	133.42599			
654.75000	87.54800	148.95900			
654.75000	77.73300	160.97400			
654.75000	61.18800	162.54401			
654.75000	44.56500	162.40100			
654.75000	30.76700	159.88000			
654.75000	23.07500	159.88000			
654.75000	15.38400	159.88000			
654.75000	7.69200	159.88000			
654.75000	0.00000	159.88000			
&BPNODE	TNODE= 3,	TNPC= 0,	TINTC= 0,	&END	
&SECT1	STX= 0.0000,	STY= 0.0000,	STZ= 0.0000,	SCALE= 1.0000,	
	ALF= 0.0,	THETA= 0.0,			
INMODE=	4,	TNODS= 0,	TNPS= 0,	TINTS= 0,	&END
681.50000	0.00000	137.90900			
681.50000	6.42500	137.90900			
681.50000	12.85000	137.90900			
681.50000	19.27499	137.90900			
681.50000	25.70000	137.90900			
681.50000	29.20000	137.90900			
681.50000	35.71001	117.27800			
681.50000	53.95200	106.51900			
681.50000	58.47400	107.08000			
681.50000	62.99500	107.64000			
681.50000	75.26300	117.16200			
681.50000	80.33099	131.93800			
681.50000	90.13100	146.81900			
681.50000	81.01500	160.26199			
681.50000	63.71100	163.72200			
681.50000	46.12100	163.43100			
681.50000	34.17400	157.39799			
681.50000	25.63000	157.39799			
681.50000	17.08701	157.39799			
681.50000	8.54300	157.39799			
681.50000	0.00000	157.39799			
&BPNODE	TNODE= 3,	TNPC= 0,	TINTC= 0,	&END	
&SECT1	STX= 0.0000,	STY= 0.0000,	STZ= 0.0000,	SCALE= 1.0000,	
	ALF= 0.0,	THETA= 0.0,			
INMODE=	4,	TNODS= 0,	TNPS= 0,	TINTS= 0,	&END
708.25000	0.00000	139.06200			
708.25000	6.42500	139.06200			
708.25000	12.85000	139.06200			
708.25000	19.27499	139.06200			
708.25000	25.70000	139.06200			
708.25000	29.26601	139.06200			
708.25000	35.69501	118.71001			
708.25000	54.06700	108.46100			
708.25000	58.26801	108.92799			
708.25000	62.46800	109.39400			
708.25000	74.49001	117.63400			
708.25000	80.79900	130.96800			

708.25000	90.33501	145.56000		
708.25000	80.97400	158.83400		
708.25000	63.68401	164.15700		
708.25000	45.76801	163.93201		
708.25000	34.06700	154.70700		
708.25000	25.55000	154.70700		
708.25000	17.03300	154.70700		
708.25000	8.51700	154.70700		
708.25000	0.00000	154.70700		
&BPNODE TNODE= 3, TNPC= 0, TINTC= 0,			&END	
&SECT1 STX= 0.0000, STY= 0.0000, STZ= 0.0000, SCALE= 1.0000,				
ALF= 0.0, THETA= 0.0,				
INMODE= 4, TNODS= 0, TNPS= 0, TINTS= 0,			&END	
735.00000	0.00000	140.36000		
735.00000	6.45400	140.36000		
735.00000	12.90700	140.36000		
735.00000	19.36099	140.36000		
735.00000	25.81400	140.36000		
735.00000	29.58299	140.36000		
735.00000	36.01500	120.47501		
735.00000	54.13699	110.34300		
735.00000	58.08000	110.83099		
735.00000	62.02300	111.32001		
735.00000	73.89600	118.48900		
735.00000	80.95399	130.47701		
735.00000	89.65700	145.00101		
735.00000	79.34300	157.84599		
735.00000	62.82700	164.46300		
735.00000	45.31700	163.97099		
735.00000	34.00000	152.56300		
735.00000	25.50000	152.56300		
735.00000	17.00000	152.56300		
735.00000	8.50000	152.56300		
735.00000	0.00000	152.56300		
&BPNODE TNODE= 3, TNPC= 0, TINTC= 0,			&END	
&SECT1 STX= 0.0000, STY= 0.0000, STZ= 0.0000, SCALE= 1.0000,				
ALF= 0.0, THETA= 0.0,				
INMODE= 4, TNODS= 0, TNPS= 0, TINTS= 0,			&END	
761.75000	0.00000	142.78600		
761.75000	6.75600	142.79800		
761.75000	13.51100	142.81000		
761.75000	20.26801	142.81200		
761.75000	27.02400	142.81100		
761.75000	31.02400	142.83000		
761.75000	37.15500	122.34599		
761.75000	56.11900	113.10899		
761.75000	59.46800	113.41299		
761.75000	62.81599	113.71600		
761.75000	73.71600	119.99499		
761.75000	80.60100	130.53500		
761.75000	86.92300	144.64999		
761.75000	75.72800	157.15300		
761.75000	60.27200	164.18500		
761.75000	43.89200	161.66600		

```

761.75000 34.00000 150.97701
761.75000 25.49899 150.98100
761.75000 16.99699 150.98399
761.75000 8.50100 151.01100
761.75000 0.00000 151.01300
&BPNODE TNODE= 3, TNPC= 0, TINTC= 0, &END
&SECT1 STX= 0.0000, STY= 0.0000, STZ= 0.0000, SCALE= 1.0000,
ALF= 0.0, THETA= 0.0,
INMODE= 4, TNODS= 3, TNPS= 0, TINTS= 0, &END
788.50000 0.00000 142.32100
788.50000 8.00600 142.88200
788.50000 15.95800 143.92400
788.50000 23.88600 145.17599
788.50000 31.81400 146.42799
788.50000 34.59599 149.06599
788.50000 37.10200 125.63800
788.50000 57.66400 114.92500
788.50000 60.67500 115.44900
788.50000 63.68700 115.97301
788.50000 74.24100 122.92000
788.50000 80.74300 133.89400
788.50000 80.03300 146.55701
788.50000 72.40300 156.48100
788.50000 58.70100 162.17999
788.50000 44.10600 158.66901
788.50000 34.59599 149.06599
788.50000 26.10899 150.95200
788.50000 17.36700 151.13800
788.50000 8.74800 152.44600
788.50000 0.00000 152.16499
&BPNODE TNODE= 3, TNPC= 0, TINTC= 0, &END
&PATCH1 IREV= 0, IDPAT= 2, MAKE= 0, KCOMP= 2, KASS= 3, &END
F14 EXHAUST CONE #22
&SECT1 STX= 0.0000, STY= 0.0000, STZ= 0.0000, SCALE= 1.0000,
ALF= 0.0, THETA= 0.0,
INMODE= 4, TNODS= 0, TNPS= 0, TINTS= 0, &END
788.50000 34.59599 149.06599
788.50000 37.10200 125.63800
788.50000 57.66400 114.92500
788.50000 60.67500 115.44900
788.50000 63.68700 115.97301
788.50000 74.24100 122.92000
788.50000 80.74300 133.89400
788.50000 80.03300 146.55701
788.50000 72.40300 156.48100
788.50000 58.70100 162.17999
788.50000 44.10600 158.66901
788.50000 34.59599 149.06599
&BPNODE TNODE= 3, TNPC= 0, TINTC= 0, &END
&SECT1 STX= 0.0000, STY= 0.0000, STZ= 0.0000, SCALE= 1.0000,
ALF= 0.0, THETA= 0.0,
INMODE= 4, TNODS= 3, TNPS= 0, TINTS= 0, &END
813.00000 45.48801 144.40100

```

813.00000	45.73599	131.46500		
813.00000	57.16100	125.38600		
813.00000	58.82700	125.66600		
813.00000	60.49300	125.94701		
813.00000	66.12399	129.47099		
813.00000	69.17999	135.35300		
813.00000	68.91200	142.06400		
813.00000	65.01801	147.42999		
813.00000	57.82100	150.74899		
813.00000	49.94901	149.25301		
813.00000	45.48801	144.40100		
&BPNODE TNODE= 3, TNPC= 0, TINTC= 0,			&END	
&PATCH1 IREV=0, IDPAT= 2, MAKE= 0, KCOMP= 2, KASS= 3, &END				
F14 FUSELAGE TIP #23				
&SECT1 STX= 0.0000, STY= 0.0000, STZ= 0.0000, SCALE= 1.0000,				
ALF= 0.0, THETA= 0.0,				
INMODE= 4, TNODS= 0, TNPS= 0, TINTS= 0,			&END	
788.50000	0.00000	142.32100		
788.50000	8.00600	142.88200		
788.50000	15.95800	143.92400		
788.50000	23.88600	145.17599		
788.50000	31.81400	146.42799		
788.50000	34.59599	149.06599		
788.50000	26.10899	150.95200		
788.50000	17.36700	151.13800		
788.50000	8.74800	152.44600		
788.50000	0.00000	152.16499		
&BPNODE TNODE= 3, TNPC= 0, TINTC= 0,			&END	
&SECT1 STX= 0.0000, STY= 0.0000, STZ= 0.0000, SCALE= 1.0000,				
ALF= 0.0, THETA= 0.0,				
INMODE= 4, TNODS= 0, TNPS= 0, TINTS= 0,			&END	
813.00000	0.00000	145.46100		
813.00000	5.13400	145.23100		
813.00000	10.26700	144.99899		
813.00000	15.35800	144.29700		
813.00000	22.44901	146.59500		
813.00000	24.42900	149.31200		
813.00000	21.57300	152.52100		
813.00000	14.38900	152.59100		
813.00000	7.20500	152.03600		
813.00000	0.00000	151.85500		
&BPNODE TNODE= 3, TNPC= 0, TINTC= 0,			&END	
&SECT1 STX= 0.0000, STY= 0.0000, STZ= 0.0000, SCALE= 1.0000,				
ALF= 0.0, THETA= 0.0,				
INMODE= 4, TNODS= 3, TNPS= 0, TINTS= 0,			&END	
834.00000	0.00000	147.53500		
834.00000	5.20300	147.53500		
834.00000	10.40600	147.53500		
834.00000	15.60900	147.53500		
834.00000	20.81200	147.53500		
834.00000	20.81200	149.53500		
834.00000	15.60900	149.53500		
834.00000	10.40600	149.53500		

```

      834.00000    5.20300   149.53500
      834.00000    0.00000   149.53500
&BPNODE TNODE=    3, TNPC=    0, TINTC=    0,                &END

&PATCH1 IREV= 0, IDPAT= 2, MAKE= 0, KCOMP= 2, KASS= 4,    &END
F14 FUSELAGE TIP COVER #24
&SECT1 STX= 0.0000, STY= 0.0000, STZ= 0.0000, SCALE= 1.0000,
      ALF=    0.0, THETA= 0.0,
      INMODE= 4, TNODS= 0, TNPS= 0, TINTS= 0,                &END
      834.00000    0.00000   148.53500
      834.00000    0.00000   148.53500
      834.00000    0.00000   148.53500
      834.00000    0.00000   148.53500
      834.00000    0.00000   148.53500
      834.00000    0.00000   148.53500
      834.00000    0.00000   148.53500
      834.00000    0.00000   148.53500
      834.00000    0.00000   148.53500
      834.00000    0.00000   148.53500
&BPNODE TNODE=    3, TNPC=    0, TINTC=    0,                &END
&SECT1 STX= 0.0000, STY= 0.0000, STZ= 0.0000, SCALE= 1.0000,
      ALF=    0.0, THETA= 0.0,
      INMODE= 4, TNODS= 3, TNPS= 0, TINTS= 0,                &END
      834.00000    0.00000   149.53500
      834.00000    5.20300   149.53500
      834.00000   10.40600   149.53500
      834.00000   15.60900   149.53500
      834.00000   20.81200   149.53500
      834.00000   20.81200   147.53500
      834.00000   15.60900   147.53500
      834.00000   10.40600   147.53500
      834.00000    5.20300   147.53500
      834.00000    0.00000   147.53500
&BPNODE TNODE=    3, TNPC=    0, TINTC=    0,                &END

&PATCH1 IREV= 0, IDPAT= 2, MAKE= 0, KCOMP= 2, KASS= 4,    &END
F14 EXHAUST COVER #25
&SECT1 STX= 0.0000, STY= 0.0000, STZ= 0.0000, SCALE= 1.0000,
      ALF=    0.0, THETA= 0.0,
      INMODE= 4, TNODS= 0, TNPS= 0, TINTS= 0,                &END
      813.00000   57.33299   138.00000
      813.00000   57.33299   138.00000
      813.00000   57.33299   138.00000
      813.00000   57.33299   138.00000
      813.00000   57.33299   138.00000
      813.00000   57.33299   138.00000
      813.00000   57.33299   138.00000
      813.00000   57.33299   138.00000
      813.00000   57.33299   138.00000
      813.00000   57.33299   138.00000
      813.00000   57.33299   138.00000
      813.00000   57.33299   138.00000
&BPNODE TNODE=    3, TNPC=    0, TINTC=    0,                &END
&SECT1 STX= 0.0000, STY= 0.0000, STZ= 0.0000, SCALE= 1.0000,

```

```

ALF= 0.0, THETA= 0.0,
INMODE= 4, TNODS= 3, TNPS= 0, TINTS= 0, &END
813.00000 45.48801 144.40100
813.00000 49.94901 149.25301
813.00000 57.82100 150.74899
813.00000 65.01801 147.42999
813.00000 68.91200 142.06400
813.00000 69.17999 135.35300
813.00000 66.12399 129.47099
813.00000 60.49300 125.94701
813.00000 58.82700 125.66600
813.00000 57.16100 125.38600
813.00000 45.73599 131.46500
813.00000 45.48801 144.40100
&BPNODE TNODE= 3, TNPC= 0, TINTC= 0, &END

&PATCH1 IREV= 0, IDPAT= 1, MAKE= 0, KCOMP= 2, KASS= 3, &END
F14 WING #26
&SECT1 STX= 0.0000, STY= 0.0000, STZ= 0.0000, SCALE= 1.0000,
ALF= 0.0, THETA= 0.0,
INMODE= 4, TNODS= 0, TNPS= 0, TINTS= 0, &END
626.37207 85.03799 159.84200
605.66089 88.13400 158.54201
587.26099 95.70599 157.50301
571.02002 103.62601 156.68201
556.78906 111.56599 156.15401
544.42896 119.92999 155.97301
533.80591 123.47000 156.09300
524.79297 127.78599 156.44701
517.27002 126.83701 156.89799
511.12305 125.66400 157.50500
506.24194 124.81900 158.46100
502.52588 124.46500 161.01900
506.24194 125.32700 163.75900
511.12305 126.10500 165.30200
517.27002 125.32400 166.69701
524.79297 124.90900 167.69901
533.80591 119.49400 168.57700
544.42896 112.61700 168.84599
556.78906 103.03000 168.47600
571.02002 98.51700 167.31900
587.26099 90.91499 165.54300
605.66089 85.64600 163.09500
626.37207 85.03799 159.84200
&BPNODE TNODE= 3, TNPC= 0, TINTC= 0, &END
&SECT1 STX= 0.0000, STY= 0.0000, STZ= 0.0000, SCALE= 1.0000,
ALF= 0.0, THETA= 0.0,
INMODE= 4, TNODS= 0, TNPS= 0, TINTS= 0, &END
622.3692 92.0181 142.7208
604.7296 95.1021 153.6552
587.26099 102.70599 157.50301
571.02002 110.62601 156.68201
556.78906 118.56599 156.15401
544.42896 126.92999 155.97301

```

533.80591	130.47000	156.09300
524.79297	134.78599	156.44701
517.27002	133.83701	156.89799
511.12305	132.66400	157.50500
506.24194	131.81900	158.46100
502.52588	131.46500	161.01900
506.24194	132.32700	163.75900
511.12305	133.10500	165.30200
517.27002	132.32400	166.69701
524.79297	131.90900	167.69901
533.80591	126.49400	168.57700
544.42896	119.61700	168.84599
556.78906	110.03000	168.47600
571.02002	105.51700	167.31900
587.26099	97.91499	165.54300
607.2193	92.2753	157.2231
622.3692	92.0181	142.7208

```

&BPNODE TNODE= 3, TNPC= 0, TINTC= 0, &END
&SECT1 STX= 0.0000, STY= 0.0000, STZ= 0.0000, SCALE= 1.0000,
ALF= 0.0, THETA= 0.0,
INMODE= 4, TNODS= 0, TNPS= 0, TINTS= 0, &END

```

631.606	169.4923	142.01
615.33	169.4796	151.994
598.78296	169.58299	156.26801
583.83203	169.58299	155.82899
570.73193	169.58299	155.67200
559.35498	169.58299	155.73100
549.57593	169.58299	155.92799
541.28003	169.58299	156.20799
534.35498	169.58299	156.56599
528.69604	169.58299	157.05499
524.20313	169.58299	157.80901
520.78296	169.58299	159.97400
524.20313	169.58299	162.53000
528.69604	169.58299	163.84399
534.35498	169.58299	164.90700
541.28003	169.58299	165.73300
549.57593	169.58299	166.25101
559.35498	169.58299	166.36600
570.73193	169.58299	165.95799
583.83203	169.58299	164.92900
598.78296	169.58299	163.23801
617.5477	169.1831	155.1908
631.606	169.4923	142.01

```

&BPNODE TNODE= 3, TNPC= 0, TINTC= 0, &END
&SECT1 STX= 0.0000, STY= 0.0000, STZ= 0.0000, SCALE= 1.0000,
ALF= 0.0, THETA= 0.0,
INMODE= 4, TNODS= 0, TNPS= 0, TINTS= 0, &END

```

634.9622	211.0303	142.0361
620.5685	211.0325	150.6627
606.11182	211.13400	154.95799
592.97974	211.13400	154.50200
581.47485	211.13400	154.33400
571.48169	211.13400	154.38200

562.89380	211.13400	154.55400
555.60669	211.13400	154.79401
549.52466	211.13400	155.09399
544.55469	211.13400	155.49500
540.60864	211.13400	156.11200
537.60474	211.13400	157.96201
540.60864	211.13400	160.18401
544.55469	211.13400	161.32001
549.52466	211.13400	162.25800
555.60669	211.13400	163.02499
562.89380	211.13400	163.55499
571.48169	211.13400	163.75200
581.47485	211.13400	163.49300
592.97974	211.13400	162.67700
606.11182	211.13400	161.26100
622.5768	210.7639	153.5582
634.9622	211.0303	142.0361

```

&BPNODE TNODE= 3, TNPC= 0, TINTC= 0, &END
&SECT1 STX= 0.0000, STY= 0.0000, STZ= 0.0000, SCALE= 1.0000,
ALF= 0.0, THETA= 0.0,
INMODE= 4, TNODS= 0, TNPS= 0, TINTS= 0, &END

```

638.2167	252.5822	141.9295
625.6762	252.6031	149.1553
613.43481	252.68600	153.38300
602.12476	252.68600	152.84801
592.21387	252.68600	152.60500
583.60571	252.68600	152.58099
576.20874	252.68600	152.68900
569.93164	252.68600	152.86700
564.69287	252.68600	153.09900
560.41187	252.68600	153.41701
557.01270	252.68600	153.92101
554.42578	252.68600	155.49300
557.01270	252.68600	157.43500
560.41187	252.68600	158.43401
564.69287	252.68600	159.27200
569.93164	252.68600	159.98300
576.20874	252.68600	160.52000
583.60571	252.68600	160.80000
592.21387	252.68600	160.71100
602.12476	252.68600	160.14999
613.43481	252.68600	159.06599
627.5032	252.3588	151.7894
638.2167	252.5822	141.9295

```

&BPNODE TNODE= 3, TNPC= 0, TINTC= 0, &END
&SECT1 STX= 0.0000, STY= 0.0000, STZ= 0.0000, SCALE= 1.0000,
ALF= 0.0, THETA= 0.0,
INMODE= 4, TNODS= 0, TNPS= 0, TINTS= 0, &END

```

641.4686	294.1341	141.81
630.7969	294.1714	147.6581
620.76270	294.23706	151.84200
611.27271	294.23706	151.23700
602.95679	294.23706	150.91499
595.73462	294.23706	150.80600

589.52686	294.23706	150.83600
584.26074	294.23706	150.94299
579.86475	294.23706	151.10201
576.27173	294.23706	151.33000
573.41968	294.23706	151.71500
571.24976	294.23706	153.00600
573.41968	294.23706	154.66901
576.27173	294.23706	155.53101
579.86475	294.23706	156.26500
584.26074	294.23706	156.91100
589.52686	294.23706	157.43900
595.73462	294.23706	157.78600
602.95679	294.23706	157.85500
611.27271	294.23706	157.55000
620.76270	294.23706	156.80901
632.4114	293.9556	149.9858
641.4686	294.1341	141.81

```

&BPNODE TNODE= 3, TNPC= 0, TINTC= 0, &END
&SECT1 STX= 0.0000, STY= 0.0000, STZ= 0.0000, SCALE= 1.0000,
ALF= 0.0, THETA= 0.0,
INMODE= 4, TNODS= 0, TNPS= 0, TINTS= 0, &END

```

644.7274	335.6856	141.7054
635.9524	335.736	146.2158
628.08862	335.78906	150.39900
620.41870	335.78906	149.74001
613.69873	335.78906	149.34000
607.86182	335.78906	149.13600
602.84473	335.78906	149.06500
598.58862	335.78906	149.07700
595.03564	335.78906	149.14500
592.13281	335.78906	149.27200
589.82764	335.78906	149.52699
588.07373	335.78906	150.54601
589.82764	335.78906	151.91701
592.13281	335.78906	152.64101
595.03564	335.78906	153.26401
598.58862	335.78906	153.83000
602.84473	335.78906	154.32899
607.86182	335.78906	154.71899
613.69873	335.78906	154.92500
620.41870	335.78906	154.86700
628.08862	335.78906	154.48000
637.2959	335.5563	148.1527
644.7274	335.6856	141.7054

```

&BPNODE TNODE= 3, TNPC= 0, TINTC= 0, &END
&SECT1 STX= 0.0000, STY= 0.0000, STZ= 0.0000, SCALE= 1.0000,
ALF= 0.0, THETA= 0.0,
INMODE= 4, TNODS= 3, TNPS= 0, TINTS= 0, &END

```

648.0172	372.5153	141.08
641.1824	372.5725	144.3174
635.71191	372.60010	149.03300
629.86084	372.60010	148.35500
624.73486	372.60010	147.90900
620.28296	372.60010	147.64000

616.45703	372.60010	147.48500	
613.20996	372.60010	147.39600	
610.50098	372.60010	147.34000	
608.28589	372.60010	147.30499	
606.52783	372.60010	147.36200	
605.18994	372.60010	148.07100	
606.52783	372.60010	149.15700	
608.28589	372.60010	149.74100	
610.50098	372.60010	150.24899	
613.20996	372.60010	150.72400	
616.45703	372.60010	151.17000	
620.28296	372.60010	151.56700	
624.73486	372.60010	151.87199	
629.86084	372.60010	152.02699	
635.71191	372.60010	151.98399	
642.1627	372.4414	145.7307	
648.0172	372.5153	141.08	
&BPNODE	TNODE= 3,	TNPC= 0,	TINTC= 0, &END
&PATCH1	IREV=0, IDPAT=1, MAKE=26, KCOMP=2, KASS=4,		&END
	F14 WING TIP #27		
&PATCH2	ITYP=1, TNODS=3, TNPS=3, TINTS=3, NPTTIP=0,		&END
&PATCH1	IREV=0, IDPAT=1, MAKE=0, KCOMP=2, KASS=3,		&END
	HORIZONTAL TAIL #28		
&SECT1	STX= 684.6, STY= 92.0, STZ= 145.5, SCALE= 0.96000,		
	ALF= -4.9, THETA= 0.0,		
	INMODE= 4, TNODS= 0, TNPS= 0, TINTS= 0,		&END
148.600	0.0	0.0	
141.170	0.0	-0.549	
133.74	0.0	-1.080	
126.31	0.0	-1.609	
118.88	0.0	-2.135	
111.45	0.0	-2.637	
104.02	0.0	-3.101	
96.59	0.0	-3.512	
89.16	0.0	-3.866	
81.73	0.0	-4.15	
74.3	0.0	-4.346	
66.87	0.0	-4.446	
59.44	0.0	-4.452	
52.01	0.0	-4.376	
44.58	0.0	-4.223	
37.15	0.0	-3.992	
29.72	0.0	-3.676	
22.29	0.0	-3.26	
14.86	0.0	-2.71	
11.145	0.0	-2.364	
7.43	0.0	-1.951	
3.715	0.0	-1.457	
1.857	0.0	-1.066	
1.114	0.0	-0.836	
0.743	0.0	-0.689	
0.0	0.0	0.0	

```

&BPNODE TNODE= 2, TNPC= 15, TINTC= 0, &END
  0.0 0.0 0.0
  0.743 0.0 0.689
  1.114 0.0 0.836
  1.857 0.0 1.066
  3.715 0.0 1.457
  7.43 0.0 1.951
  11.145 0.0 2.364
  14.86 0.0 2.71
  22.29 0.0 3.26
  29.72 0.0 3.676
  37.15 0.0 3.992
  44.58 0.0 4.223
  52.01 0.0 4.376
  59.44 0.0 4.452
  66.87 0.0 4.446
  74.3 0.0 4.346
  81.73 0.0 4.15
  89.16 0.0 3.866
  96.59 0.0 3.512
  104.02 0.0 3.101
  111.45 0.0 2.633
  118.88 0.0 2.135
  126.31 0.0 1.609
  133.74 0.0 1.080
  141.17 0.0 0.549
  148.6 0.0 0.0
&BPNODE TNODE= 3, TNPC= 15, TINTC= 0, &END
&SECT1 STX= 808.0, STY= 202.7, STZ= 138.7, SCALE= 0.2133,
  ALF= 0.0, THETA= 0.0,
  INMODE= 0, TNODS= 3, TNPS= 5, TINTS= 0, &END

&PATCH1 IREV=0, IDPAT=1, MAKE=28, KCOMP=2, KASS=4, &END
  HORIZONTAL TAIL TIP #29
&PATCH2 ITYP=1, TNODS=3, TNPS=2, TINTS=3, NPTTIP=0, &END

&PATCH1 IREV=0, IDPAT=1, MAKE=-28, KCOMP=2, KASS=4, &END
  HORIZONTAL TAIL TIP #30
&PATCH2 ITYP=1, TNODS=3, TNPS=3, TINTS=3, NPTTIP=0, &END

&PATCH1 IREV=0, IDPAT=2, MAKE=0, KCOMP=2, KASS=3, &END
  VERTICAL TAIL #31
&SECT1 STX= 680.0, STY= 56.5, STZ= 166.0, SCALE= 1.0000,
  ALF= 0.0, THETA= 0.0,
  INMODE= 4, TNODS= 0, TNPS= 0, TINTS= 0, &END
  123.0 0.0 0.0
  116.85 0.455 0.0
  110.7 0.894 0.0
  104.550 1.332 0.0
  98.4 1.762 0.0
  92.25 2.183 0.0
  86.1 2.567 0.0
  79.95 2.907 0.0
  73.8 3.2 0.0

```

67.65	3.435	0.0			
61.5	3.597	0.0			
55.350	3.68	0.0			
49.2	3.685	0.0			
43.05	3.622	0.0			
36.9	3.495	0.0			
30.75	3.305	0.0			
24.6	3.043	0.0			
18.45	2.698	0.0			
12.3	2.243	0.0			
9.225	1.956	0.0			
6.15	1.614	0.0			
3.075	1.206	0.0			
1.537	0.883	0.0			
0.922	0.692	0.0			
0.615	0.57	0.0			
0.0	0.0	0.0			
&BPNODE	TNODE=	2, TNPC=	12, TINTC=	0,	&END
0.0	0.0	0.0			
0.615	-0.57	0.0			
0.922	-0.692	0.0			
1.537	-0.883	0.0			
3.075	-1.206	0.0			
6.15	-1.614	0.0			
9.225	-1.956	0.0			
12.3	-2.243	0.0			
18.45	-2.698	0.0			
24.6	-3.043	0.0			
30.75	-3.305	0.0			
36.9	-3.495	0.0			
43.05	-3.622	0.0			
49.2	-3.685	0.0			
55.350	-3.68	0.0			
61.5	-3.597	0.0			
67.65	-3.435	0.0			
73.8	-3.2	0.0			
79.95	-2.907	0.0			
86.1	-2.567	0.0			
92.25	-2.183	0.0			
98.4	-1.762	0.0			
104.550	-1.332	0.0			
110.7	-0.894	0.0			
116.85	-0.455	0.0			
123.0	0.0	0.0			
&BPNODE	TNODE=	3, TNPC=	12, TINTC=	0,	&END
&SECT1	STX=	787.0, STY=	65.4, STZ=	266.0, SCALE=	0.35772,
	ALF=	0.0, THETA=	0.0,		
	INMODE=	0, TNODS=	3, TNPS=	5, TINTS=	0,
					&END
&PATCH1	IREV=0, IDPAT=1, MAKE=31, KCOMP=2, KASS=4,				&END
	VERTICAL TAIL TIP #32				
&PATCH2	ITYP=1, TNODS=5, TNPS=3, TINTS=3, NPTTIP=0,				&END

```

&WAKE1 IDWAK=1, IFLXW=0, &END
  T34 WING WAKE
&WAKE2 KWPACH=9, KWSIDE=4, KWLINE=2, KWPAN1=0, &END
  KWPAN2=0, NODEW=0, INITIAL=1,
&WAKE2 KWPACH=6, KWSIDE=4, KWLINE=4, KWPAN1=0, &END
  KWPAN2=0, NODEW=0, INITIAL=1,
&WAKE2 KWPACH=2, KWSIDE=2, KWLINE=0, KWPAN1=0, &END
  KWPAN2=0, NODEW=3, INITIAL=1,
&SECT1 STX=1900.0, STY=0.0, STZ=0.0, SCALE=1.0, &END
  ALF=0.0, THETA=0.0,
  INMODE=-1, TNODS=3, TNPS=15, TINTS=1,
&WAKE1 IDWAK=1, IFLXW=0, &END
  T34 TAIL WAKE
&WAKE2 KWPACH=7, KWSIDE=2, KWLINE=0, KWPAN1=0, &END
  KWPAN2=0, NODEW=3, INITIAL=1,
&SECT1 STX=1500.0, STY=0.0, STZ=0.0, SCALE=1.0, &END
  ALF=0.0, THETA=0.0,
  INMODE=-1, TNODS=3, TNPS=15, TINTS=1,

&WAKE1 IDWAK=1, IFLXW=0, &END
  F14 HORIZONTAL TAIL WAKE
&WAKE2 KWPACH=28, KWSIDE=4, KWLINE=0, KWPAN1=0, &END
  KWPAN2=0, NODEW=3, INITIAL=1,
&SECT1 STX=1800.0, STY=0.0, STZ=0.0, SCALE=1.0, &END
  ALF=0.0, THETA=0.0,
  INMODE=-1, TNODS=3, TNPS=15, TINTS=0,

&WAKE1 IDWAK=1, IFLXW=0, &END
  F14 VERTICAL TAIL WAKE
&WAKE2 KWPACH=31, KWSIDE=2, KWLINE=0, KWPAN1=0, &END
  KWPAN2=0, NODEW=3, INITIAL=1,
&SECT1 STX=1800.0, STY=0.0, STZ=0.0, SCALE=1.0, &END
  ALF=0.0, THETA=0.0,
  INMODE=-1, TNODS=3, TNPS=15, TINTS=0,

&WAKE1 IDWAK=1, IFLXW=0, &END
  F14 WING WAKE
&WAKE2 KWPACH=26, KWSIDE=4, KWLINE=0, KWPAN1=0, &END
  KWPAN2=0, NODEW=0, INITIAL=1,
&WAKE2 KWPACH=21, KWSIDE=2, KWLINE=13, KWPAN1=1, &END
  KWPAN2=1, NODEW=0, INITIAL=1,
&WAKE2 KWPACH=21, KWSIDE=3, KWLINE=1, KWPAN1=8, &END
  KWPAN2=8, NODEW=0, INITIAL=1,
&WAKE2 KWPACH=21, KWSIDE=2, KWLINE=12, KWPAN1=2, &END
  KWPAN2=2, NODEW=0, INITIAL=1,
&WAKE2 KWPACH=21, KWSIDE=3, KWLINE=2, KWPAN1=9, &END
  KWPAN2=10, NODEW=0, INITIAL=1,
&WAKE2 KWPACH=21, KWSIDE=2, KWLINE=10, KWPAN1=3, &END
  KWPAN2=0, NODEW=0, INITIAL=1,
&WAKE2 KWPACH=22, KWSIDE=2, KWLINE=5, KWPAN1=0, &END
  KWPAN2=0, NODEW=0, INITIAL=1,
&WAKE2 KWPACH=25, KWSIDE=4, KWLINE=7, KWPAN1=0, &END
  KWPAN2=0, NODEW=0, INITIAL=1,

```

```

&WAKE2 KWPACH=25, KWSIDE=2, KWLINE=11, KWPAN1=0,
      KWPAN2=0, NODEW=0, INITIAL=1, &END
&WAKE2 KWPACH=22, KWSIDE=4, KWLINE=1, KWPAN1=0,
      KWPAN2=0, NODEW=0, INITIAL=1, &END
&WAKE2 KWPACH=23, KWSIDE=2, KWLINE=5, KWPAN1=0,
      KWPAN2=0, NODEW=0, INITIAL=1, &END
&WAKE2 KWPACH=24, KWSIDE=4, KWLINE=5, KWPAN1=0,
      KWPAN2=0, NODEW=5, INITIAL=1, &END
&SECT1 STX=-511.0, STY=0.0, STZ=2004.0, SCALE=1.0,
      ALF=11.0, THETA=0.0,
      INMODE=4, TNODS=2, TNPS=0, TINTS=0, &END
651.0 372.5153 140.0
651.0 335.686 140.57
650.0 294.134 141.04
645.0 252.5822 139.54
643.9 211.0303 138.02
643.0 169.4923 136.313
640.0 120.0 133.91
635.0 95.0 133.0
656.0 82.0 148.0
656.0 88.5 142.0
683.0 92.0 141.0
683.0 83.0 129.0
684.0 77.0 116.0
711.0 77.0 116.5
739.0 76.0 117.0
764.0 76.2 118.3
789.5 75.0 121.4
817.0 66.5 128.0
817.0 57.333 136.5
817.0 45.5 143.0
792.0 34.596 148.0
817.0 26.0 148.0
838.0 20.812 148.5
838.0 0.0 148.5
&BPNODE TNODE=3, TNPC=0, TINTC=0, &END
&SECT1 STX=-511.0, STY=0.0, STZ=2004.0, SCALE=1.0,
      ALF=11.0, THETA=0.0,
      INMODE=4, TNODS=2, TNPS=0, TINTS=0, &END
656.0 372.515 137.0
656.0 335.7 136.0
654.0 294.1 135.5
653.0 252.582 135.0
653.0 211.0 134.0
653.0 169.5 132.0
645.0 130.0 131.5
645.0 125.0 130.0
660.0 105.0 130.0
665.0 98.0 131.0
687.0 94.0 135.0
687.0 85.0 127.0
687.0 79.0 115.5
715.0 78.0 116.0
743.0 77.0 116.0

```

768.0	76.5	117.5	
794.0	75.5	120.5	
821.0	66.5	127.5	
821.0	57.4	135.5	
821.0	45.5	142.0	
798.0	34.6	147.0	
821.0	26.0	147.0	
842.0	20.8	147.5	
842.0	0.0	147.5	
&BPNODE TNODE=3, TNPC=0, TINTC=0,			&END
&SECT1 STX=-511.0, STY=0.0, STZ=2004.0, SCALE=1.0,			
ALF=11.0, THETA=0.0,			
INMODE=4, TNODS=2, TNPS=0, TINTS=0,			&END
666.0	372.5	133.0	
666.0	335.7	132.0	
666.0	294.1	131.5	
663.0	252.6	132.0	
663.0	211.0	131.5	
663.0	169.5	130.0	
660.0	130.0	127.0	
660.0	125.0	125.0	
668.0	110.0	125.0	
668.0	107.0	125.0	
691.0	96.0	130.0	
691.0	88.0	125.0	
691.0	80.0	115.0	
720.0	78.5	115.5	
748.0	77.5	115.5	
773.0	77.0	115.0	
799.0	75.6	120.0	
826.0	66.6	127.0	
826.0	57.4	135.0	
826.0	45.5	141.5	
815.0	34.6	146.5	
826.0	26.0	146.5	
848.0	20.8	147.0	
848.0	0.0	147.0	
&BPNODE TNODE=3, TNPC=0, TINTC=0,			&END
&SECT1 STX=-511.0, STY=0.0, STZ=2004.0, SCALE=1.0,			
ALF=11.0, THETA=0.0,			
INMODE=4, TNODS=2, TNPS=0, TINTS=0,			&END
695.0	372.5	121.0	
695.0	335.7	121.0	
695.0	294.1	121.0	
695.0	252.6	121.0	
695.0	211.0	121.0	
695.0	169.5	121.0	
695.0	130.0	121.0	
695.0	125.0	115.0	
695.0	120.0	115.0	
695.0	115.0	115.0	
695.0	100.0	125.0	
695.0	90.0	115.0	
695.0	85.0	110.0	

728.0	80.0	115.0	
756.0	81.0	112.0	
781.0	80.0	114.0	
806.0	75.6	120.0	
834.0	66.6	127.0	
834.0	57.4	135.0	
834.0	45.5	141.5	
834.0	34.6	146.5	
834.0	26.0	146.5	
856.0	20.8	147.0	
856.0	0.0	147.0	
&BPNODE TNODE=3, TNPC=0, TINTC=0,			&END
&SECT1 STX=-511.0, STY=0.0, STZ=2004.0, SCALE=1.0,			
ALF=11.0, THETA=0.0,			
INMODE=4, TNODS=2, TNPS=0, TINTS=0,			&END
760.0	372.5	105.0	
760.0	335.7	105.0	
760.0	294.1	105.0	
760.0	252.6	105.0	
760.0	211.0	105.0	
760.0	169.5	105.0	
760.0	130.0	105.0	
760.0	125.0	105.0	
760.0	120.0	105.0	
760.0	115.0	105.0	
760.0	105.0	110.0	
760.0	100.0	110.0	
760.0	95.0	105.0	
760.0	85.0	110.0	
760.0	82.0	110.0	
791.0	80.0	110.0	
816.0	75.6	120.0	
844.0	66.6	126.5	
844.0	57.4	134.5	
844.0	45.5	141.0	
844.0	34.6	146.0	
844.0	26.0	146.0	
865.0	20.8	146.5	
865.0	0.0	146.5	
&BPNODE TNODE=3, TNPC=0, TINTC=0,			&END
&SECT1 STX=-511.0, STY=0.0, STZ=2004.0, SCALE=1.0,			
ALF=11.0, THETA=0.0,			
INMODE=4, TNODS=2, TNPS=0, TINTS=0,			&END
870.0	372.5	95.0	
870.0	335.7	95.0	
870.0	294.1	95.0	
870.0	252.6	95.0	
870.0	211.0	95.0	
870.0	169.5	95.0	
870.0	130.0	95.0	
870.0	125.0	95.0	
870.0	120.0	95.0	
870.0	115.0	95.0	
870.0	105.0	100.0	

870.0	100.0	100.0
870.0	95.0	100.0
870.0	90	100.0
870.0	85.0	105.0
870.0	80.0	105.0
870.0	75.6	120.0
870.0	66.6	126.5
870.0	57.4	134.5
870.0	45.5	141.0
870.0	34.6	146.0
870.0	26.0	146.0
870.0	20.8	146.0
870.0	0.0	146.0

```
&BPNODE TNODE=3, TNPC=0, TINTC=0, &END
&SECT1 STX=1000.0, STY=0.0, STZ=0.0, SCALE=1.0,
ALF=11.0, THETA=0.0,
INMODE=-1, TNODS=3, TNPS=20, TINTS=3, &END
```

```
&VS1 NVOLR= 0, NVOLC= 0, &END
&VS2 X0= -2.0000, Y0= 0.0000, Z0= -2.0000, &END
&VS3 X1= 2.0000, Y1= 0.0000, Z1= -2.0000, NPT1= 20, &END
&VS4 X2= -2.0000, Y2= 0.0000, Z2= -2.0000, NPT2= 0, &END
&VS5 X3= -2.0000, Y3= 0.0000, Z3= 2.0000, NPT3= 40, &END
```

```
&VS6 XR0= 0.0000, YR0= 0.0000, ZR0= 0.0000, &END
&VS7 XR1= 0.0000, YR1= 10.0000, ZR1= 0.0000, &END
XR2= 0.0000, YR2= 0.0000, ZR2= 1.0000, &END
&VS8 R1= 0.5000, R2= 5.0000, PHI1= 0.0, PHI2=330.0, &END
&VS9 NRAD= 10, NPHI= 12, NLEN= 5, &END
```

```
&SLIN1 NSTLIN=16, &END
&SLIN2 SX0=-110.0, SY0=40.0, SZ0=5.0, &END
SU=50.0, SD=450.0, DS=5.0, &END
&SLIN2 SX0=-110.0, SY0=40.0, SZ0=15.0, &END
SU=50.0, SD=450.0, DS=5.0, &END
&SLIN2 SX0=-110.0, SY0=40.0, SZ0=25.0, &END
SU=50.0, SD=450.0, DS=5.0, &END
&SLIN2 SX0=-110.0, SY0=40.0, SZ0=35.0, &END
SU=50.0, SD=450.0, DS=5.0, &END
&SLIN2 SX0=-110.0, SY0=40.0, SZ0=45.0, &END
SU=50.0, SD=450.0, DS=5.0, &END
&SLIN2 SX0=-110.0, SY0=40.0, SZ0=55.0, &END
SU=50.0, SD=450.0, DS=5.0, &END
&SLIN2 SX0=-110.0, SY0=40.0, SZ0=65.0, &END
SU=50.0, SD=450.0, DS=5.0, &END
&SLIN2 SX0=-110.0, SY0=40.0, SZ0=75.0, &END
SU=50.0, SD=450.0, DS=5.0, &END
&SLIN2 SX0=-110.0, SY0=40.0, SZ0=85.0, &END
SU=50.0, SD=450.0, DS=5.0, &END
&SLIN2 SX0=-110.0, SY0=40.0, SZ0=95.0, &END
SU=50.0, SD=450.0, DS=5.0, &END
&SLIN2 SX0=-110.0, SY0=40.0, SZ0=-5.0, &END
SU=50.0, SD=450.0, DS=5.0, &END
```

```
&SLIN2  SX0=-110.0,  SY0=40.0,  SZ0=-15.0,
SU=50.0,  SD=450.0,  DS=5.0,                &END
&SLIN2  SX0=-110.0,  SY0=40.0,  SZ0=-25.0,
SU=50.0,  SD=450.0,  DS=5.0,                &END
&SLIN2  SX0=-110.0,  SY0=40.0,  SZ0=-35.0,
SU=50.0,  SD=450.0,  DS=5.0,                &END
&SLIN2  SX0=-110.0,  SY0=40.0,  SZ0=-45.0,
SU=50.0,  SD=450.0,  DS=5.0,                &END
&SLIN2  SX0=-110.0,  SY0=40.0,  SZ0=-55.0,
SU=50.0,  SD=450.0,  DS=5.0,                &END
```

LIST OF REFERENCES

1. Naval Safety Center, *Summary of Mid-Air Collisions During Formation Flight*, Compiled by Mr. C. Byrd, NSC Code 10, February 1993.
2. Headquarters Air Force Safety Agency, HQ AFSA/SERD, *1982 To Date Mid-Air Collision Summary*, Compiled by LtCol. J. R. Perkins, USAF, Director of Reports and Analysis, February 1993.
3. Chief of Naval Air Training, *T-34C Formation Flight Training Instruction*, CNAT P-357 (Rev. 05-93) PAT, 23 April 1993.
4. Hurt, H. H., *Aerodynamics For Naval Aviators*, pp. 383-385, Aviation Maintenance Publishers, Inc., 1965
5. Air Force Human Resources Lab, AFHRL-TR-74-102, *Transfer of Training with Formation Flight Trainer*, by G. B. Reid, M. L. Cyrus, December 1974.
6. Aircraft Engineering Vol. 43, Num. 7, *Formation Flight Technology*, by T. K. Speer, E. C. Mill, and J. L. Tate, July 1971.
7. National Aeronautics and Space Administration, NASA-TM-4465, *Summary of the Effects of Engine Throttle Response on Airplane Formation-Flying Qualities*, by K. R. Walsh, March 1993.
8. Analytical Methods, Inc., NASA-CR-151974, *Formation Flying Benefits Based on Vortex Lattice Calculations*, by B. Maskew, April 1977.
9. Lyons, D. F., *Aerodynamic Analysis of a U.S. Navy and Marine Corps Unmanned Air Vehicle*, Master's Thesis, Naval Postgraduate School, Monterey, California, June 1989.
10. Rixey, J. W., *A Multi-Faceted Engineering Study of Aerodynamic Errors of the Service Aircraft Instrumentation Package (SAIP)*, Master's Thesis, Naval Postgraduate School, Monterey, California, September 1992.
11. NASA Technical Memorandum 102851, *Potential Flow Theory and Operation Guide for the Panel Code PMARC*, by D. L. Ashby, M. R. Dudley, S. K. Iguchi, L. Browne, and J. Katz, January 1991.
12. Naval Postgraduate School, W. R. Church Computer Center, *Visualization Laboratory User's Guide*, pp. 4-5, 18 June 1993.

13. Naval Air Systems Command, Report Number SD-507-3-2, *Detailed Specification for Model T-34C Airplane Single Engine Turboprop Training Airplane, FY-78 Procurement*, pp. 15-18 and 8-A, 15 February 1978.
14. Grumman Aircraft Corporation, Report Number A51-335-R-70-2, *F-14A Stability and Control, and Flying Qualities Report, Status III, Part II, Aerodynamic Characteristics and Dimensional Data*, pp. 3-3 through 3-13 and 6-35 through 6-37, June 1970.
15. COSMIC, The University of Georgia, *GVS General Visualization System Handbook*, S. R. Keith, p. 1-7, 1993.
16. Smetana, F. O., *Computer Assisted Analysis of Aircraft Performance Stability and Control*, pp. 57-102, McGraw-Hill Book Company, 1984.
17. Perkins, Courtland D., and Hage, Robert E., *Airplane Performance Stability and Control*, p. 224, John Wiley & Sons, Inc., 1950.
18. Abbot, I. H., and Von Doenhoff, A. E., *Theory of Wing Sections*, Dover Publications, Inc., 1959.
19. Roskam, J., *Airplane Flight Dynamics and Automatic Flight Controls*, Part 1, pp. 592-609, Roskam Aviation and Engineering Corporation, 1982.
20. Nelson, Robert C., *Flight Stability and Automatic Control*, p. 252, McGraw-Hill Book Company, 1989.
21. NAVAIRWARCENACDIV, F-14 Six Degree of Freedom Simulator Data, Man Flight Simulator Building, Patuxent River, Maryland., 14 July 1993.

INITIAL DISTRIBUTION LIST

	No. Copies
1. Defense Technical Information Center Cameron Station Alexandria, Virginia 22304-6145	2
2. Library, Code 52 Naval Postgraduate School Monterey, California 93943-5002	2
3. Mr. Jonah Ottensoser Naval Air Systems Command, AIR-53011C Washington, D. C. 20361-5300	2
4. Chairman, Code AA Department of Aeronautics and Astronautics Naval Postgraduate School Monterey, California 93943-5000	1
5. Professor Richard M. Howard, Code AA/Ho Department of Aeronautics and Astronautics Naval Postgraduate School Monterey, California 93943-5000	3
6. Professor Oscar Biblarz, Code AA/Bi Department of Aeronautics and Astronautics Naval Postgraduate School Monterey, California 93943-5000	1
7. LCdr. David B. Porter, USN 936 Forest Road Lancaster, Pennsylvania 17601	2
8. Mr. Dale Ashby Full-Scale Aerodynamics Research Division NASA Ames Research Center Moffet Field, California 94035	1
9. Commanding Officer Training Squadron Six Attn: Lt. Glen B. Freeman, USCG 7700 U.S.S. Enterprise St. Suite 102 Milton, Florida 32570-5100	1

10. LtCol. Steven Grossmeyer 1
Aviation Safety Program, Code 034
Naval Postgraduate School
Monterey, California 93943-5000
11. LtCol. Jerry R. Perkins 1
HQ AFSA/SERD
918 First Ave, Room 330
Norton AFB, California 92409-7001